

Developing a Surface-initiated  
Polymerization System from a Redox-  
switchable Catalyst for Polyamide Synthesis

Kexing Xiao

A thesis  
submitted to the Faculty of  
the department of Chemistry  
in partial fulfillment  
of the requirements for the degree of  
Master of Science

Boston College  
Morrissey College of Arts and Sciences  
Graduate School

May 2022



# **Developing a Surface-initiated Polymerization System from a Redox-switchable Catalyst for Polyamide Synthesis**

Kexing Xiao

Advisor: Professor Jeffery A. Byers

**Abstract** This thesis discusses the development of a surface-initiated N-carboxyanhydride (NCA) polymerization system from a redox-switchable catalyst for polyamide synthesis and further efforts towards the synthesis of polypeptide-based materials through the integration of NCA synthesis and its polymerization. In Chapter one, the most used methods to obtain polypeptide-based materials as well as their significant limitations are introduced. A new strategy is presented to access the polypeptide-based materials based on the integrated catalysis under spatial and temporal control. In Chapter two, a strategy to allow the attachment of a redox-switchable NCA polymerization catalyst on surface of titania for the synthesis of polyamide brushes will be demonstrated. Investigations about the kinetics of this surface-initiated ring-opening polymerization will be presented by carrying out the reaction in batch and under flow. Chapter three will discuss efforts towards achieving the integration of NCA synthesis and NCA polymerization, which includes an additional anchoring method to support polymerization catalyst and compatibility tests between the two separate reactions.

## Table of Contents

<b>1. Chapter 1. Synthetic Methods for Polypeptide-based Macromolecules .....</b>	<b>1</b>
1.1 Synthetic polypeptide-based materials .....	1
1.2 Solid phase peptide synthesis: overview and limitations .....	2
1.3 N-carboxyanhydride (NCA) polymerization: overview and limitations .....	5
1.3.1 Controlled NCA polymerization methods .....	9
1.3.2 Recent efforts towards the development of controlled NCA polymerization with accelerated rate .....	15
1.3.3 Recent efforts towards the development of moisture-tolerant controlled NCA polymerization .....	24
1.4 Synthesis of polypeptide-based materials using integrated catalysis .....	31
1.5 Conclusions .....	35
References .....	37
<b>2. Chapter 2. Surface-initiated NCA Polymerizations from Redox-switchable Catalysts .....</b>	<b>53</b>
2.1 Introduction .....	53
2.2 Redox-switchable NCA Polymerization Catalyst .....	54
2.3 Synthesis of the iron(I)-TiO <sub>2</sub> nanoparticles .....	58
2.4 Polymerization of Sar-NCA with the iron(I) containing TiO <sub>2</sub> nanoparticles .....	61
2.5 Direct attachment of iron(I) on spin-coated TiO <sub>2</sub> electrode and surface-initiated NCA polymerization from flat surface .....	68
2.6 Redox behavior of surface-supported iron(I) towards the NCA polymerization .....	71
2.7 Kinetics of surface-initiated NCA polymerization from iron(I)-TiO <sub>2</sub> plate .....	74
2.8 Conclusions .....	81

Experimental Section .....	83
References .....	92
<b>3. Chapter 3. Efforts towards Integrated Catalysis of Polyamide Synthesis.....</b>	<b>101</b>
3.1 Introduction .....	101
3.2 Different attachment methods of polymerization catalyst on surface .....	102
3.2.1 Preparation of modified surface as the substrate .....	103
3.2.2 Attempts to introduce functionalized ligands on modified substrates.....	109
3.3 Compatibility tests for integration of NCA synthesis and its polymerization.....	115
3.3.1 A new NCA synthesis methodology from amino acids and CO <sub>2</sub> .....	115
3.3.2 Polymerizations of 6-membered ring NCA by iron catalysts.....	117
3.3.3 Polymerization of 5-membered ring NCA by iron(I) complex 2.1 .....	120
3.4 Conclusions .....	121
Experimental Section .....	123
References .....	135

## ABBREVIATIONS

$\delta$	chemical shift
AMM	activated monomer mechanism
AAMMA	accelerated amine mechanism by monomer activation
ATR-FTIR	attenuated total reflection
[BAr <sub>4</sub> <sup>F24</sup> ]	tetrakis(3,5-bis(trifluoromethyl)phenyl)borate
Bn	benzyl
Boc	tert-butyloxycarbonyl
BPTMS	(3-bromopropyl)trimethoxysilane
Bu	butyl
BUTCS	11-bromoundecyltrichlorosilane
CCP	covalent cooperative polymerization
[CoCp <sub>2</sub> ]	cobaltocenium
CPTMS	(3-chloropropyl)trimethoxysilane
CV	cyclic voltammetry
DIPEA	diisopropylethylamine
DMF	N,N-Dimethylformamide
DOSY	diffusion-ordered spectroscopy
E <sub>1/2</sub>	half-wave potential or redox potential
Et	ethyl
equiv.	equivalents(s)
Fc	ferrocene
Fmoc	fluorenylmethyloxycarbonyl
g	gram(s)

G3	Grubbs' third generation catalyst
GPC	gel permeation chromatography
h	hour(s)
HBTU	hexafluorophosphate benzotriazole tetramethyl uronium
HF	hydrofluoric acid
HMDS	hexamethyldisilazane
HMPA	hexamethylphosphoramide
HOBT	hydroxybenzotriazole
HVT	high vacuum technique
ICP-OES	inductively coupled plasma optical emission spectrometry
LiHMDS	lithium hexamethyldisilazide
M	molarity (mol/L)
Me	methyl
$M_n$	number-average molecular weight
$M_w$	weight average molecular weight
NAM	normal amine mechanism
NCA	N-carboxyanhydride
NHC	N-heterocyclic carbenes
NMR	nuclear magnetic resonance
PDI	pyridyl diimine
Ph	phenyl
RAFT	reversible addition-fragmentation polymerization
ROMP	ring-opening metathesis polymerization
ROP	ring-opening polymerization
SAM	self-assembled monolayer

SPPS	solid phase peptide synthesis
T <sub>3</sub> P	propanephosphonic acid anhydride
<sup>t</sup> Bu	tert-butyl
TFA	trifluoroacetic acid
TGA	thermalgravimetric analysis
THF	tetrahydrofuran
TMS	trimethylsilyl
TREN	triethylaminetriamine
V	volt(s)
XPS	X-ray photoelectron spectroscopy

## List of Figures

**Figure 1.1** Principal of solid phase peptide synthesis (SPPS). T is the temporary protecting group for N-terminus of amino acids. P<sub>n</sub> is the permanent protecting group for the side chains of amino acids. The most commonly used T and P<sub>n</sub> protecting groups are fluorenylmethyloxycarbonyl (Fmoc) and tert-butyl (tBu), respectively. Typical procedures for Fmoc-based SPPS are: i) Fmoc deprotection: 20% piperidine in N,N-dimethylformamide (DMF); ii) activation of carboxyl acid group of free amino acid: diisopropylethylamine (DIPEA) in DMF; iii) coupling step: Hexafluorophosphate benzotriazole tetramethyl uronium (HBTU) as the coupling agent with the addition of 2 equiv of hydroxybenzotriazole (HOBT) in DMF to suppress racemization ; iv) removal of Fmoc group: 20% piperidine in DMF; v) deprotection of side-chain and cleavage of peptide from solid support: 95% trifluoroacetic acid (TFA) aqueous solution. ....3

**Figure 1.2** Synthesis and schematic representation of a “hinged” polypeptide obtained from BLG-NCA polymerization initiated by 1,6-diaminohexane compared with a single polypeptide resulted from hexylamine-initiated polymerization. Adapted with permission from *J. Am. Chem. Soc.*, **2019**, *141*(22), 8680. Copyright 2019 American Chemical Society. ....24

**Figure 1.3** The synthesis of multiblock copolypeptides via accelerated polymerizations of N-carboxyanhydrides (NCAs) in a water/chloroform biphasic system. Reprinted with permission from *ACS Macro Lett.* **2019**, *8*, 11, 1517–1521. Copyright 2019 American Chemical Society.....27

<b>Figure 1.4</b> General scheme for integrated catalysis to access sequence-defined polymeric materials.....	31
<b>Figure 1.5</b> Iron-based catalysts for the redox-switchable polymerization of lactide and epoxide: Fe(II) is active towards lactide polymerization while the oxidized Fe(III) can initiate the epoxide polymerization only. Recreated from ref. 92.....	33
<b>Figure 1.6</b> Design of integrated catalysis system for synthesis of sequence-defined polypeptides. The system is composed of two separate catalysis reactions: synthesis of NCAs from amino acids and CO <sub>2</sub> and polymerizations of in-situ formed NCAs with the release of CO <sub>2</sub> . .....	35
<b>Figure 2.1</b> Iron bis(iminopyridine) monoalkoxide complexes used in redox-switchable polymerizations of N-carboxyanhydride (NCAs) and cyclohexene oxide: iron(I) complex <b>2.1</b> is active to initiate polymerization of NCAs, such as BLG-NCA and Sar-NCA; after being oxidized, the formed iron(II) complex <b>2.2</b> is only active towards epoxide polymerization like the iron(II) bisalkoxide complex <b>1.2</b> . Recreated from Ref. 30.....	56
<b>Figure 2.2</b> Proposed coordination-insertion mechanism for Sar-NCA polymerization catalyzed by complex <b>2.1</b> and co-catalyzed by a Lewis acid co-catalyst, [CoCp <sub>2</sub> ][BAr <sub>4</sub> <sup>F24</sup> ]. The Lewis acidic co-catalyst could serve two functions: to activate NCA for insertion and to prevent product inhibition. Recreated from Ref. 30. ....	58
<b>Figure 2.3</b> Iron-based catalysts reported for the redox-switchable polymerization of lactide and epoxides are extended to the solid state by appending iron-based catalysts to titania nanoparticles through protonolysis reaction. Application of an	

electrochemical switch to a conducting substrate containing electrically isolated zones coated with these particles enables patterning of surfaces with two different polymer brushes. Recreated from Ref. 32.....59

**Figure 2.4** Surface-initiated Sar-NCA polymerization from immobilized Fe(I) **2.7@TiO<sub>2</sub>** nanoparticles and Characterizations of the resulting poly(sarcosine)-coated TiO<sub>2</sub> nanoparticles. (a) Scheme for the surface-initiated Sar-NCA polymerization from **2.7@TiO<sub>2</sub>** powder; (b) FT-IR characterization of the poly(sarcosine)-coated TiO<sub>2</sub> nanoparticles; (c) TGA analysis of the poly(sarcosine)-coated TiO<sub>2</sub> nanoparticles. ...63

**Figure 2.5** Removal and characterizations of poly(sarcosine) cleaved from the TiO<sub>2</sub> nanoparticles with iodomethane treatment. (a) Reaction scheme to cleave poly(sarcosine) from TiO<sub>2</sub> powders; (b) TGA analysis of the cleaved TiO<sub>2</sub> nanoparticles after iodomethane treatment; (c) FT-IR of the cleaved TiO<sub>2</sub> nanoparticles after iodomethane treatment. ....64

**Figure 2.6** Quantitative characterizations of the poly(sarcosine) cleaved from the surface of TiO<sub>2</sub> nanoparticles. (a) GPC analysis of the poly(sarcosine) cleaved off TiO<sub>2</sub> particles; (b) <sup>1</sup>H-NMR spectrum of poly(sarcosine) cleaved off TiO<sub>2</sub> particles; (c) <sup>1</sup>H-NMR spectrum of the poly(sarcosine) obtained from the iron (I) alkoxide **2.1** initiated Sar-NCA polymerization. ....66

**Figure 2.7** Anchoring the iron(I) alkyl complex **2.7** onto the surface of spin-coated TiO<sub>2</sub> plate for surface-initiated Sar-NCA polymerization. ....69

**Figure 2.8** XPS and ATR FT-IR and characterizations for the plate after Sar-NCA polymerization. (a) XPS survey scan spectra of poly(sarcosine)-plate; (b) C1s XPS

spectra of poly(sarcosine)-plate; (c) FT-IR analysis of plate after surface-initiated NCA polymerization and a controlled plate that is prepared by drop casting a layer of pre-synthesized poly(sarcosine)..... 70

**Figure 2.9** Redox behavior of supported iron(I) catalyst **2.7@TiO<sub>2</sub>** towards NCA polymerization can be tuned by applying electrochemical potential (top); (a) Cyclic voltammetry (CV) curve for surface-anchored iron(I) **2.7@TiO<sub>2</sub>** plate; (b) CV measurement of surface-anchored iron(I) **2.7@TiO<sub>2</sub>** plate with the insertion of a small amount of poly(sarcosine) between the substrate and iron complex; c) CV curve for molecular iron(I) alkoxide complex **2.1**.<sup>30</sup> 0.1 M THF solution of Bu<sub>4</sub>PF<sub>6</sub> was used as the electrolyte; Working electrode: **2.7@TiO<sub>2</sub>** plate; Counter electrode: platinum wire, Reference electrode: lithium strip; Scan rate is 50 mV/s; The peak at about -1.4 V vs Fc<sup>+</sup>/Fc on Figure 2.9 (b) belongs to the TiO<sub>2</sub> background. .... 73

**Figure 2.10** Evolution of NCA conversion versus reaction time for NCA polymerizations on **2.7@TiO<sub>2</sub>** plates carried out in the batch with stirring at 1000 rpm. .... 76

**Figure 2.11** Design of the microfluidic cell used for the heterogeneous surface-initiated Sar-NCA polymerization from **2.7@TiO<sub>2</sub>** plate. .... 77

**Figure 2.12** Plots for NCA conversion and rate constant versus flow rate for NCA polymerizations on **2.7@TiO<sub>2</sub>** plates carried out in the microfluidic cell. .... 81

**Figure S 2.1** Original <sup>1</sup>H NMR of the cleaved poly(sarcosine) in CDCl<sub>3</sub>. Specific analysis is shown in Figure 2.6 (b). .... 88

**Figure S 2.2** <sup>1</sup>H NMR of precipitated homogeneous poly(sarcosine) in CDCl<sub>3</sub>. .... 90

<b>Figure S 2.3</b> $^1\text{H}$ NMR of the homogeneous poly(sarcosine) after the iodomethane treatment in $\text{CDCl}_3$ .....	91
<b>Figure S 2.4</b> Diffusion ordered spectroscopy (DOSY) of the homogeneous poly(sarcosine) after iodomethane treatment. Only single polymer species existed after the methyl iodide treatment. ....	91
<b>Figure 3.1</b> Drawbacks of attaching catalyst through iron center ((a), method described in Chapter 2) versus advantages of anchoring catalyst through modified ligands ((b), method discussed in Chapter 3). ....	102
<b>Figure 3.2</b> Formation of halide-terminated SAMs on the $\text{TiO}_2$ plate that was prepared by spin-coating a layer of $\text{TiO}_2$ P25 nanoparticles on an FTO-glass slide. (a) Cl-terminated SAM on spin-coated $\text{TiO}_2$ plate using (3-chloropropyl)trimethoxysilane (CPTMS); (b) Br-terminated SAM on spin-coated $\text{TiO}_2$ plate using (3-bromopropyl)trimethoxysilane (BPTMS); (c) Br-terminated SAM on spin-coated $\text{TiO}_2$ plate using 11-bromoundecyltrichlorosilane (BUTCS); Water contact angles and XPS were used as the characterizations for the plates to confirm the successful introduction of halide elements on their hydrophobic surfaces. ....	105
<b>Figure 3.3</b> Preparations of OH-terminated SAMs of different lengths from (a) the Cl-terminated propylorganosilane-modified spin-coated $\text{TiO}_2$ plate or (b) Br-terminated undecylorganosilane-modified spin-coated $\text{TiO}_2$ plate using the hydrolysis reaction condition shown in entry 9 of Table 3.1. XPS analysis and water contact angles are included.....	109
<b>Figure 3.4</b> Iron complexes used for the NCA polymerization studies.....	117

<b>Figure S 3.1</b>	$^1\text{H}$ NMR of ethyl ester-functionalized PDI ligand <b>3.2</b> in $\text{CDCl}_3$ . .....	131
<b>Figure S 3.3</b>	FT-IR of ethyl ester-functionalized PDI ligand <b>3.2</b> . .....	132
<b>Figure S 3.4</b>	Paramagnetic $^1\text{H}$ NMR of iron dichloride complex <b>3.5</b> in $\text{C}_6\text{D}_6$ . .....	133
<b>Figure S 3.5</b>	FT-IR of ethyl ester-functionalized. iron dichloride complex <b>3.5</b> . .....	133
<b>Figure S 3.6</b>	$^1\text{H}$ NMR after hydrolysis and removal of iron from complex <b>3.5</b> . .....	134

## List of Schemes

- Scheme 1.1** Proposed mechanisms for the synthesis of  $\alpha$ -amino acid N-carboxyanhydrides (NCAs) using Leuchs method and Fuchs–Farthing method. ....6
- Scheme 1.2** Two common mechanisms of traditional N-carboxyanhydride (NCA) polymerizations initiated by amines: (a) normal amine mechanism (NAM) and (b) activated monomer mechanism (AMM). ....7
- Scheme 1.3** Carbamic acid–CO<sub>2</sub> equilibrium in N-carboxyanhydride (NCA) ring-opening polymerization (ROP) through normal amine mechanism (NAM). ....9
- Scheme 1.4** Mechanisms for controlled N-carboxyanhydride (NCA) polymerizations initiated by transition metal complexes: (a) zerovalent bpyNi(COD) (bpy = 2,2'-bipyridyl, COD = 1,5-cyclooctadiene) or (PMe<sub>3</sub>)<sub>4</sub>Co; (b) nickelacycle imitators. .... 11
- Scheme 1.5** Mechanism for controlled N-carboxyanhydride (NCA) polymerization through the usage of ammonium salts. .... 13
- Scheme 1.6** Trimethylsilyl (TMS) mechanism for controlled N-carboxyanhydride (NCA) polymerization initiated by silazane derivatives including hexamethyldisilazane (HMDS) or a variety of N-TMS amines. .... 14
- Scheme 1.7** Controlled N-carboxyanhydride (NCA) polymerization initiated by triethylaminetriamine (TREN) follows the accelerated amine mechanism by monomer activation (AAMMA) mechanism ..... 16
- Scheme 1.8** Mechanism for controlled N-carboxyanhydride (NCA) polymerizations mediated by (a) N-heterocyclic carbenes (NHC) in the presence of primary amine as the initiator; (b) 1,3-bis(2-hydroxyhexafluoroisopropyl)benzene (1,3-Bis-HFAB) from

an aminoalcohol initiator, N,N-dimethylethanolamine (DMEA). .....	18
<b>Scheme 1.9</b> (a) Trimethylsilyl phenylsulfide (PhS-TMS) mediated N-carboxyanhydride (NCA) polymerization and (b) Synthesis of trimethyl stannyl phenyl sulfide (PhS-SnMe <sub>3</sub> ) and PhS-SnMe <sub>3</sub> mediated NCA polymerization. ....	20
<b>Scheme 1.10</b> Polymerization of BLG-NCA initiated by <i>exo</i> -norbornene (NB) forms linear polypeptides (PBLG <sub>m</sub> ). Ring-opening metathesis polymerization (ROMP) of NB with ruthenium catalyst G3 forms PNB <sub>n</sub> that can act as macroinitiators for the polymerization of BLG-NCA forming brush polymers. The resulting polypeptide chains spontaneously fold into $\alpha$ -helices after obtaining a degree of polymerization (DP) between 8 and 12.....	23
<b>Scheme 1.11</b> Mechanism for NCA polymerization initiated by lithium hexamethyldisilazide (LiHMDS) where controlled insertion of NCA monomer is enabled by the nucleophilic attack of N-terminal lithium carbamate due to its weak basicity. ....	25
<b>Scheme 1.12</b> Ring-opening polymerization and in situ self-assembly (ROPISA) in water of BLG-NCA and Leu-NCA monomer by initiated by a $\alpha$ -amino-poly(ethylene oxide) (PEG). ....	28
<b>Scheme 1.13</b> Mechanism for the superfast N-carboxyanhydride (NCA) polymerization initiated by tetrabutylammonium carboxylate. ....	29
<b>Scheme 2.1</b> Protonolysis reaction can allow the support of iron(I) complex <b>2.7</b> covalently on P25 titania nanoparticles to afford <b>2.7@TiO<sub>2</sub></b> . The iron loading on the resulting <b>2.7@TiO<sub>2</sub></b> sample was within 0.25-0.80 wt%. ....	61

<b>Scheme 3.1</b> Reaction scheme for the synthesis of methyl ester-functionalized bis(imino)pyridine (PDI) ligand <b>3.1</b> .	110
<b>Scheme 3.2</b> Transesterification reaction of methyl ester-functionalized PDI ligand <b>3.1</b> in ethanol (a) without and (b) with the addition of ZnCl <sub>2</sub> . With adding ZnCl <sub>2</sub> , the reaction afforded 96% of an ethyl ester-functionalized PDI compound <b>3.2</b> and a small amount (4%) of the mono-substituted ketone byproduct <b>3.3</b> as evident by <sup>1</sup> H NMR spectroscopy.	111
<b>Scheme 3.3</b> Transesterification reaction of methyl ester-functionalized PDI ligand <b>3.2</b> with ethanol in the presence of FeCl <sub>2</sub> . Upon removal of iron species, 85% of the ethyl ester-functionalized PDI ligand <b>3.2</b> and 15% of the methyl ester-functionalized PDI ligand <b>3.1</b> (~15%) were obtained as evident by <sup>1</sup> H NMR spectroscopy.	113
<b>Scheme 3.4</b> Proposal to attach PDI ligand on titania substrate through (i) transesterification reaction to introduce alkyne group on ligand backbone followed by (ii) a click reaction between the ligand on azide-terminated SAM surface.	115
<b>Scheme 3.5</b> Optimal conditions for the synthesis of benzylisatoic anhydride from unprotected β-amino acid and CO <sub>2</sub> directly in one-pot; 1 equivalence of anthralinic acid under 300 psi of CO <sub>2</sub> with T <sub>3</sub> P (3 equivalence), DIPEA (4 equivalence) and DMAP (1 equivalence) in acetonitrile at 70 °C for 24 h.	116

## List of Tables

<b>Table 2.1</b> Kinetics of Fe(I)-catalyzed Sar-NCA polymerization from TiO <sub>2</sub> plate carried out in the batch.....	75
<b>Table 2.2</b> Kinetics of the NCA polymerization from <b>2.7@TiO<sub>2</sub></b> plate carried out in the microfluidic cell under different flow rate and residence time <sup>a</sup> of the Sar-NCA solution via a single cycle. <sup>b</sup> .....	78
<b>Table 3.1</b> Reaction conditions for hydrolysis of terminal -Cl groups on SAMs and the corresponding XPS characterization results. <sup>a</sup> .....	108
<b>Table 3.2</b> Polymerization of 6-membered ring N-benzylisatoic anhydride by different iron complexes. <sup>a</sup> .....	119
<b>Table 3.3</b> N-Bn Gly-NCA polymerizations catalyzed by iron(I) complex <b>2.1</b> with or without the addition of co-catalyst. <sup>a</sup> .....	121

## Acknowledgement

First and foremost, I must thank the support and continued love of my family, especially my parents. They always encourage me to do whatever I would like to do or try and believe that I have the talent to achieve any goal I aspire to. Without each of you, I'd be nowhere near the person I am today, and the person I'm still working on becoming. I am especially sorry for my grandmother, who kept talking about me in her last days and I did not spend a lot of time video chatting with her because I was busy with my experiments and oral exam. I missed the last chance to see her before she went to heaven, and I really wish her peace in Paradise.

I am very appreciative of my advisor, Prof. Jeffery Byers, who spent a lot of time and effort to guide me in both chemistry and research and provided opportunities for me to being involved in a big collaborative team. I was motivated by his passion towards chemistry and attention to details for being a researcher and I believe it will certainly benefit me a lot in the future. I would also like to thank all the previous and current students in the Byers group I have worked with: Dr. Matthew Thompson, Dr. Chet Tyrol, Dr. Alex Wong, Jiangwei (Eric) Liu, Connor Gallin, Banruo Li, Marcin Kazmierczak, Stephanie Johnson, William Thompson, Christine Vo, Tharani Rathnayake, Beau Fountaine. You all provide me a lot of support and helps. Specifically, all the senior students helped me a lot in the lab during the pandemic shifts and make me become more used to working in an organic lab. I would like to thank Matt for teaching me a lot about the things related to my second project after failure of my first project. It really relived a lot of my pressure in certain time. Special

thank you to Banruo and Marcin for going through this process from the start with me. I hope you both enjoy your future days and keep doing what you are interested in. In addition, I would like to acknowledge the NSF-Center for Integrated Catalysis (NSF-CIC). Thanks for all helpful suggestions and expertise shared by all the excellent PIs: Prof. Dunwei Wang, Prof. Chong Liu, Prof. Loi Do, Prof. Alex Miller, Prof. Paula Diaconescu. With being involved in this big coherent team, I got to learn various research fields and how to work with people in different personalities. I would like to thank my collaborators, Haochuan Zhang, Brandon Jolly, Connor Gallin, Dr. Thi Tran, Yi Shen and Shijie (Jenny) Deng. A lot of research shown in my thesis would not have been possible without their efforts. Furthermore, I want to thank Prof. Peter Zhang and Prof. Shi-yuan Liu for serving on my thesis committee and providing helpful feedback and continued support. Thank you both for reading my thesis.

Finally, I would like to express my sincere gratitude to Boston College and the Chemistry Department. Dale Mahoney, Lynne Houlihan, Ian Parr, Jing Jin, Marek Domin and Thusitha Jayasundera have been constant sources of help in academics and instrumentation. I also would like to thank Prof. Lynne O'Connell for all the helps and accommodations in my teaching. Additionally, I would like to thank a lot of my friends who I made here for providing me a lot of mental support.

## Chapter 1. Synthetic Methods for Polypeptide-based Macromolecules

### 1.1 Synthetic polypeptide-based materials

Proteins are one of the most essential biomacromolecules that provide structural and mechanical support for cells, tissues, and organs, catalyze different biochemical reactions and regulate cell behaviors.<sup>1-4</sup> The various functions of natural proteins originate from a wide choice of  $\alpha$ -amino acids as well as control of peptide sequences.<sup>5</sup> Inspired by the complex structures and versatile functions of natural proteins, significant efforts have been dedicated to obtaining the synthetic polypeptides. Because of their biocompatibility and biodegradability, polypeptide-based materials have been widely used in biomedicine and biotechnology applications, such as tissue engineering, drug delivery, and therapeutics.<sup>5-7</sup> Compared with typical polymers, polypeptides exhibit a great deal of chemical diversity through the amino acid side chains, where numerous functional groups can also be incorporated into polypeptide materials in addition to the canonical amino acids.<sup>8</sup> Depending on the amino acid side chains, polypeptides can adopt certain ordered conformations and self-assemble into precisely defined structures through non-covalent interactions, such as hydrogen bonding, van der Waals forces and  $\pi$ - $\pi$  stacking. The resulting hierarchical architectures or complicated functions enable the polypeptide-based materials for specific applications.<sup>9,10</sup>

Synthetic polypeptides can be generated through protein biosynthesis<sup>11</sup>, solid phase peptide synthesis (SPPS)<sup>12</sup>, and  $\alpha$ -amino acid N-carboxyanhydrides (NCA) polymerization<sup>13,14</sup>. Protein biosynthesis can be used to synthesize polypeptides with

precision chain lengths and sequences by introducing an engineered recombinant plasmid into a bacterial host.<sup>11</sup> However, the microbial synthesis is only useful for the preparation of peptides with natural amino acid residues, and it often suffers from low yields, limited post-translational modifications, and complex productions. Among the three synthetic methods, the latter two are more commonly used by chemists. An overview for each of the approaches and their apparent drawbacks will be discussed in this chapter, respectively.

## **1.2 Solid phase peptide synthesis: overview and limitations**

Solid-phase peptide synthesis (SPPS) was first introduced by Bruce Merrifield<sup>12</sup> and won him the Nobel Prize in Chemistry in 1984.<sup>15</sup> The principles of SPPS are illustrated in Figure. 1.1. The N-protected C-terminal amino-acid residue is anchored through its carboxyl group to a resin yielding a covalently linked peptide that will ultimately produce a C-terminal acid or a C-terminal amide peptide. After loading the first amino acid, the desired peptide sequence is assembled in a linear manner from the C-terminus to the N-terminus by repetitive cycles of N<sup>α</sup> deprotection and amino acid coupling reactions. Side-chain functional groups of amino acids must be masked with permanent protecting groups (P<sub>n</sub>) that are stable during peptide elongation. The α-amino group is protected by temporary protecting group (T) that can be easily removed under mild conditions which helps to preserve peptide integrity and reduces the rate of epimerization. After coupling, the excess of reactants is removed by simple filtration and washings. The temporary N-terminal protecting group is removed allowing the addition of the next N-protected amino acid residue by

activation of its  $\alpha$ -carboxylic acid. This deprotection-coupling process will be repeated until the desired sequence is obtained. In the final step, the peptide is released from the resin with the simultaneous removal of side-chain  $P_n$ .

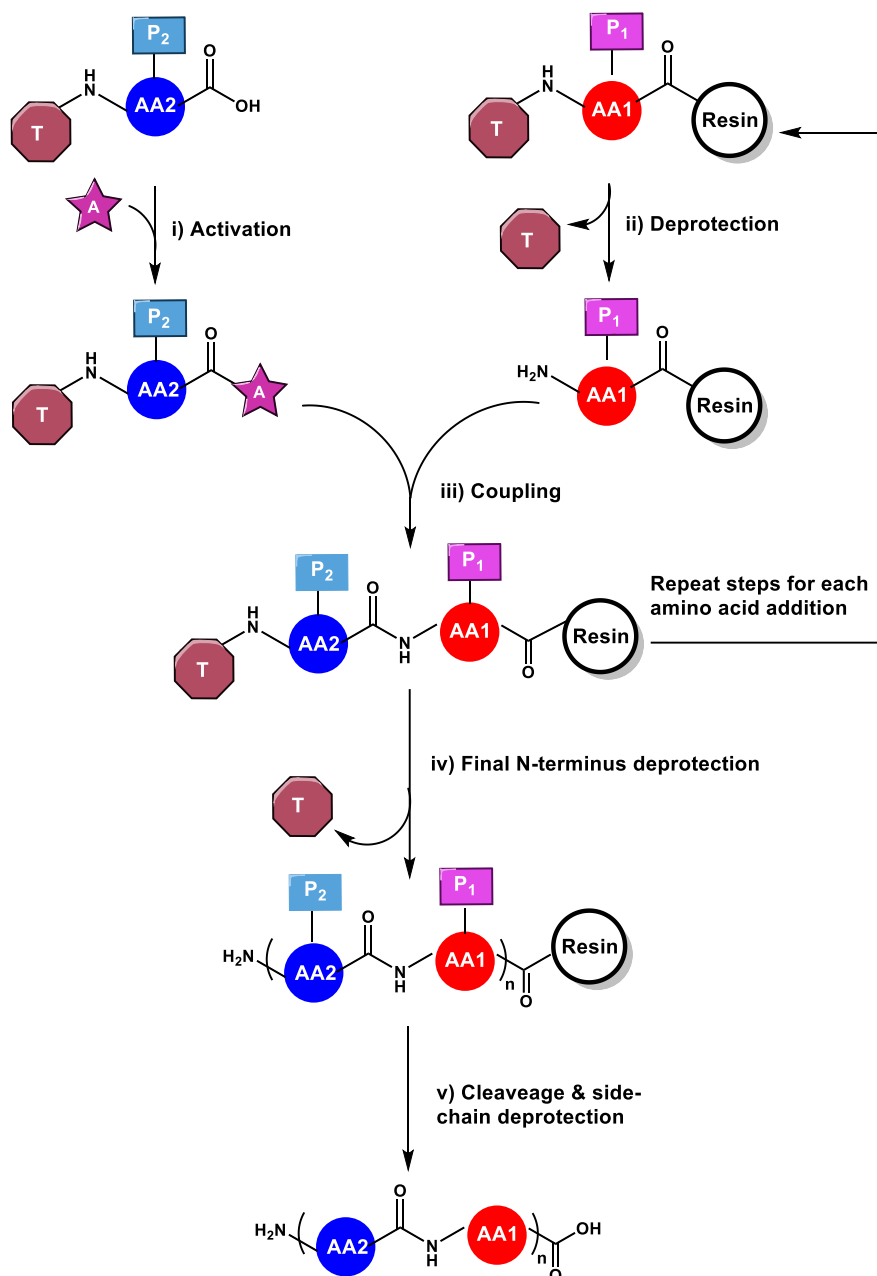


**Figure 1.1** Principial of solid phase peptide synthesis (SPPS). T is the temporary protecting group for N-terminus of amino acids. P<sub>n</sub> is the permanent protecting group for the side chains of amino acids. The most commonly used T and P<sub>n</sub> protecting groups are fluorenylmethyloxycarbonyl (Fmoc) and tert-butyl (tBu),

respectively. Typical procedures for Fmoc-based SPPS are: i) Fmoc deprotection: 20% piperidine in N,N-dimethylformamide (DMF); ii) activation of carboxyl acid group of free amino acid: diisopropylethylamine (DIPEA) in DMF; iii) coupling step: Hexafluorophosphate benzotriazole tetramethyl uronium (HBTU) as the coupling agent with the addition of 2 equiv of hydroxybenzotriazole (HOBT) in DMF to suppress racemization ; iv) removal of Fmoc group: 20% piperidine in DMF; v) deprotection of side-chain and cleavage of peptide from solid support: 95% trifluoroacetic acid (TFA) aqueous solution.

A feature in the SPPS is the temporary protecting groups used for amino acids. The two most widely used combinations are the Boc/Bn<sup>16</sup> and the Fmoc/<sup>t</sup>Bu<sup>17</sup> approaches for T/P<sub>n</sub> protecting groups, respectively. For the former strategy, the Boc group is normally removed by trifluoroacetic acid (TFA) treatment, and side-chain protecting groups and peptide–resin linkages are removed at the end of the synthesis with the addition of anhydrous hydrofluoric acid (HF). Although this method achieves efficient synthesis of large peptides and small proteins, safety concern about the usage of highly toxic HF limits its application. In addition, the use of strongly acidic conditions can destroy the structural integrity of peptides containing acid-sensitive sequences. The Fmoc strategy is often preferred over the Boc strategy for routine synthesis, because the former is based upon an orthogonal protecting group strategy. The approach uses the base–labile N-Fmoc group for protection of the  $\alpha$ -amino function, acid–labile side-chain protecting groups and acid–labile linkers that constitute the C-terminal amino acid protecting groups, which allows the removal of

temporary and permanent orthogonal protections by different mechanisms. Importantly, the final deprotection and cleavage of the peptide from the solid support can be achieved using milder acidic conditions.<sup>18</sup> Therefore, Fmoc-based SPPS has become the method of choice for routine synthesis of peptides.

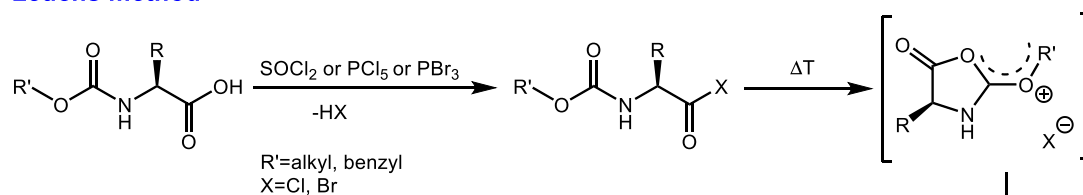
As a robust and routine method, SPPS has been employed to prepare polypeptides with precisely controlled amino acid sequences by successive couplings of amino acids. However, the maximum chain length is restricted to about 50 amino acid residues due to the statistical accumulation of resin-bound byproducts from incomplete reactions and impurities in the solvent, reagents, and protected amino acids used.<sup>19,20</sup> In addition, the scale of polypeptide obtained from SPPS is limited to milligram quantities. Moreover, the tedious stoichiometric coupling, protection and deprotection steps result in low overall yields, possible racemization<sup>21</sup> and generation of stoichiometric wastes that could lead to accumulation of chemical waste.<sup>22</sup> Because of the important applications of peptides as “medium-sized” molecular medicine,<sup>23</sup> the development of greener alternatives for synthetic peptides is desirable from a green chemistry perspective.<sup>24</sup>

### **1.3 N-carboxyanhydride (NCA) polymerization: overview and limitations**

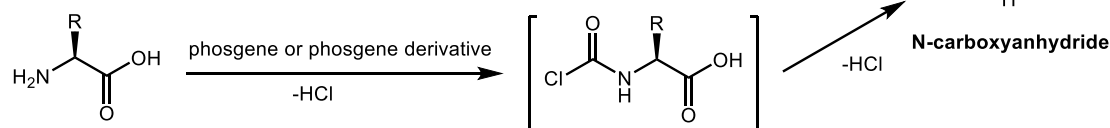
Ring-opening polymerization (ROP) of N-carboxyanhydrides (NCAs) derived from  $\alpha$ -amino acids is the most applied polymerization technique for people to obtain synthetic polypeptide-based materials.<sup>25</sup> By using this approach, high molecular weight polypeptide-based materials composed of natural or non-proteinogenic amino acids can be formed efficiently on a multigram scale. The origin of this method can be

traced back to 1906 when Hermann Leuchs first reported the synthesis of  $\alpha$ -amino acid N-carboxyanhydrides.<sup>26</sup> Since then, numerous research has been devoted to the formation of well-controlled polypeptide-based macromolecules with narrow molecular weight distributions.

#### Leuchs method



#### Fuchs-Farthing method

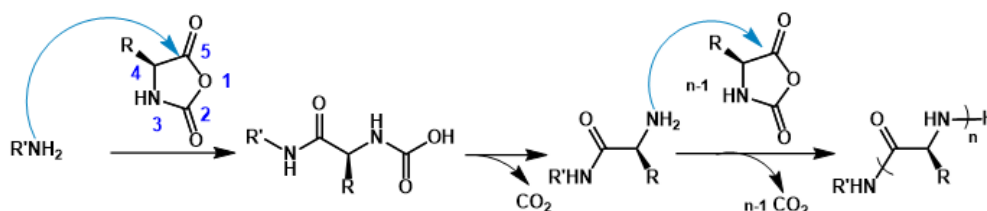


**Scheme 1.1** Proposed mechanisms for the synthesis of  $\alpha$ -amino acid N-carboxyanhydrides (NCAs) using Leuchs method and Fuchs–Farthing method.

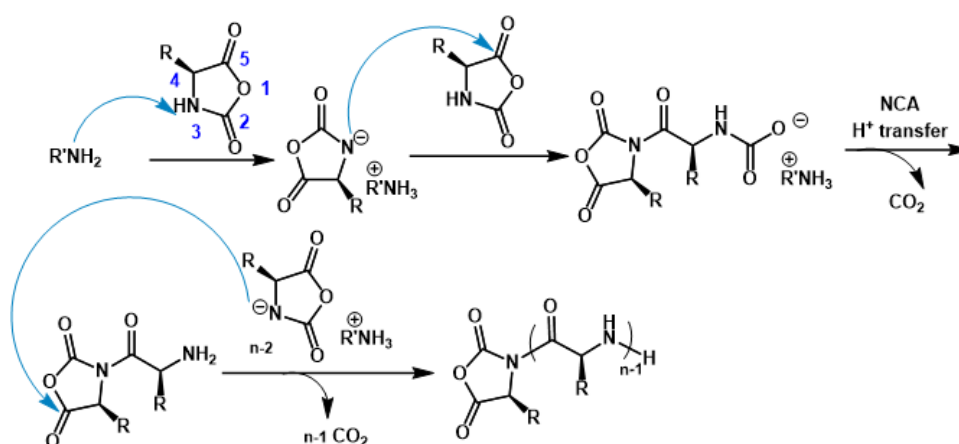
NCA can be synthesized either by the reaction of N-alkyloxycarbonyl-amino acids with halogenating agents (e.g.,  $\text{PBr}_3$ ,  $\text{PCl}_5$ ,  $\text{SOCl}_2$ ) leading to the formation of carcinogenic alkyl halides (Leuchs method<sup>26–28</sup>); or by the treatment of  $\alpha$ -amino acids with phosgene (Scheme 1.1, Fuchs–Farthing method<sup>29,30</sup>) (Scheme 1.1). Triphosgene<sup>31</sup>, trichloromethyl chloroformate<sup>32</sup> and di-tert-butyltricarboxylate<sup>33</sup> have been used as phosgene substitutes, allowing phosgene to form in situ during NCA synthesis. Mostly recrystallization but also flash chromatography can be applied for the purifications of NCAs to remove byproducts generated during NCA synthesis including HCl, HCl–amino acid salts and 2-isocyanatoacyl chlorides as they can

inhibit or quench the propagation of the polymer chains during NCA polymerization and thus, affect the synthesis of polypeptides.<sup>34–36</sup>

**(a) Normal Amine Mechanism (NAM)**



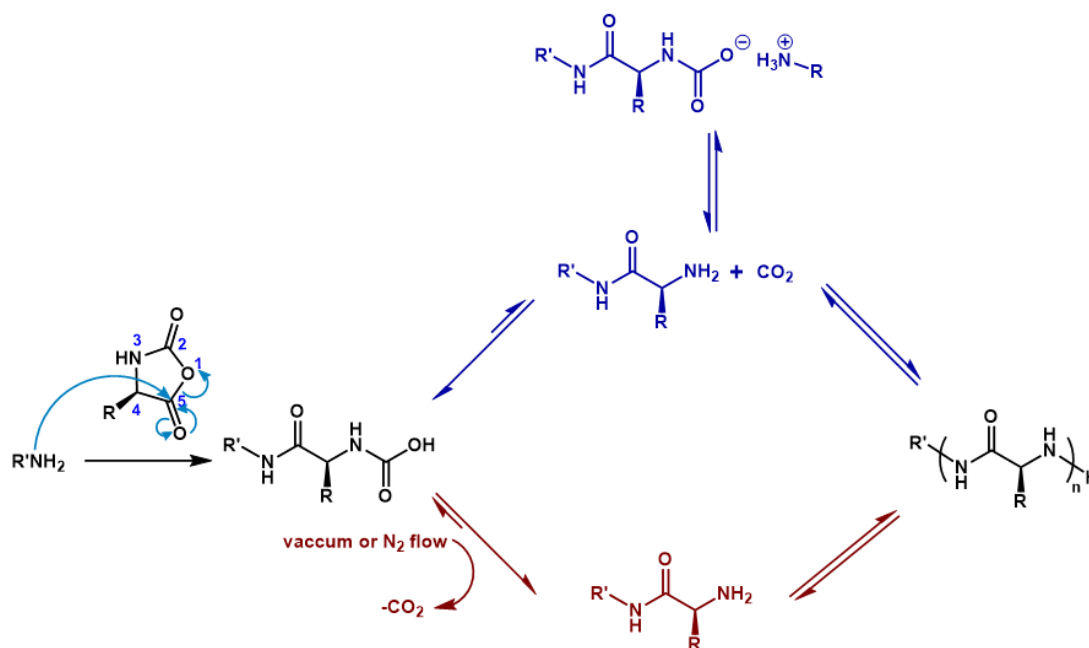
**(b) Activated Monomer Mechanism (AMM)**



**Scheme 1.2** Two common mechanisms of traditional N-carboxyanhydride (NCA) polymerizations initiated by amines: (a) normal amine mechanism (NAM) and (b) activated monomer mechanism (AMM).

The traditional NCA polymerization proceeds via two mechanisms: the normal amine mechanism (NAM) and the activated monomer mechanism (AMM), as depicted in Scheme 1.2.<sup>13</sup> The initiation mechanism of an NCA is determined by the relative nucleophilicity and basicity of the initiator.<sup>36</sup> The initiator must have sufficient nucleophilicity to attack the 5-C=O of the NCA, resulting in opening of the NCA ring and proton transfer to form a carbamic acid intermediate. Decarboxylation of the carbamic acid generates a free amino group which continues to serve as a

nucleophile for chain propagation through the NAM. However, if the initiator is very basic, deprotonation of the NCA can occur, and the resulting nucleophile initiates chain growth through the unwanted AMM. Generally, nucleophiles like primary amines are the initiators for NCA polymerizations proceeding via NAM. Nevertheless, these initiators are prone to side-reactions with solvents, water contaminants, end-group termination and other competing mechanisms (such as AMM). Consequently, the reactions often lack the control of chain-end fidelity making it hard to access the synthesis of more complex polymer architectures like block copolymers with high molecular weights and narrow dispersity.<sup>37-41</sup> Furthermore, the reaction rates can be sluggish due to inhibition from CO<sub>2</sub> reacting with propagating polymer chains.<sup>42</sup> As depicted in Scheme 1.3, the loss of CO<sub>2</sub> from the carbamic acid is the rate-determining step in NAM. Therefore, with the efficient removal of CO<sub>2</sub> from the reaction mixture, the decarboxylation of the carbamic acid continuously shifts the equilibrium to generate active amine for further chain propagation and thus, first-order kinetics are observed.<sup>43,44</sup> However, without removal of CO<sub>2</sub>, the carbamic acid dominates and the formation of carbamic acid salt is favored, which reduces the nucleophilicity of the active polymer chain end and presents different polymerization kinetics.



**Scheme 1.3** Carbamic acid–CO<sub>2</sub> equilibrium in N-carboxyanhydride (NCA) ring-opening polymerization (ROP) through normal amine mechanism (NAM).

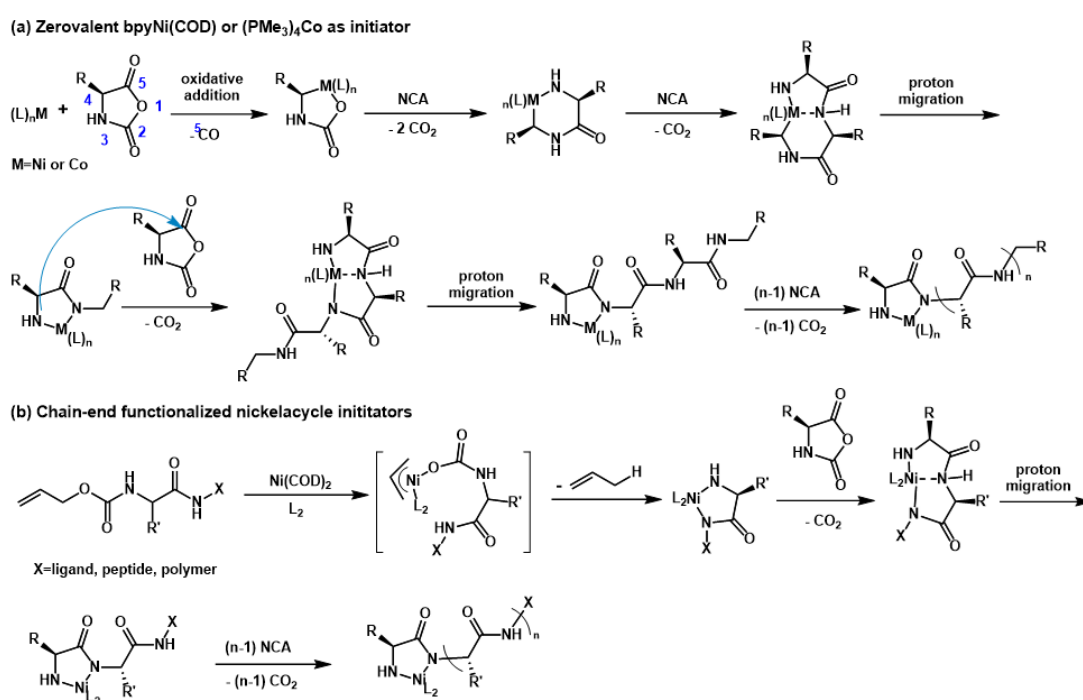
### 1.3.1 Controlled NCA polymerization methods

In the past decade, numerous efforts have been made towards improving the control of NCA polymerization. Generally, two different approaches were taken to prevent chain termination in NCA polymerization. When compared to NAM, the first approach builds on different reaction mechanisms by the formations of a dormant polymer chain end. On the other hand, the second strategy achieves the great control of NCA polymerization by optimizing the NAM conditions themselves. Herein, several key strategies to mediate the controlled NCA polymerizations are discussed with their mechanisms and potential drawbacks.

In 1997, Deming discovered a new class of NCA polymerization initiators based on the zerovalent nickel complex  $bpyNi(COD)$  ( $bpy = 2,2'$ -bipyridyl,  $COD = 1,5$ -cyclooctadiene) or cobalt complex  $(PMe_3)_4Co$ .<sup>45,46</sup> The usage of the transition

metal complexes allowed insertion of NCA monomers leaving the polymer chain end intact. Therefore, a controlled (“living”) NCA polymerization was enabled for the first time. The mechanism for this controlled NCA polymerization is depicted in Scheme 1.4 a. The metal initiators react with NCA monomers first to afford, by oxidative addition to the anhydride bonds of NCA, metallacyclic complexes, which react with a second NCA monomer to give a 6-membered amido-alkyl metallacycle. The amido-alkyl metallacycle then reacts with another NCA to give a large metallacycle after the simultaneous elimination of CO<sub>2</sub>. Migration of an amide proton to the metal-bound carbon results in the formation of a 5-membered amido-amidate complex, an active polymerization intermediate.<sup>47</sup> The propagation then proceeds through this 5-membered amido-amidate complex by attack of the nucleophilic amido group on the electrophilic 5-C=O of NCA to regenerate the active species upon CO<sub>2</sub> elimination and proton migration. Using these zerovalent nickel or cobalt complexes as initiators, homo- and co-polypeptides with controlled high molecular weights and narrow molecular weight distributions ( $M_w/M_n < 1.2$ ) can be synthesized in almost quantitative yields. However, one limitation of this methodology is that the active propagating amido-amidate species are generated in situ and thus do not permit for controlled functionalization of the polypeptide chain ends. To solve this problem, Curtin and Deming synthesized the Ni amido-amidates by quantitative reaction of alloc- $\alpha$ -aminoamides and L<sub>2</sub>Ni(COD) (L = donor ligand) (Scheme 1.4 b).<sup>48,49</sup> These species were used as initiators to efficiently catalyze the living polymerizations of NCAs affording block co-polypeptides with controlled sequences and diverse chain-

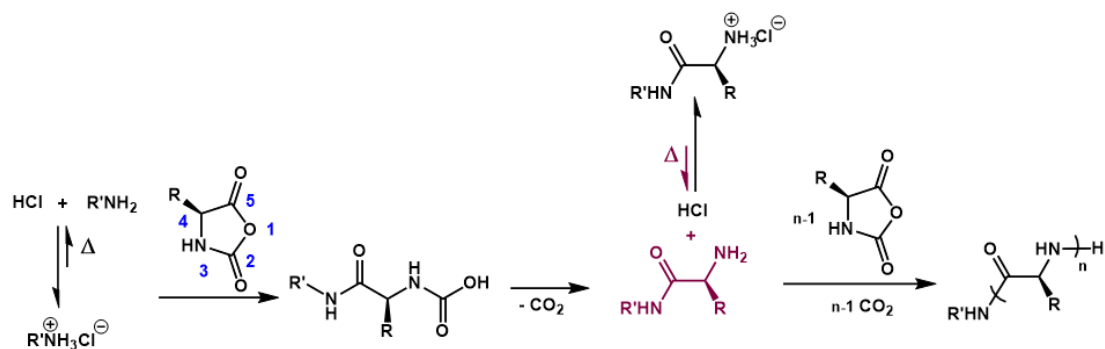
end functionalities. Overall, metal catalysis is highly useful in the synthesis of high-molecular weight (MW) block and hybrid polypeptides. However, it requires careful choice of ligand, solvent and temperature conditions in order to access the chelating metallacyclic intermediates that afford controlled polymerizations. In addition, concerns associated with the removal of heavy metal residues have somewhat curtailed the use of metal catalysts for NCA ROP used in biomedical applications.



**Scheme 1.4** Mechanisms for controlled N-carboxyanhydride (NCA) polymerizations initiated by transition metal complexes: (a) zerovalent  $\text{bpyNi(COD)}$  ( $\text{bpy} = 2,2'$ -bipyridyl,  $\text{COD} = 1,5$ -cyclooctadiene) or  $(\text{PMe}_3)_4\text{Co}$ ; (b) nickelacycle initiators.

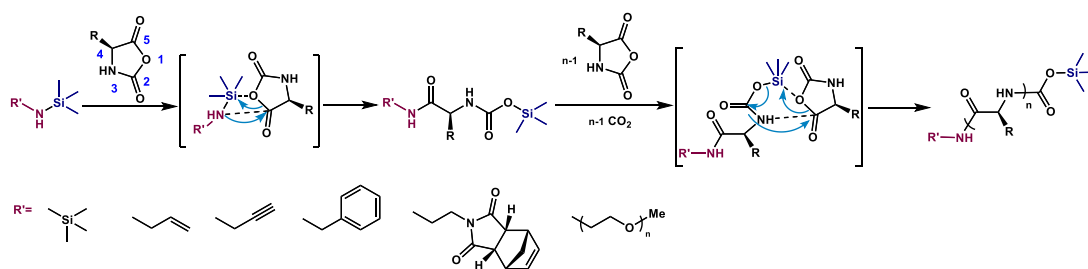
Although the discovery of effective metal catalysts for NCA ROP drove the field of controlled ring opening polymerization of NCA forward in the late 1990s, the primary amine-initiated NCA polymerization is still the most widely used technique.

Different experimental techniques have been investigated and optimized to give well-defined polypeptides. Vayaboury and co-workers reported that low temperature (0 °C) could suppress the side reactions in the polymerizations of  $\epsilon$ -trifluoroacetyl-L-lysine NCA (TFA-Lys NCA) initiated by n-hexylamine, giving rise to a homo-polyamide with monomodal molecular weight distribution.<sup>50,51</sup> The elimination of the termination reactions at low temperature was attributed to the higher activation energy of the side reaction than that of chain propagation. In 2004, Hadjichristidis and co-workers showed that using highly purified chemicals and high vacuum technique (HVT), homo- and block polypeptides with high and controlled molecular weights could be prepared.<sup>52</sup> In this approach, the highly purified solvent and initiator, the suppression of the carbamic acid–CO<sub>2</sub> equilibrium after the efficient removal of CO<sub>2</sub> as well as the side reaction between DMF and the end groups of propagating polymer chains were accounted for the great control during the polymerization. The advantages of the HVT for the preparation of well-defined polypeptides were also demonstrated by Messman and co-workers.<sup>53</sup> Nevertheless, the reaction time for NCA polymerization initiated by primary amine at lower temperature is usually much longer (3 days). Side reactions cannot be diminished when carrying out the polymerization at room temperature even with the application of vacuum.<sup>37</sup> HVT can promote the control of NCA polymerization by removal of the CO<sub>2</sub>, however, the polymerization must be conducted in specially designed apparatus to avoid loss of reagents and solvent. Difficulties with scaling up might be experienced with the application of HVT.



**Scheme 1.5** Mechanism for controlled N-carboxyanhydride (NCA) polymerization through the usage of ammonium salts.

To help the control of amine-initiated polymerizations, the protonated amine salts were examined as initiators by Schlaad<sup>40</sup> and Vicent<sup>41</sup> in 2003 and 2013, respectively. As depicted in Scheme 1.5, the reduced nucleophilicity of amine salt initiator can be exploited to achieve more controlled polymerizations in a manner similar to the reversible-deactivation radical polymerizations, where great control is achieved through an equilibrium between dormant amine salts and active amine sites. The reaction temperature ( $40 < T < 80$  °C) affects the equilibrium, with higher temperature favoring a shift towards higher concentrations of free primary amines. Polypeptides with narrow molecular weight distributions were obtained through this method, though extended reaction time was necessary (3 days) and incomplete polymerization could occur due to the low reactivity of the active sites.



**Scheme 1.6** Trimethylsilyl (TMS) mechanism for controlled N-carboxyanhydride (NCA) polymerization initiated by silazane derivatives including hexamethyldisilazane (HMDS) or a variety of N-TMS amines.

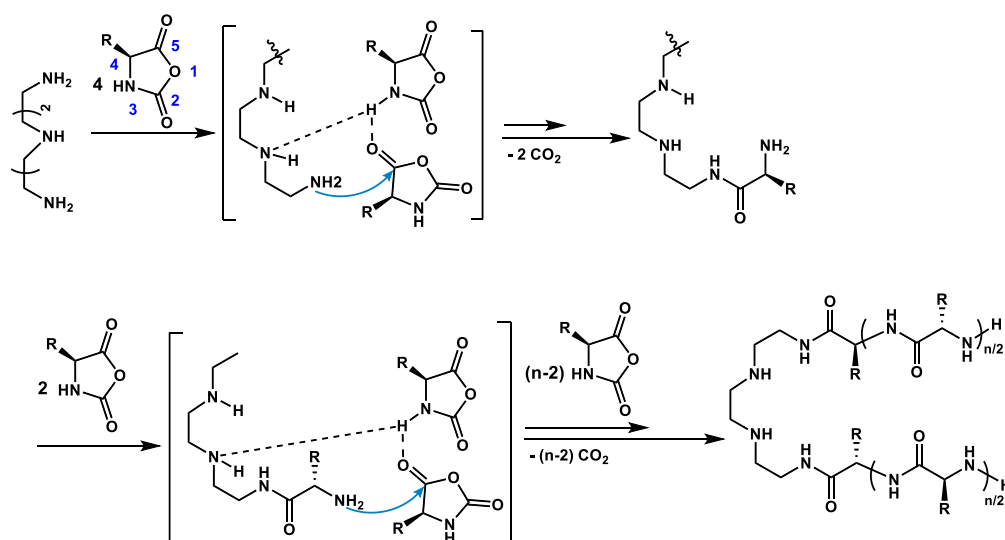
A further established method of controlled NCA polymerization relies on the organosilicons or their salts as initiators. In 2007, Lu and Cheng discovered hexamethyldisilazane (HMDS) as the initiator to successfully mediate a controlled  $\gamma$ -benzyl L-glutamate NCA (BLG-NCA) polymerization.<sup>54</sup> A variety of trimethylsilyl (TMS) amines were then exploited by the same group in 2008 for the controlled polymerizations of NCAs, such as BLG-NCA and  $\epsilon$ -Cbz-l-lysine NCA (Lys-NCA).<sup>55</sup> The improved control of polymerization catalyzed by silazane or its derivative in comparison to primary amine was attributed to a new mechanism that differs from NAM and AMM. As shown in Scheme 1.6, the TMS moiety transfers in a concerted way to CO-1 forming a terminal TMS carbamate group. Propagation of the polypeptide chains then proceeds through the transfer of the TMS group from the terminal TMS carbamate to the incoming monomer followed by the formation of a new TMS carbamate propagating group. Noteworthy, all polymerizations initiated by the TMS amines can be finished within 12–24 h at room temperature under atmospheric pressure, in contrast to the controlled polymerizations that require either

particular temperature or high vacuum. In addition, facile functionalization of the C-termini of polypeptides can be achieved due to readily available N-TMS amines. However, the NCA polymerizations following TMS mechanism still need to be conducted under anhydrous condition since the NH-Si bond can be readily cleaved upon exposure to moisture or acidic condition.

### **1.3.2 Recent efforts towards the development of controlled NCA polymerization with accelerated rate**

Despite the excellent control of NCA polymerizations can be achieved using the methods discussed above, the polymerization rates are usually slow, taking up to several days to finish. With the prolonged polymerization time, side reactions such as chain terminations and monomer degradation become significant.<sup>13,37</sup> Therefore, one of the main focuses in the past ten years is to improve the rates of NCA polymerizations. The accelerated NCA polymerizations have been enabled by either the efficient removal of released CO<sub>2</sub>,<sup>56</sup> cooperative interaction from the secondary structures of polypeptides<sup>57,58</sup> or design of new catalyst systems, such as allied amines,<sup>59,60</sup> organosilyl salts,<sup>61</sup> N-heterocyclic carbenes (NHC),<sup>62,63</sup> aminoalcohols<sup>64,65</sup>, novel Lewis pairs,<sup>66-68</sup> fluorinated molecules<sup>69</sup> and crown ether.<sup>70</sup> The reduction of contribution from side reactions and increase of polymerization rate not only simplified the preparation process of polypeptides but also allowed the access of polymer materials that were difficult to prepare using conventional polymerization with normal rate.<sup>71,72</sup>

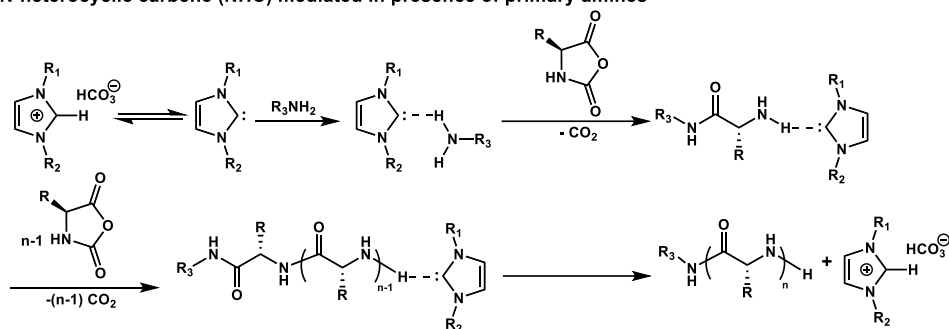
As mentioned in section 1.3.1, the release of CO<sub>2</sub> can significantly impact the kinetics of NCA polymerization (Scheme 1.3). Several groups have reported the controlled polymerizations of NCA facilitated by efficient removal of CO<sub>2</sub> through high vacuum or N<sub>2</sub> purging.<sup>37,42,52,53</sup> In 2013, Wooley and co-workers demonstrated that the removal of CO<sub>2</sub> with precise N<sub>2</sub> flow could accelerate the polymerization of BLG-NCA initiated by n-hexylamine, producing polypeptides with desired MWs and narrow molecular weight distributions.<sup>56</sup> The use of N<sub>2</sub> flow facilitated the decarboxylation of carbamic acid intermediates to generate nucleophilic amino groups, which promoted the chain propagation. Living NCA polymerization under N<sub>2</sub> flow was demonstrated, in contrast with that without N<sub>2</sub> flow, where ill-defined polypeptides with broader molecular weight distributions were obtained due to significant side reactions.



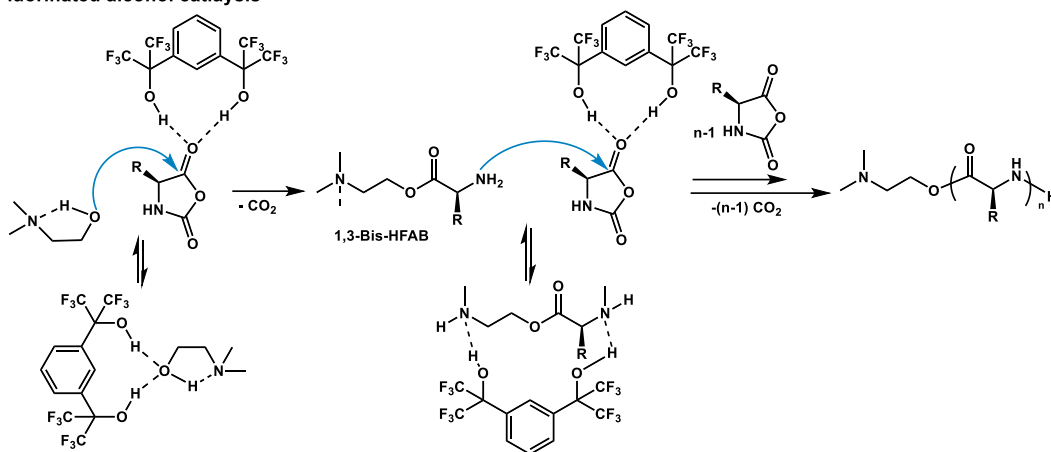
**Scheme 1.7** Controlled N-carboxyanhydride (NCA) polymerization initiated by triethylaminetriamine (TREN) follows the accelerated amine mechanism by monomer activation (AAMMA) mechanism

Accelerated polymerizations of NCAs can also be achieved by utilizing new initiation systems based on modified amine initiators. A key finding from Hadjichristidis's group was the unique NCA polymerization kinetics initiated by triethylaminetriamine (TREN), an initiator containing a sterically hindered tertiary amine and three primary amines.<sup>59</sup> TREN exhibited faster propagation rate than that catalyzed by the primary amine. Moreover, TREN-initiated NCA ROP did not give rise to uncontrolled high molecular products unlike other tertiary amines which normally promote the AMM pathway. The key of the controlled NCA polymerization was attributed to the presence of the tertiary amine at the core of TREN. As depicted in Scheme 1.7, accelerated amine mechanism by monomer activation (AAMMA) was proposed by the authors to elucidate the polymerization process. While the central tertiary amine group cannot effectively abstract proton from NCA monomer for an initiation through AMM, it plays an essential role in the activation of NCA monomer through hydrogen bonding leading to faster propagation. A further work of the same team using an initiator system containing primary and secondary amines which exhibited rate acceleration and produced linear polypeptide materials.<sup>60</sup>

(a) N-heterocyclic carbene (NHC) mediated in presence of primary amines



(b) Fluorinated alcohol catalysis



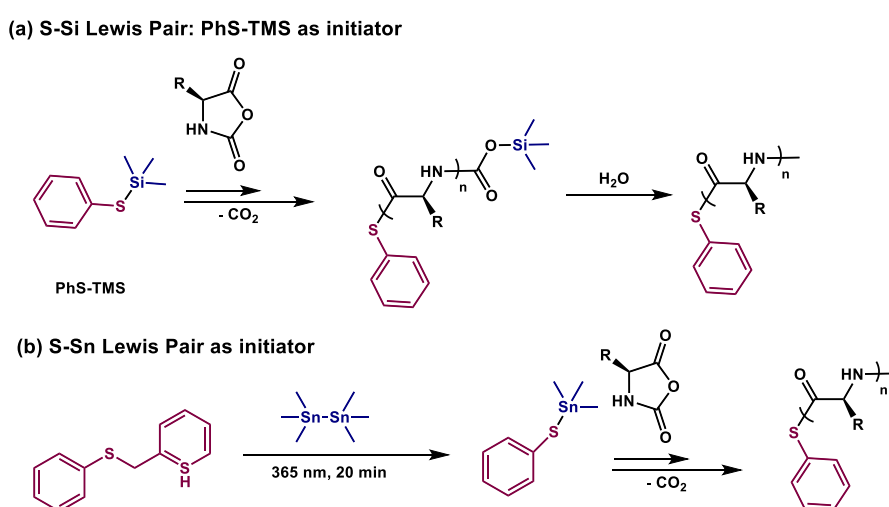
**Scheme 1.8** Mechanism for controlled N-carboxyanhydride (NCA) polymerizations mediated by (a) N-heterocyclic carbenes (NHC) in the presence of primary amine as the initiator; (b) 1,3-bis(2-hydroxyhexafluoroisopropyl)benzene (1,3-Bis-HFAB) from an aminoalcohol initiator, N,N-dimethylethanolamine (DMEA).

NCA polymerization catalysis through hydrogen bonding, as discussed above, is a powerful strategy to obtain well-controlled polypeptides due to the stabilization capacity enabled by hydrogen bonds. N-heterocyclic carbenes (NHC), a class of organocatalysts, commonly applied for ROP of lactides, have been used for NCA ROPs by Kim's group.<sup>63</sup> The NHC-mediated polymerization proceeds rapidly in the presence and absence of primary amines, resulting in well-defined linear and cyclic polypeptides, respectively. The proposed mechanism for the NHC-mediated NCA polymerization is displayed in Scheme 1.8 a. The NHC preferentially hydrogen bonds

with the initiator and  $\omega$ -terminus of the growing polypeptide, if an amine initiator is added, which affords a controlled NCA ROP. In the absence of a primary amine initiator, the NHC not only initiates the polymerization but also mediates the chain propagation as counterions, following a zwitterionic mechanism. In addition, another class of controlled NCA polymerization initiators that have been investigated is aminoalcohols. In 2019, Hadjichristidis and co-workers exploited 1,3-bis(2-hydroxyhexafluoroisopropyl)benzene (1,3-Bis-HFAB) to mediate the NCA polymerization from an aminoalcohol initiator, N,N-dimethylethanolamine (DMEA).<sup>64</sup> As shown in Scheme 1.8 b, 1,3-Bis-HFAB can activate the initiating alcohol and the NCA monomer through hydrogen bonding without inducing polymerization by itself. In the propagation, 1,3-Bis-HFAB continues to act as the hydrogen donor to the NCA, and silences the tertiary amine present in DMEA. A reversible exchange between active and inactive polymer chains is facilitated, resulting in the fast polymerization kinetics and well-defined polypeptide.

Further modification based on silazane derivatives initiators was explored as well to promote the NCA polymerization rate. In 2016, Lu and co-workers applied the trimethylsilyl phenylsulfide (PhS-TMS) to mediate well-controlled polymerizations of a varied range of NCAs (Scheme 1.9 a).<sup>61</sup> Mechanistic studies suggested that the polymerization also followed the TMS mechanism: a reactive TMS carbamate was generated during the chain initiation and continued to regulate the chain propagation through a TMS transfer process. Compared with the previously reported N-TMS amine initiator, the sulfur is, in general, more nucleophilic but less basic than nitrogen,

and the S–Si bond is more reactive than the N–Si bond. Thus, the PhS-TMS provides a faster chain initiation than a N-TMS amine with minimized AMM, which together ensure a living polymerization with better control. Well-controlled polypeptides from a lot of functionalized Glutamate (Glu) NCAs were synthesized under great controls except for  $\gamma$ -chloropropyl-L-glutamate NCA. The thiol-reactivity of this monomer may pose disadvantageous interactions with the initiator.



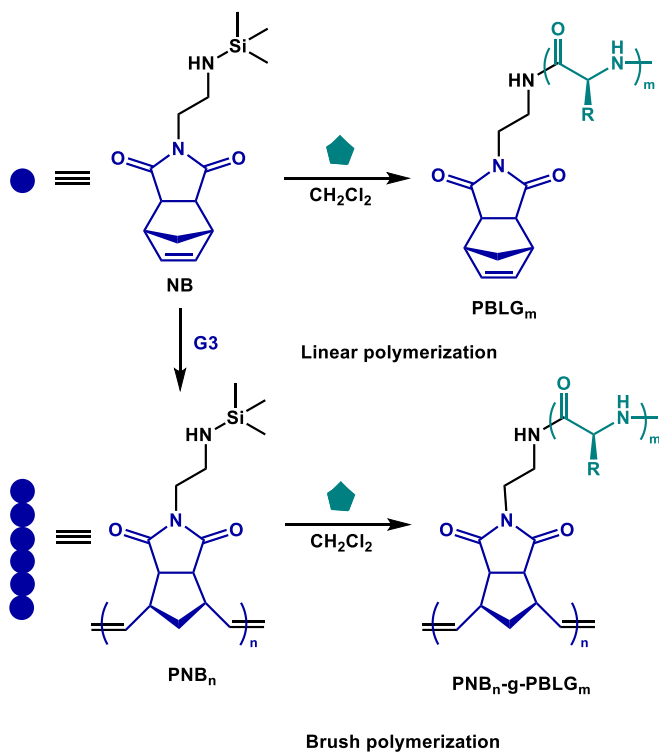
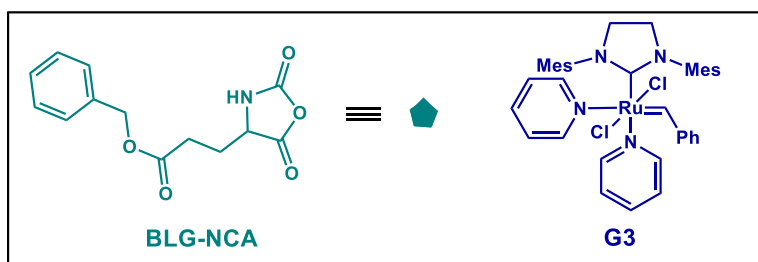
**Scheme 1.9** (a) Trimethylsilyl phenylsulfide (PhS-TMS) mediated N-carboxyanhydride (NCA) polymerization and (b) Synthesis of trimethyl stannyl phenyl sulfide (PhS-SnMe<sub>3</sub>) and PhS-SnMe<sub>3</sub> mediated NCA polymerization.

Besides regulating the chain propagation species in NCA ROP utilizing a single Lewis acid agent, the NCA ROP mediated by novel Lewis pairs was investigated. In 2018, Lu and co-workers developed a new initiation system relying on a sulfur-stannum Lewis pair, trimethyl stannyl phenyl sulfide (PhS-SnMe<sub>3</sub>) (Scheme 1.9 b).<sup>67</sup> This Lewis pair can withstand exposure to air but is more easily cleaved than the reported PhS-TMS previously examined by the same group. The

kinetics of this polymerization system exhibited solvent-dependent features. In DMF, the ROP of Z lysine NCA exhibited two stage-character: a great proportion of the monomer was consumed rapidly in the first stage (67% in 7 min) while a slower polymerization rate with chain termination was observed in the second stage. The polymerizations were also conducted in THF, a solvent of lower polarity that may likely stabilize the S–Sn bond. A first-order kinetic character with respect to monomer concentration was obtained while the polymerization rate was significantly slower. Based on these observations, a cosolvent mixture of DMF and THF was applied to afford linear polypeptides of varying molecular weights, some as high as 150 kg/mol. Notably, the polymerization speed was 4 times faster than the similar PhS-TMS system where the polymerization was completed within a few hours. The fast polymerization was attributed to the S–Sn Lewis pair that resulted in a more reactive trimethylstannyl group during the propagation.

Accelerated NCA polymerization was explored depending on the helical secondary structures of polypeptides as well. Covalent cooperative polymerization (CCP) of NCAs in solvents with low dielectric constants was developed by Cheng, Lin, and co-workers.<sup>57, 58</sup> Unlike the polymerization in traditional polar solvents like DMF or THF, the cooperative interactions of  $\alpha$ -helical macrodipoles in close proximity could facilitate the chain propagation process, leading to an accelerated ROP of NCA in solvents with low dielectric constants including dichloromethane, chloroform and 1,2-dichloroethane. In 2017, the CCP was first reported, where the trimethylsilyl (TMS) amine substituted *exo*-norbornene (NB) was used as the

monomer to prepare a linear polypeptide based on the BLG-NCA polymerization.<sup>57</sup> A macroinitiator (PNB) could also be synthesized from the ring-opening metathesis polymerization (ROMP) of functionalized NB monomer using ruthenium catalyst G3. Through the usage of PNB macroinitiator, the formation of brush polymers was enabled after the BLG-NCA polymerization (Scheme 1.10). Compared with the single-site initiator, the propagation rate of BLG-NCA polymerization in dichloromethane from the brushlike macroinitiator PNB was found to be more than 1000 times faster. The proximity-induced rate acceleration was further evidenced by polymerizing NCAs from macroinitiators with different initiator densities. A significant decrease of polymerization rate was observed with smaller density of initiating sites, even when the concentrations of initiators were maintained the same. In a following investigation, the same team reported such a cooperative effect even with simple diamino initiators.<sup>58</sup> The polymerization initiated by diamines proceeds via the formation of “hinged” polypeptides, which are two blocks of helical chains connected head-to-head by the diamine molecules in the polymerization solution (Figure 1.2). Faster polymerization was observed with shorter alkyl length between the primary amine initiating sites, which further validated the relationship between polymerization rates and distances of macrodipoles. Noteworthy, the chain propagation rate of the NCA polymerization was increased by more than 600 times when initiated by 1,6-diaminohexane in helicogenic solvents compared to that of the NCA polymerization initiated by its linear analogue (hexylamine).



**Scheme 1.10** Polymerization of BLG-NCA initiated by *exo*-norbornene (NB) forms linear polypeptides (PBLG<sub>m</sub>). Ring-opening metathesis polymerization (ROMP) of NB with ruthenium catalyst G3 forms PNB<sub>n</sub> that can act as macroinitiators for the polymerization of BLG-NCA forming brush polymers. The resulting polypeptide chains spontaneously fold into  $\alpha$ -helices after obtaining a degree of polymerization (DP) between 8 and 12.

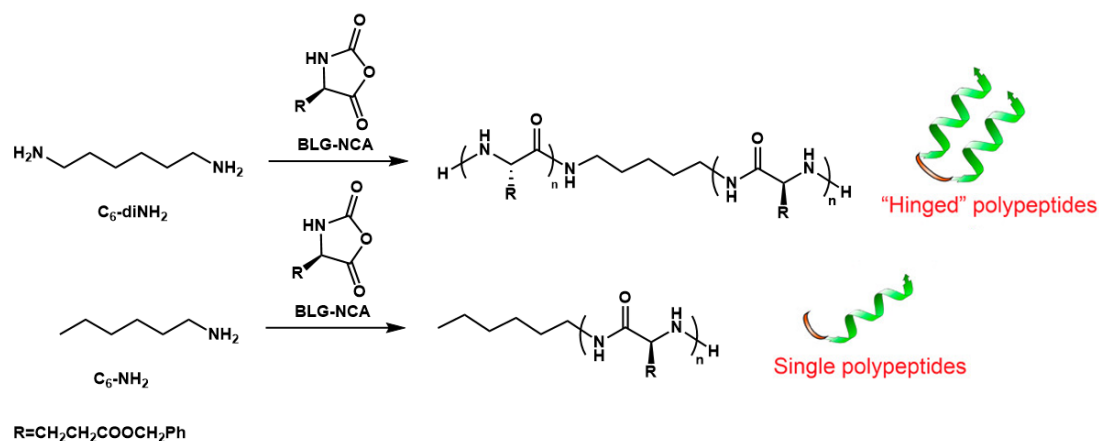
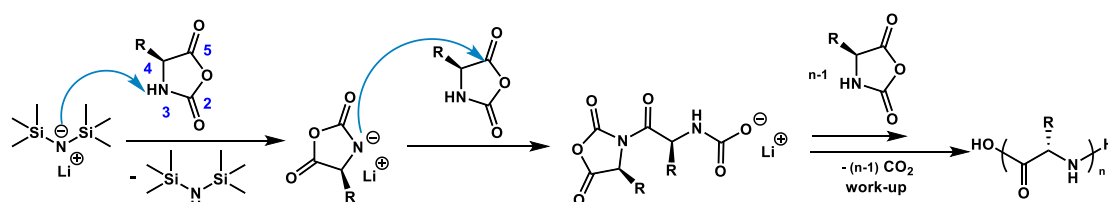


**Figure 1.2** Synthesis and schematic representation of a “hinged” polypeptide obtained from BLG-NCA polymerization initiated by 1,6-diaminohexane compared with a single polypeptide resulted from hexylamine-initiated polymerization. Adapted with permission from *J. Am. Chem. Soc.*, **2019**, *141*(22), 8680. Copyright 2019 American Chemical Society.

### 1.3.3 Recent efforts towards the development of moisture-tolerant controlled NCA polymerization

Although extensive efforts have been spent towards the enhancement of NCA polymerization rates, these reactions still need to be carefully carried out using strict anhydrous chemicals (such as purified NCAs, catalysts and solvents) or setups (such as glovebox and Schlenk line). The fear of moisture has been a great challenge for NCA polymerizations until recent progress on fast and moisture-insensitive NCA polymerizations using lithium/sodium/potassium hexamethyldisilazide as the initiator,<sup>73,74</sup> using primary amine as the initiator in biphasic system<sup>75,76</sup> or aqueous polymerization process.<sup>77</sup> Herein, a brief overview about these moisture-tolerant polymerizations systems is described in this section.

In 2018, Liu and co-workers developed a superfast polymerization of NCA using lithium hexamethyldisilazide (LiHMDS) as the initiator.<sup>73</sup> The proposed mechanism for this novel NCA polymerization is depicted in Scheme 1.11. As a non-nucleophilic base, LiHMDS deprotonates the NH-3 position of the NCA in a similar manner to other strong bases. Instead of deprotonation of another NCA monomer as it is typical for AMM, however, the N-terminal lithium carbamate will attack 5-C=O due to its weak basicity. Much faster polymerization was observed ( $\leq 15$  min), especially with high  $[M]_0/[I]_0$  ratios for the synthesis of high-MW well-controlled polypeptides. In addition, the authors demonstrated the feasibility of open vessel polymerization of NCAs with the LiHMDS system in untreated THF at 60% relative humidity. This work highlights the importance of accelerated NCA polymerizations, which downplays the requirements for strict anhydrous conditions. More importantly, this work leads to the envision that the fast polymerization might outpace water-induced side reactions and minimize the generation of undesired contaminants, enabling the polymerization in the presence of moisture and even aqueous phase.



**Scheme 1.11** Mechanism for NCA polymerization initiated by lithium hexamethyldisilazide (LiHMDS) where controlled insertion of NCA monomer is enabled by the nucleophilic attack of N-terminal lithium carbamate due to its weak basicity.

Biphasic system has been applied to the primary amine-initiated NCA polymerization to not only accelerates the polymerization rate but also makes the reaction water-insensitive. Emulsions are normally used for the polymerizations of monomers with initiators that are not miscible in the same solvent. Typically, it is carried out by emulsification of two immiscible phases such as dichloromethane and water, followed by the addition of initiator to the bulk phase. The high surface area of an emulsion allows for high reaction rates with the removal of waste products enabled by the amphiphilic environment.<sup>78,79</sup> In 2019, Cheng and co-workers employed a water-in-oil emulsion to the NCA polymerization for the first time.<sup>75</sup> In this work, methoxy poly(ethylene glycol)-block-poly( $\gamma$ -benzyl-L-glutamate) amine (PEG-PBLG; PEG=5 kg/mol, PBLG=9.8 kg/mol), an amphiphilic diblock copolymer bearing an amino terminus, was used as the macroinitiator for NCA polymerization in a water/dichloromethane biphasic system. Owing to the hydrophilicity, the PEG segments containing the terminal free amine groups tended to localize at the interface of the two phases. On the other hand, the hydrophobic PBLG block with  $\alpha$ -helical secondary structure thermodynamically favored positioning at the interface of the emulsion and dispersed in the bulk of the dichloromethane phase. The usage of interfacially anchored and closely packed  $\alpha$ -helical macroinitiator afforded a well-controlled PBLG extension and exhibited remarkable kinetics—the polymerization rate was enhanced 100-fold compared to conventional BLG-NCA polymerization in dichloromethane. The acceleration of polymerization rate was attributed to the  $\alpha$ -helicity of the macroinitiator and the increased surface area of the emulsion.

Importantly, the ultrafast polymerization kinetics can outpace water-induced side reactions, allowing the preparation of well-defined polypeptides even in the presence of water. In addition, acidic impurities present in crude NCA monomers could be eliminated in situ as these partition towards the aqueous phase. Owing to these benefits, this bioinspired polymerization strategy was further applied to successfully synthesize multiblock copolypeptides by the same group.<sup>76</sup> By using a water/chloroform biphasic system, narrowly dispersed ( $\mathcal{D} < 1.1$ ) copolypeptides with previously unattained high number of blocks (up to 20) and fast polymerization rates (on average <15 min/block) were obtained.

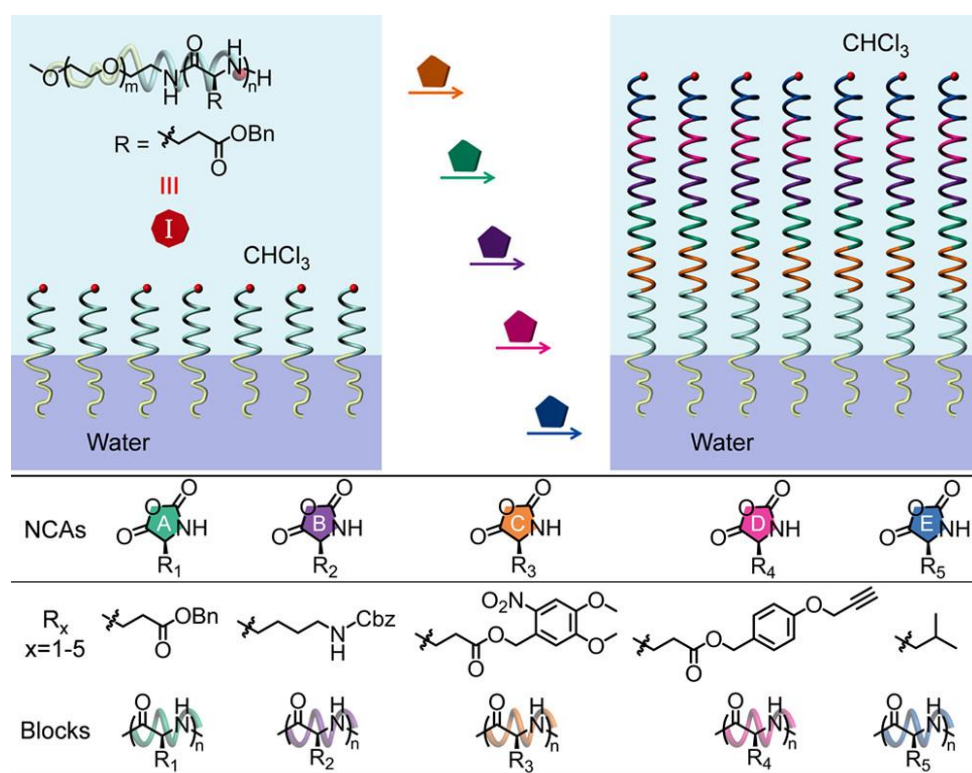
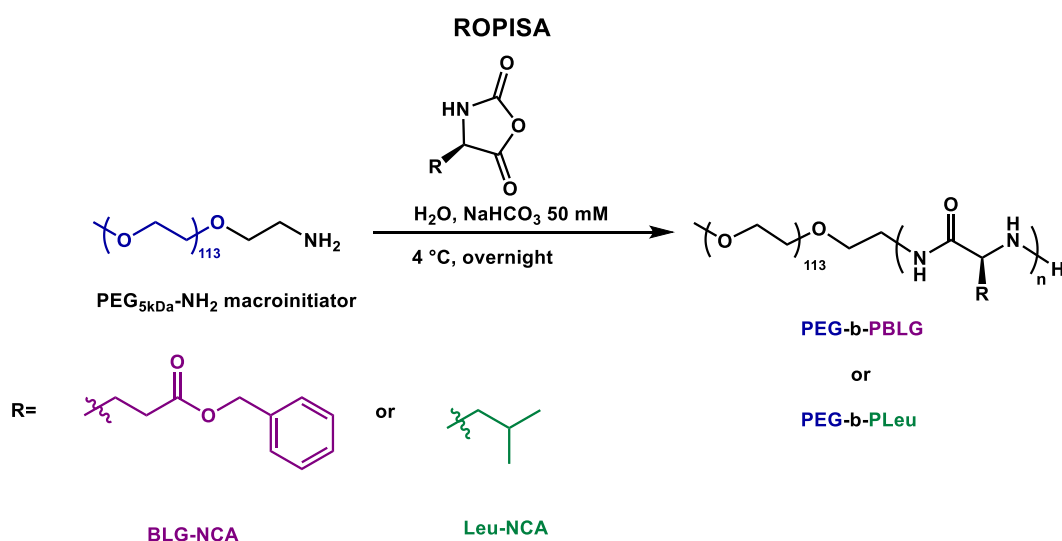


**Figure 1.3** The synthesis of multiblock copolypeptides via accelerated polymerizations of N-carboxyanhydrides (NCAs) in a water/chloroform biphasic system. Reprinted with permission from *ACS Macro Lett.* **2019**, 8, 11, 1517–1521.

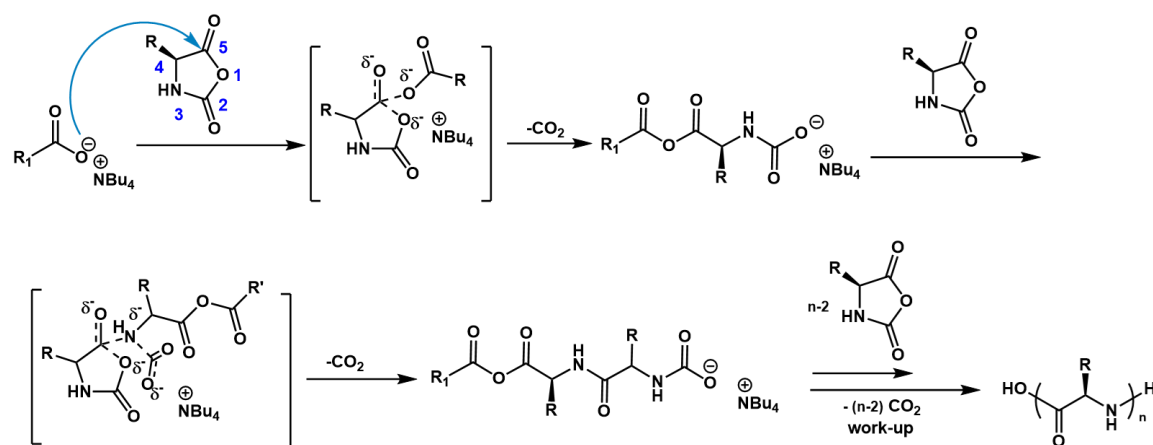
Copyright 2019 American Chemical Society.

Another water-tolerant NCA ROP method relies on the polymerization induced self-assembly (PISA). PISA, particularly mediated by RAFT polymerization, has been extensively studied and can be carried out in emulsion or dispersion.<sup>80,81</sup> In PISA processes, the solid content, length of the macro-initiating block and degree of polymerization are important factors which impact the morphology of attainable particles.<sup>82</sup> In 2020, Lecommandoux, Bonduelle and co-workers reports an aqueous ring-opening polymerization induced self-assembly (ROPISA) of NCA system.<sup>77</sup> A hydrophilic  $\alpha$ -amino-poly(ethylene oxide) was utilized as the macroinitiator for the polymerization of BLG-NCA or L-leucine NCA (Leu-NCA) in an aqueous sodium bicarbonate buffer (pH 8.5) at 4 °C, affording well-defined amphiphilic diblock copolymers that could simultaneously form needle-like nanoparticles (Scheme 1.12). The protection of the NCA monomers from hydrolysis in the presence of water was enabled through the spontaneous in-situ self-assembly.



**Scheme 1.12** Ring-opening polymerization and in situ self-assembly (ROPISA) in water of BLG-NCA and Leu-NCA monomer by initiated by a  $\alpha$ -amino-poly(ethylene oxide) (PEG).

Very recently, Liu and co-workers developed a superfast NCA polymerization using tetraalkylammonium carboxylate as a new class of initiator.<sup>83</sup> Mechanistic studies indicate that carboxylate initiates NCA polymerization by nucleophilic addition to the 5-C=O on the NCA ring and propagates in a concerted manner using the terminal tetraalkylammonium carbamate as the reactive center (Scheme 1.13). The superfast polymerization rate was attributed to the difference of this propagation center, compared with that of primary amine which requires hydrogen transfer to release CO<sub>2</sub> over an extra decarboxylation step. In addition, the bulky tetraalkylammonium cations was proposed to not only increase the solubility of the carboxylates to facilitate the polymerization,<sup>84</sup> but also stabilize the usually unstable carbamate anion.<sup>85</sup> Overall, this polymerization is insensitive to water and can proceed in open vessels at ambient condition to provide homo- or block polypeptides (15 blocks) with variable lengths and narrow molecular weight distributions. Tedious purification steps for NCAs can be avoided when aqueous environment is applied to achieve the one-pot synthesis of polypeptide nanoparticles.



**Scheme 1.13** Mechanism for the superfast N-carboxyanhydride (NCA) polymerization initiated by tetraalkylammonium carboxylate.

Although a variety of achievements have been demonstrated for the generations of well-defined polypeptide-based materials eliminating side reactions and requirement for anhydrous conditions, some drawbacks still remain. Compared with the natural polypeptides, the greatest limitation for the synthetic polypeptides that are accessible from NCA polymerization method, is their significantly simplified sequence. Since the repetitive additions of NCA monomers could accumulate impurities, chain propagation would be inhibited, and more significant side reactions might occur. Even with the usage of recently developed ultrafast controlled NCA ROP strategies to outpace side reactions, careful conditions are required. more importantly, the number of different NCAs incorporated into the backbones of the resulting block polypeptides is less than five.<sup>76,86,87</sup> The composition of the polypeptides is mainly limited to BLG-based amino acids, which might limit the potential applications for these biomacromolecules.<sup>58,76, 77,83</sup>

Besides the limit of sophisticated polymer sequences that are accessible from controlled NCA ROPs, other drawbacks also exist. For example, the relatively unstable NCAs are prone to ring openings in the presence of water, making it crucial to work under anhydrous conditions. Another issue is the synthesis of the NCA monomer itself. To date, the most common method for preparing NCAs involves phosgene or its derivatives, but the high toxicity and legal restrictions on their usage poses significant safety regulation issues. Rigorous purifications are required in order to remove any formed byproducts that will inhibit or shut down the most of NCA polymerizations. Therefore, a mild, facile and safe process for synthesizing a wide

range of NCAs with high purities in good yields based on green reagents is also needed.

#### 1.4 Synthesis of polypeptide-based materials using integrated catalysis

Owing to the limitations of existing methods for polypeptides synthesis, an efficient, mild, easy-to-use strategy to expand the monomer scopes for producing sequence-defined polypeptide-based materials of high molecular weights on a large-scale is in demand. To achieve that, the concept of integrated catalysis was introduced to allow the synthesis of sequence-defined polymeric materials from pools of abundant feedstocks in a single reactor with spatiotemporal control (Figure 1.4).

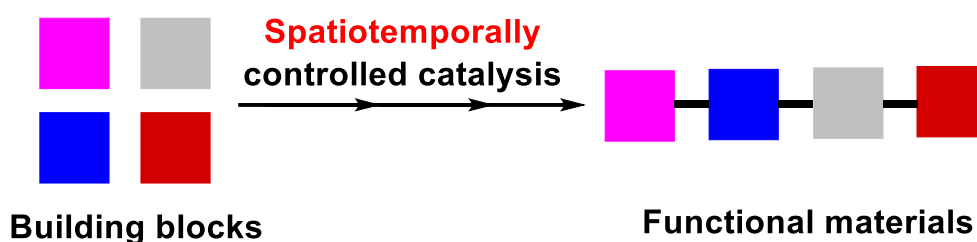


**Figure 1.4** General scheme for integrated catalysis to access sequence-defined polymeric materials.

Specifically, the polyamides are proposed to be generated directly from unprotected amino acids by coupling two reactions for the synthesis and in-situ polymerization of NCAs. In our integrated catalysis design, the first catalysis aims to utilize natural feedstocks  $\text{CO}_2$  and unprotected amino acids for synthesis of NCAs. The second catalysis then allows the polymerizations of in-situ formed NCAs directly without their isolation, which in turn, will release  $\text{CO}_2$  to be utilized in a second round of NCA synthesis. This integrated catalysis strategy can be used to target with high

level of complexity synthesis with the aid of spatially separated and switchable catalysts to overcome incompatibilities that normally occur during multiple catalytic cycles.

Switchable catalysis can allow the in-situ generation of different products by switching the reactivities towards different reactions in response to an applied stimulus (such as light, mechanical force, redox, pH etc.) Among the many possible external stimuli, redox chemistry is an efficient tool for development of redox-switchable ROP to access sophisticated polymer microstructures by altering catalyst oxidation state. Common strategies include introducing redox active moieties (e.g. ferrocene) in ligand frameworks<sup>88</sup> or using redox-active elements to serve as the sites for catalysis.<sup>89-92</sup> The Byers group has been investigating a redox-switchable polymerization system based on iron alkoxide complexes containing bis(imino)pyridine ligands.<sup>90,92-94</sup> The oxidation states of iron centers in these complexes was found to determine the orthogonal polymerization activity towards different monomer. For instance, iron (II) complex **1.1** and iron (III) complex **1.2** can toggle between catalyzing the ROP of lactide and epoxide when either redox reagents<sup>92</sup> or electrochemical potentials<sup>95</sup> are applied (Figure 1.5). Such a unique selectivity offers the opportunity for the synthesis of block copolymers<sup>92</sup>, cross-linked polymer networks<sup>96</sup>, and polymer-modified surface patterns<sup>97</sup>.

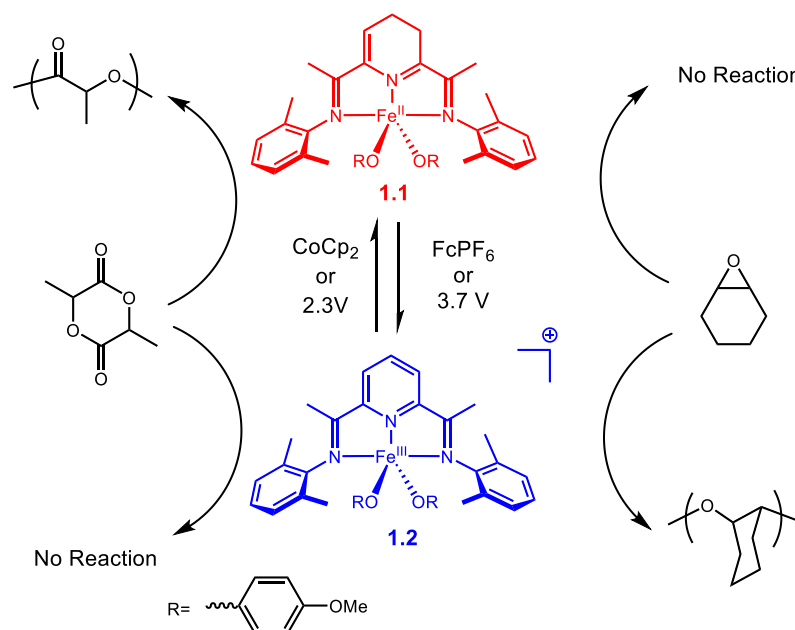


**Figure 1.5** Iron-based catalysts for the redox-switchable polymerization of lactide and epoxide: Fe(II) is active towards lactide polymerization while the oxidized Fe(III) can initiate the epoxide polymerization only. Recreated from ref. 92.

Using these kind of redox-switchable catalysts, temporal control of polymerization can be enabled by tuning the oxidation states of iron centers with redox reagents or electrochemical potentials. In parallel, spatial control can be achieved by anchoring polymerization catalysts on surfaces, which can separate different catalysts from each other. To mitigate potential mass transport limitations for heterogeneous surface reactions, the integrated catalysis will be carried out ideally by the application of continuous flow. Temporal control can also be demonstrated by flowing in and out different required reagents at desired time for different catalysis. Overall, the incorporation of NCAs can be achieved in a timely manner with the spatiotemporal control (Figure 1.6). In this design, unprotected amino acids and  $\text{CO}_2$  can be coupled catalytically to form the NCAs. Accumulation of waste or acidic

impurities can be avoided by using the natural abundant CO<sub>2</sub> and unprotected amino acids. In a following step, the supported redox-switchable polymerization catalyst will be activated through electrochemical method to directly polymerize the in-situ formed NCAs, which will avoid their facile decomposition and the necessity for future purifications. The polyamide chain will keep growing until achieving the desirable length with the concomitant release of CO<sub>2</sub>. To eliminate any incompatibility issues or side reactions, the polymerization catalyst will then be deactivated allowing the NCA synthesis to proceed individually with the recycled CO<sub>2</sub> in the single reactor. NCA polymerization catalyst can be activated again through the electrochemical method once a second kind of NCAs is formed. Polymerization of the in-situ formed NCAs will result in chain extensions from the active polymer chain ends and thus, incorporate different polypeptide compositions. After iterative steps, sequence-defined polyamides with sophisticated compositions can be obtained upon their removal from the surface. Noteworthy, this goal has not been achieved yet. All the research described in this thesis is designed to reach this ultimate goal.

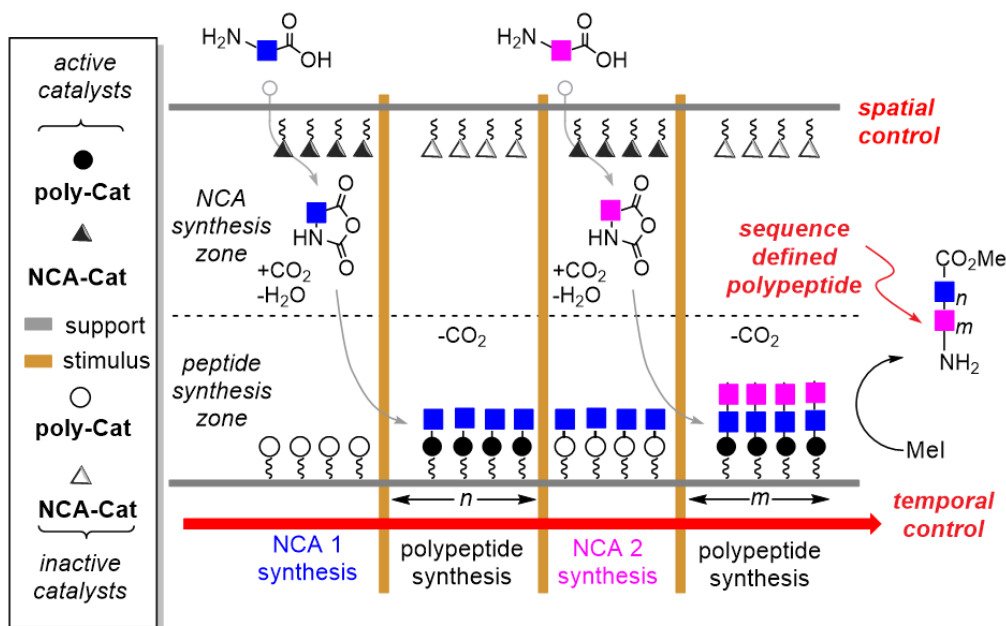


**Figure 1.6** Design of integrated catalysis system for synthesis of sequence-defined polypeptides. The system is composed of two separate catalysis reactions: synthesis of NCAs from amino acids and  $\text{CO}_2$  and polymerizations of in-situ formed NCAs with the release of  $\text{CO}_2$ .

## 1.5 Conclusions

There has been a significant long history for people to develop and improve synthetic methods in to efficiently obtain polypeptide-based materials with controlled sequences, sophisticated microstructures, high molecular weights, and narrow dispersity. Current existing methods for generating polypeptides all have their own advantages and limitations. Recombinant techniques for expressing peptides in microorganisms are scalable and yield high molecular weight, sequence-defined polypeptides but require specialized equipment that is not readily available in most synthetic laboratories, in addition to being time and cost-intensive. SPPS is a powerful routine technique that allows the automated synthesis of relatively complex sequences

through convenient isolation and purifications steps, yet the length of polypeptide is typically limited to 100 amino acids with generation of significant amount of chemical waste. On the other hand, NCA polymerization is a highly versatile technique for the preparation of higher molecular weight synthetic polypeptides on a multigram scale, but it lacks the ability to synthesize specific sequences and requires extended reaction time and careful operations.

We sought to fill this gap by developing an alternative and mild approach that allows the generation of sequence-defined polypeptides on a large scale. To achieve that goal, integrated catalysis will be applied by synthesis of NCAs from natural abundant unprotected amino acids and CO<sub>2</sub> followed by their polymerizations in situ. Spatial and temporal control will be employed to resolve any potential incompatibility issues between the two separate catalysis. In the following chapters, efforts towards developing a surface-initiated redox switchable NCA polymerization system will be demonstrated to allow for the spatiotemporal control of NCA polymerization needed for the integrated catalysis system described above. Additional efforts towards integrated catalysis from amino acids to polypeptide will be discussed, including different methods for anchoring catalysts on the surface and compatibility tests for reaction conditions of current NCA methodology and NCA polymerization.

## References

- (1) Dobson, C. M. Protein Folding and Misfolding. *Nature* **2003**, *426*, 884–890. DOI:10.1038/nature02261.
- (2) Lutz, J. F.; Börner, H. G. Modern Trends in Polymer Bioconjugates Design. *Prog. Polym. Sci.* **2008**, *33* (1), 1–39. DOI: 10.1016/J.PROGPOLYMSCI.2007.07.005.
- (3) Maji, S. K.; Perrin, M. H.; Sawaya, M. R.; Jessberger, S.; Vadodaria, K.; Rissman, R. A.; Singru, P. S.; Nilsson, K. P. R.; Simon, R.; Schubert, D.; Eisenberg, D.; Rivier, J.; Sawchenko, P.; Vale, W.; Riek, R. Functional Amyloids as Natural Storage of Peptide Hormones in Pituitary Secretory Granules. *Science*, **2009**, *325* (5938), 328–332. DOI: 10.1126/science.1173155.
- (4) Gomes, S.; Leonor, I. B.; Mano, J. F.; Reis, R. L.; Kaplan, D. L. Natural and Genetically Engineered Proteins for Tissue Engineering. *Prog. Polym. Sci.* **2012**, *37* (1), 1–17. DOI: 10.1016/j.progpolymsci.2011.07.003.
- (5) Deming, T. J. Synthetic Polypeptides for Biomedical Applications. *Prog. Polym. Sci.* **2007**, *32* (8–9), 858–875. DOI: 10.1016/j.progpolymsci.2007.05.010.
- (6) Lu, H.; Wang, J.; Song, Z.; Yin, L.; Zhang, Y.; Tang, H.; Tu, C.; Lin, Y.; Cheng, J. Recent Advances in Amino Acid N-Carboxyanhydrides and Synthetic Polypeptides: Chemistry, Self-Assembly and Biological Applications. *Chem. Commun.* **2013**, *50* (2), 139–155. DOI:10.1039/C3CC46317F.
- (7) Rad-Malekshahi, M.; Lempsink, L.; Amidi, M.; Hennink, W. E.; Mastrobattista,

- E. Biomedical Applications of Self-Assembling Peptides. *Bioconjug. Chem.* **2016**, *27* (1), 3–18. DOI: 10.1021/acs.bioconjchem.5b00487.
- (8) Ge, C.; Liu, S.; Liang, C.; Ling, Y.; Tang, H. Synthesis and UCST-Type Phase Behavior of  $\alpha$ -Helical Polypeptides with Y-Shaped and Imidazolium Pendants. *Polym. Chem.* **2016**, *7* (38), 5978–5987. DOI: 10.1039/C6PY01287F.
- (9) Whitesides, G. M.; Grzybowski, B. Self-Assembly at All Scales. *Science*, **2002**, *295* (5564), 2418–2421. DOI: 10.1126/science.1070821.
- (10) Jones, R. Why Nanotechnology Needs Better Polymer Chemistry. *Nat. Nanotechnol.* **2008**, *3* (12), 699–700. DOI: 10.1038/nnano.2008.349.
- (11) van Hest, J. C. M.; Tirrell, D. A. Protein-Based Materials, toward a New Level of Structural Control. *Chem. Commun.* **2001**, *19* (19), 1897–1904. DOI: 10.1039/B105185G.
- (12) Merrifield, R. B. Solid Phase Peptide Synthesis. I. The Synthesis of a Tetrapeptide. *J. Am. Chem. Soc.* **1963**, *85* (14), 2149–2154. DOI: 10.1021/ja00897a025.
- (13) Hadjichristidis, N.; Iatrou, H.; Pitsikalis, M.; Sakellariou, G. Synthesis of Well-Defined Polypeptide-Based Materials via the Ring-Opening Polymerization of  $\alpha$ -Amino Acid N-Carboxyanhydrides. *Chem. Rev.* **2009**, *109* (11), 5528–5578. DOI: 10.1021/CR900049T.
- (14) Kricheldorf, H. R.; Kricheldorf, H. R. Polypeptides and 100 Years of Chemistry of  $\alpha$ -Amino Acid N-Carboxyanhydrides. *Angew. Chemie Int. Ed.* **2006**, *45* (35), 5752–5784. DOI: 10.1002/ANIE.200600693.

- (15) Merrifield, R. B.; Merrifield, [ R B. Solid Phase Synthesis (Nobel Lecture). *Angew. Chemie Int. Ed. English* **1985**, *24* (10), 799–810. DOI:10.1002/ANIE.198507993.
- (16) SCHNölzer, M.; ALEWOOD, P.; JONES, A.; ALEWOOD, D.; KENT, S. B. H. In Situ Neutralization in Boc-Chemistry Solid Phase Peptide Synthesis. *Int. J. Pept. Protein Res.* **1992**, *40* (3–4), 180–193. DOI: 10.1111/J.1399-3011.1992.TB00291.X.
- (17) Carpino, L. A.; Han, G. Y. 9-Fluorenylmethoxycarbonyl Function, a New Base-Sensitive Amino-Protecting Group. *J. Am. Chem. Soc.* **1970**, *92* (19), 5748–5749. DOI: 10.1021/JA00722A043.
- (18) Behrendt, R.; White, P.; Offer, J. Advances in Fmoc Solid-Phase Peptide Synthesis. *J. Pept. Sci.* **2016**, *22* (1), 4–27. DOI: 10.1002/PSC.2836.
- (19) Klok, H. A. Peptide/Protein-Synthetic Polymer Conjugates: Quo Vadis. *Macromolecules* **2009**, *42* (21), 7990–8000. DOI: 10.1021/ma901561t.
- (20) Cavalli, S.; Albericio, F.; Kros, A. Amphiphilic Peptides and Their Cross-Disciplinary Role as Building Blocks for Nanoscience. *Chem. Soc. Rev.* **2009**, *39* (1), 241–263. DOI:10.1039/B906701A.
- (21) Bacsa, B.; Horváti, K.; Bősze, S.; Andrae, F.; Kappe, C. O. Solid-Phase Synthesis of Difficult Peptide Sequences at Elevated Temperatures: A Critical Comparison of Microwave and Conventional Heating Technologies. *J. Org. Chem.* **2008**, *73* (19), 7532–7542. DOI: 10.1021/jo8013897.
- (22) Aqueous cross-coupling Qi, P.; Sheldon, R. A. The E Factor: Fifteen Years On.

- Green Chem.* **2007**, *9* (12), 1273–1283. DOI:10.1039/B713736M.
- (23) Pattabiraman, V. R.; Bode, J. W. Rethinking Amide Bond Synthesis. *Nature*, **2011**, *480* (7378), 471–479. DOI: 10.1038/nature10702.
- (24) Bryan, M. C.; Dunn, P. J.; Entwistle, D.; Gallou, F.; Koenig, S. G.; Hayler, J. D.; Hickey, M. R.; Hughes, S.; Kopach, M. E.; Moine, G.; Richardson, P.; Roschangar, F.; Steven, A.; Weiberth, F. J. Key Green Chemistry Research Areas from a Pharmaceutical Manufacturers' Perspective Revisited. *Green Chem.* **2018**, *20* (22), 5082–5103. DOI: 10.1039/C8GC01276H.
- (25) Cheng, J.; Deming, T. J. Synthesis of Polypeptides by Ring-Opening Polymerization of  $\alpha$ -Amino Acid -Carboxyanhydrides. *Top. Curr. Chem.* **2011**, *310*, 1–26. DOI: 10.1007/128\_2011\_173.
- (26) Leuchs, H. Ueber Die Glycin-Carbonsäure. *Berichte der Dtsch. Chem. Gesellschaft* **1906**, *39* (1), 857–861. DOI: 10.1002/CBER.190603901133.
- (27) Leuchs, H.; Manasse, W. Über Die Isomerie Der Carbäthoxyl-Glycyl Glycinester. *Berichte der Dtsch. Chem. Gesellschaft* **1907**, *40* (3), 3235–3249. DOI: 10.1002/CBER.19070400387.
- (28) Leuchs, H.; Geiger, W. Über Die Anhydride von  $\alpha$ -Amino-N-Carbonsäuren Und Die von  $\alpha$ -Aminosäuren. *Berichte der Dtsch. Chem. Gesellschaft* **1908**, *41* (2), 1721–1726. DOI: 10.1002/CBER.19080410232.
- (29) Fuchs, F. Über N-Carbonsäure-Anhydride. *Berichte der Dtsch. Chem. Gesellschaft (A B Ser.)* **1922**, *55* (9), 2943–2943. DOI: 10.1002/CBER.19220550902.

- (30) Farthing, A. C.; Reynolds, R. J. W. Anhydro-N-Carboxy-DL- $\beta$ -Phenylalanine. *Nature*, **1950**, *165* (4199), 647–647. DOI:10.1038/165647a0.
- (31) Wilder, R.; Mobashery, S. The Use of Triphosgene in Preparation of N-Carboxy .Alpha.-Amino Acid Anhydrides. *J. Org. Chem.* **2002**, *57* (9), 2755–2756. DOI: 10.1021/JO00035A044.
- (32) Katakai, R.; Iizuka, Y. An Improved Rapid Method for the Synthesis of N-Carboxy .Alpha.-Amino Acid Anhydrides Using Trichloromethyl Chloroformate. *J. Org. Chem.* **2002**, *50* (5), 715–716. DOI: 10.1021/JO00205A039.
- (33) Nagai, A.; Sato, D.; Ishikawa, J.; Ochiai, B.; Kudo, H.; Endo, T. A Facile Synthesis of N-Carboxyanhydrides and Poly( $\alpha$ -Amino Acid) Using Di-Tert-Butyltricarboxylate. *Macromolecules* **2004**, *37* (7), 2332–2334. DOI: 10.1021/ma0498464.
- (34) Iwakuha, Y.; Uno, K.; Kang, S. The Synthesis and Reactions of 2-Isocyanatoacyl Chlorides. *J. Org. Chem.* **2002**, *30* (4), 1158–1161. DOI: 10.1021/JO01015A049.
- (35) Fuller, W. D.; Verlander, M. S.; Goodman, M. A Procedure for the Facile Synthesis of Amino-Acid N-Carboxyanhydrides. *Biopolymers* **1976**, *15* (9), 1869–1871. DOI: 10.1002/BIP.1976.360150922.
- (36) Kramer, J. R.; Deming, T. J. General Method for Purification of  $\alpha$ -Amino Acid-N-Carboxyanhydrides Using Flash Chromatography. *Biomacromolecules* **2010**, *11* (12), 3668–3672. DOI: 10.1021/bm101123k.

- (37) Habraken, G. J. M.; Peeters, M.; Dietz, C. H. J. T.; Koning, C. E.; Heise, A. How Controlled and Versatile Is N-Carboxy Anhydride (NCA) Polymerization at 0 °C? Effect of Temperature on Homo-, Block- and Graft (Co)Polymerization. *Polym. Chem.* **2010**, *1* (4), 514–524. DOI: 10.1039/B9PY00337A.
- (38) Kricheldorf, H. R.; Lossow, C. V.; Schwarz, G. Primary Amine and Solvent-Induced Polymerizations of L- or D,L-Phenylalanine N-Carboxyanhydride. *Macromol. Chem. Phys.* **2005**, *206* (2), 282–290. DOI: 10.1002/MACP.200400417.
- (39) Kricheldorf, H. R.; Von Lossow, C.; Schwarz, G. Cyclic Polypeptides by Solvent-Induced Polymerizations of  $\alpha$ -Amino Acid N-Carboxyanhydrides. *Macromolecules* **2005**, *38* (13), 5513–5518. DOI: 10.1021/MA0401368.
- (40) Dimitrov, I.; Kukula, H.; Cölfen, H.; Schlaad, H. Advances in the Synthesis and Characterization of Polypeptide-Based Hybrid Block Copolymers. *Macromol. Symp.* **2004**, *215* (1), 383–393. DOI: 10.1002/MASY.200451129.
- (41) Barz, M.; Luxenhofer, R.; Zentel, R.; Vicent, M. J. Overcoming the PEG-Addiction: Well-Defined Alternatives to PEG, from Structure–Property Relationships to Better Defined Therapeutics. *Polym. Chem.* **2011**, *2* (9), 1900–1918. DOI: 10.1039/C0PY00406E.
- (42) Thunig, D.; Semen, J.; Elias, H.-G. Carbon Dioxide Influence on NCA Polymerizations. *Die Makromol. Chemie* **1977**, *178* (2), 603–607. DOI: 10.1002/MACP.1977.021780229.

- (43) Goodman, M.; Hutchison, J. Propagation Mechanism in Strong Base Initiated Polymerization of  $\alpha$ -Amino Acid N-Carboxyanhydrides. *J. Am. Chem. Soc.* **1965**, *87* (15), 3524–3525. DOI: 10.1021/ja01093a056.
- (44) Rinaudo, M.; Domard, A. Kinetics of  $\gamma$ -Benzyl-L-Glutamate NCA's Polymerizations and Molecular-Weight Distributions on Corresponding Polymers. *Biopolymers* **1976**, *15* (11), 2185–2199. DOI: 10.1002/BIP.1976.360151107.
- (45) Deming, T. J. Facile Synthesis of Block Copolypeptides of Defined Architecture. *Nature*, **1997**, *390* (6658), 386–389. DOI: 10.1038/37084.
- (46) Deming, T. J. Cobalt and Iron Initiators for the Controlled Polymerization of  $\alpha$ -Amino Acid-N-Carboxyanhydrides. *Macromolecules* **1999**, *32* (13), 4500–4502. DOI: 10.1021/ma9902899.
- (47) Deming, T. J. Amino Acid Derived Nickelacycles: Intermediates in Nickel-Mediated Polypeptide Synthesis. *J. Am. Chem. Soc.* **1998**, *120* (17), 4240–4241. DOI: 10.1021/JA980313I.
- (48) Curtin, S. A.; Deming, T. J. Initiators for End-Group Functionalized Polypeptides via Tandem Addition Reactions. *J. Am. Chem. Soc.* **1999**, *121* (32), 7427–7428. DOI: 10.1021/ja990905g.
- (49) Deming, T. J.; Curtin, S. A. Chain Initiation Efficiency in Cobalt- and Nickel-Mediated Polypeptide Synthesis. *J. Am. Chem. Soc.* **2000**, *122* (24), 5710–5717. DOI:10.1021/JA994281Q.
- (50) Vayaboury, W.; Giani, O.; Cottet, H.; Deratani, A.; Schué, F. Living

- Polymerization of  $\alpha$ -Amino Acid N-Carboxyanhydrides (NCA) upon Decreasing the Reaction Temperature. *Macromol. Rapid Commun.* **2004**, *25* (13), 1221–1224. DOI: 10.1002/MARC.200400111.
- (51) Vayaboury, W.; Giani, O.; Cottet, H.; Bonaric, S.; Schué, F. Mechanistic Study of  $\alpha$ -Amino Acid N-Carboxyanhydride (NCA) Polymerization by Capillary Electrophoresis. *Macromol. Chem. Phys.* **2008**, *209* (15), 1628–1637. DOI: 10.1002/MACP.200800096.
- (52) Aliferis, T.; Iatrou, H.; Hadjichristidis, N. Living Polypeptides. *Biomacromolecules* **2004**, *5* (5), 1653–1656. DOI: 10.1021/BM0497217.
- (53) Pickel, D. L.; Politakos, N.; Avgeropoulos, A.; Messman, J. M. A Mechanistic Study of  $\alpha$ -(Amino Acid)-n-Carboxyanhydride Polymerization: Comparing Initiation and Termination Events in High-Vacuum and Traditional Polymerization Techniques. *Macromolecules* **2009**, *42* (20), 7781–7788. DOI: 10.1021/ma901340y.
- (54) Lu, H.; Cheng, J. Hexamethyldisilazane-Mediated Controlled Polymerization of  $\alpha$ -Amino Acid N-Carboxyanhydrides. *J. Am. Chem. Soc.* **2007**, *129* (46), 14114–14115. DOI: 10.1021/ja074961q.
- (55) Lu, H.; Cheng, J. N-Trimethylsilyl Amines for Controlled Ring-Opening Polymerization of Amino Acid N-Carboxyanhydrides and Facile End Group Functionalization of Polypeptides. *J. Am. Chem. Soc.* **2008**, *130* (38), 12562–12563. DOI: 10.1021/ja803304x.
- (56) Zou, J.; Fan, J.; He, X.; Zhang, S.; Wang, H.; Wooley, K. L. A Facile

- Glovebox-Free Strategy to Significantly Accelerate the Syntheses of Well-Defined Polypeptides by N -Carboxyanhydride (NCA) Ring-Opening Polymerizations. *Macromolecules* **2013**, *46* (10), 4223–4226. DOI: 10.1021/ma4007939.
- (57) Baumgartner, R.; Fu, H.; Song, Z.; Lin, Y.; Cheng, J. Cooperative Polymerization of  $\alpha$ -Helices Induced by Macromolecular Architecture. *Nat. Chem.* **2017**, *9* (7), 614–622. DOI: 10.1038/nchem.2712.
- (58) Chen, C.; Fu, H.; Baumgartner, R.; Song, Z.; Lin, Y.; Cheng, J. Proximity-Induced Cooperative Polymerization in “Hinged” Helical Polypeptides. *J. Am. Chem. Soc.* **2019**, *141* (22), 8680–8683. DOI: 10.1021/jacs.9b02298.
- (59) Zhao, W.; Gnanou, Y.; Hadjichristidis, N. From Competition to Cooperation: A Highly Efficient Strategy towards Well-Defined (Co)Polypeptides. *Chem. Commun.* **2015**, *51* (17), 3663–3666. DOI: 10.1039/C4CC09055A.
- (60) Zhao, W.; Gnanou, Y.; Hadjichristidis, N. Fast and Living Ring-Opening Polymerization of  $\alpha$ -Amino Acid N-Carboxyanhydrides Triggered by an “Alliance” of Primary and Secondary Amines at Room Temperature. *Biomacromolecules* **2015**, *16* (4), 1352–1357. DOI: 10.1021/acs.biomac.5b00134.
- (61) Yuan, J.; Sun, Y.; Wang, J.; Lu, H. Phenyl Trimethylsilyl Sulfide-Mediated Controlled Ring-Opening Polymerization of  $\alpha$ -Amino Acid N-Carboxyanhydrides. *Biomacromolecules* **2016**, *17* (3), 891–896. DOI: 10.1021/acs.biomac.5b01588.

- (62) Sun, Y.; Hou, Y.; Zhou, X.; Yuan, J.; Wang, J.; Lu, H. Controlled Synthesis and Enzyme-Induced Hydrogelation of Poly(L-Phosphotyrosine)s via Ring-Opening Polymerization of  $\alpha$ -Amino Acid N-Carboxyanhydride. *ACS Macro Lett.* **2015**, *4* (9), 1000–1003. DOI: 10.1021/acsmacrolett.5b00429.
- (63) Zhang, Y.; Liu, R.; Jin, H.; Song, W.; Augustine, R.; Kim, I. Straightforward Access to Linear and Cyclic Polypeptides. *Commun. Chem.* **2018**, *1* (1), 1–7. DOI: 10.1038/s42004-018-0040-0.
- (64) Zhao, W.; Lv, Y.; Li, J.; Feng, Z.; Ni, Y.; Hadjichristidis, N. Fast and Selective Organocatalytic Ring-Opening Polymerization by Fluorinated Alcohol without a Cocatalyst. *Nat. Commun.* **2019**, *10* (1), 1–11. DOI: 10.1038/s41467-019-11524-y.
- (65) Zhao, W.; Gnanou, Y.; Hadjichristidis, N. Organocatalysis by Hydrogen-Bonding: A New Approach to Controlled/Living Polymerization of  $\alpha$ -Amino Acid N-Carboxyanhydrides. *Polym. Chem.* **2015**, *6* (34), 6193–6201. DOI: 10.1039/C5PY00874C.
- (66) Zhang, H.; Nie, Y.; Zhi, X.; Du, H.; Yang, J. Controlled Ring-Opening Polymerization of  $\alpha$ -Amino Acid N-Carboxy-Anhydride by Frustrated Amine/Borane Lewis Pairs. *Chem. Commun.* **2017**, *53* (37), 5155–5158. DOI: 10.1039/C7CC01440F.
- (67) Yuan, J.; Zhang, Y.; Li, Z.; Wang, Y.; Lu, H. A S-Sn Lewis Pair-Mediated Ring-Opening Polymerization of  $\alpha$ -Amino Acid N-Carboxyanhydrides: Fast Kinetics, High Molecular Weight, and Facile Bioconjugation. *ACS Macro Lett.*

- 2018**, 7 (8), 892–897. DOI: 10.1021/acsmacrolett.8b00465.
- (68) Nie, Y.; Zhi, X.; Du, H.; Yang, J. Zn(OAc)<sub>2</sub>-Catalyzing Ring-Opening Polymerization of N-Carboxyanhydrides for the Synthesis of Well-Defined Polypeptides. *Molecules* **2018**, 23 (4), 760. DOI: 10.3390/molecules23040760.
- (69) Hao, W.; Lv, Y.; Ili, J.; Feng, Z.; Onghao Ni, Y.; Hadjichristidis, N. A Synthetic Method for Site-Specific Functionalized Polypeptides: Metal-Free, Highly Active, and Selective at Room Temperature. *Angew. Chemie* **2021**, 133 (2), 902–908. DOI: 10.1002/ANGE.202009316.
- (70) Xia, Y.; Song, Z.; Tan, Z.; Xue, T.; Wei, S.; Zhu, L.; Yang, Y.; Fu, H.; Jiang, Y.; Lin, Y.; Lu, Y.; Ferguson, A. L.; Cheng, J. Accelerated Polymerization of N-Carboxyanhydrides Catalyzed by Crown Ether. *Nat. Commun.* **2021**, 12 (1), 1–8. DOI: 10.1038/s41467-020-20724-w.
- (71) Yonezumi, M.; Takaku, R.; Kanaoka, S.; Aoshima, S. Living Cationic Polymerization of  $\alpha$ -Methyl Vinyl Ethers Using SnCl<sub>4</sub>. *J. Polym. Sci. Part A Polym. Chem.* **2008**, 46 (6), 2202–2211. DOI: 10.1002/POLA.22555.
- (72) Fantin, M.; Isse, A. A.; Venzo, A.; Gennaro, A.; Matyjaszewski, K. Atom Transfer Radical Polymerization of Methacrylic Acid: A Won Challenge. *J. Am. Chem. Soc.* **2016**, 138 (23), 7216–7219. DOI: 10.1021/jacs.6b01935.
- (73) Wu, Y.; Zhang, D.; Ma, P.; Zhou, R.; Hua, L.; Liu, R. Lithium Hexamethyldisilazide Initiated Superfast Ring Opening Polymerization of Alpha-Amino Acid N-Carboxyanhydrides. *Nat. Commun.* **2018**, 9 (1), 1–10. DOI: 10.1038/s41467-018-07711-y.

- (74) Wu, Y. M.; Zhang, W. W.; Zhou, R. Y.; Chen, Q.; Xie, C. Y.; Xiang, H. X.; Sun, B.; Zhu, M. F.; Liu, R. H. Facile Synthesis of High Molecular Weight Polypeptides via Fast and Moisture Insensitive Polymerization of  $\alpha$ -Amino Acid N-Carboxyanhydrides. *Chinese J. Polym. Sci.* **2020**, *38* (10), 1131–1140. DOI: 10.1007/S10118-020-2471-1.
- (75) Song, Z.; Fu, H.; Wang, J.; Hui, J.; Xue, T.; Pacheco, L. A.; Yan, H.; Baumgartner, R.; Wang, Z.; Xia, Y.; Wang, X.; Yin, L.; Chen, C.; Rodríguez-López, J.; Ferguson, A. L.; Lin, Y.; Cheng, J. Synthesis of Polypeptides via Bioinspired Polymerization of in Situ Purified N-Carboxyanhydrides. *Proc. Natl. Acad. Sci. U. S. A.* **2019**, *166* (22), 10658–10663. DOI: 10.1073/PNAS.1901442116.
- (76) Wang, X.; Song, Z.; Tan, Z.; Zhu, L.; Xue, T.; Lv, S.; Fu, Z.; Zheng, X.; Ren, J.; Cheng, J. Facile Synthesis of Helical Multiblock Copolypeptides: Minimal Side Reactions with Accelerated Polymerization of N-Carboxyanhydrides. *ACS Macro Lett.* **2019**, *8* (11), 1517–1521. DOI: 10.1021/acsmacrolett.9b00784.
- (77) Grazon, C.; Salas-Ambrosio, P.; Ibarboure, E.; Buol, A.; Garanger, E.; Grinstaff, M. W.; Lecommandoux, S.; Bonduelle, C. Aqueous Ring-Opening Polymerization-Induced Self-Assembly (ROPISA) of N-Carboxyanhydrides. *Angew. Chemie Int. Ed.* **2020**, *59* (2), 622–626. DOI: 10.1002/ANIE.201912028.
- (78) Lovell, P. A.; El-Aasser, M. Wiley: Emulsion Polymerization and Emulsion Polymers, Wiley, New York, **1997**.

- (79) Crespy, D.; Landfester, K. Miniemulsion Polymerization as a Versatile Tool for the Synthesis of Functionalized Polymers. *Beilstein J. Org. Chem.* **2010**, *6* (1), 1132–1148. DOI: 10.3762/BJOC.6.130.
- (80) Derry, M. J.; Fielding, L. A.; Armes, S. P. Polymerization-Induced Self-Assembly of Block Copolymer Nanoparticles via RAFT Non-Aqueous Dispersion Polymerization. *Prog. Polym. Sci.* **2016**, *52*, 1–18. DOI: 10.1016/J.PROGPOLYMSCI.2015.10.002.
- (81) Yeow, J.; Boyer, C.; Nanoparticles, P.; Yeow, J.; Boyer, C. Photoinitiated Polymerization-Induced Self-Assembly (Photo-PISA): New Insights and Opportunities. *Adv. Sci.* **2017**, *4* (7), 1700137. DOI: 10.1002/ADVS.201700137.
- (82) Charleux, B.; Delaittre, G.; Rieger, J.; D’Agosto, F. Polymerization-Induced Self-Assembly: From Soluble Macromolecules to Block Copolymer Nano-Objects in One Step. *Macromolecules* **2012**, *45* (17), 6753–6765. DOI: 10.1021/ma300713f.
- (83) Wu, Y.; Chen, K.; Wu, X.; Liu, L.; Zhang, W.; Ding, Y.; Liu, S.; Zhou, M.; Shao, N.; Ji, Z.; Chen, J.; Zhu, M.; Liu, R. Superfast and Water-Insensitive Polymerization on  $\alpha$ -Amino Acid N-Carboxyanhydrides to Prepare Polypeptides Using Tetraalkylammonium Carboxylate as the Initiator. *Angew. Chemie Int. Ed.* **2021**, *60* (50), 26063–26071. DOI: 10.1002/ANIE.202103540.
- (84) Chen, X.; Van De Mark, M. R. Tetrabutylammonium Benzoate-Initiated Polymerization of Propylene Oxide. *J. Appl. Polym. Sci.* **1993**, *50* (11), 1923–

1927. DOI:10.1002/APP.1993.070501109.
- (85) Wang, M. Y.; Song, Q. W.; Ma, R.; Xie, J. N.; He, L. N. Efficient Conversion of Carbon Dioxide at Atmospheric Pressure to 2-Oxazolidinones Promoted by Bifunctional Cu(II)-Substituted Polyoxometalate-Based Ionic Liquids. *Green Chem.* **2015**, *18* (1), 282–287. DOI:10.1039/C5GC02311D.
- (86) Habraken, G. J. M.; Wilsens, K. H. R. M.; Koning, C. E.; Heise, A. Optimization of N-Carboxyanhydride (NCA) Polymerization by Variation of Reaction Temperature and Pressure. *Polym. Chem.* **2011**, *2* (6), 1322–1330. DOI: 10.1039/C1PY00079A.
- (87) Li, Z.; Deming, T. J. Tunable Hydrogel Morphology via Self-Assembly of Amphiphilic Pentablock Copolypeptides. *Soft Matter* **2010**, *6* (11), 2546–2551. DOI: 10.1039/B927137F.
- (88) Gregson, C. K. A.; Gibson, V. C.; Long, N. J.; Marshall, E. L.; Oxford, P. J.; White, A. J. P. Redox Control within Single-Site Polymerization Catalysts. *J. Am. Chem. Soc.* **2006**, *128* (23), 7410–7411. DOI: 10.1021/ja061398n.
- (89) Broderick, E. M.; Guo, N.; Wu, T.; Vogel, C. S.; Xu, C.; Sutter, J.; Miller, J. T.; Meyer, K.; Cantat, T.; Diaconescu, P. L. Redox Control of a Polymerization Catalyst by Changing the Oxidation State of the Metal Center. *Chem. Commun.* **2011**, *47* (35), 9897–9899. DOI: 10.1039/C1CC13117F.
- (90) Biernesser, A. B.; Li, B.; Byers, J. A. Redox-Controlled Polymerization of Lactide Catalyzed by Bis(Imino)Pyridine Iron Bis(Alkoxide) Complexes. *J. Am. Chem. Soc.* **2013**, *135* (44), 16553–16560. DOI: 10.1021/ja407920d.

- (91) Quan, S. M.; Wei, J.; Diaconescu, P. L. Mechanistic Studies of Redox-Switchable Copolymerization of Lactide and Cyclohexene Oxide by a Zirconium Complex. *Organometallics* **2017**, *36* (22), 4451–4457. DOI: 10.1021/acs.organomet.7b00672.
- (92) Biernesser, A. B.; Chiaie, K. R. D.; Curley, J. B.; Byers, J. A. Block Copolymerization of Lactide and an Epoxide Facilitated by a Redox Switchable Iron-Based Catalyst. *Angew. Chemie Int. Ed.* **2016**, *55* (17), 5251–5254. DOI: 10.1002/ANIE.201511793.
- (93) Delle Chiaie, K. R.; Biernesser, A. B.; Ortuño, M. A.; Dereli, B.; Iovan, D. A.; Wilding, M. J. T.; Li, B.; Cramer, C. J.; Byers, J. A. The Role of Ligand Redox Non-Innocence in Ring-Opening Polymerization Reactions Catalysed by Bis(Imino)Pyridine Iron Alkoxide Complexes. *Dalt. Trans.* **2017**, *46* (38), 12971–12980. DOI: 10.1039/C7DT03067C.
- (94) Thompson, M. S. Redox-Switchable Copolymerization: Transforming Underutilized Monomer Feedstocks to Complex Copolymers, Ph.D. Dissertation, Boston College, Boston, MA, 2021.
- (95) Qi, M.; Dong, Q.; Wang, D.; Byers, J. A. Electrochemically Switchable Ring-Opening Polymerization of Lactide and Cyclohexene Oxide. *J. Am. Chem. Soc.* **2018**, *140* (17), 5686–5690. DOI: 10.1021/jacs.8b02171.
- (96) Delle Chiaie, K. R.; Yablon, L. M.; Biernesser, A. B.; Michalowski, G. R.; Sudyn, A. W.; Byers, J. A. Redox-Triggered Crosslinking of a Degradable Polymer. *Polym. Chem.* **2016**, *7* (28), 4675–4681. DOI: 10.1039/C6PY00975A.

- (97) Qi, M.; Zhang, H.; Dong, Q.; Li, J.; Musgrave, R. A.; Zhao, Y.; Dulock, N.; Wang, D.; Byers, J. A. Electrochemically Switchable Polymerization from Surface-Anchored Molecular Catalysts. *Chem. Sci.* **2021**, *12* (26), 9042–9052.  
DOI: 10.1039/D1SC02163J.

## **Chapter 2. Surface-initiated NCA Polymerizations from Redox-switchable Catalysts**

### **2.1 Introduction**

Surface modification by the introduction of synthetic polypeptides or polyamides have been explored for a wide range of applications including biosensing,<sup>1,2</sup> molecule delivery<sup>3,4</sup> and antibiofouling/antimicrobial applications.<sup>5,6</sup> While conventional deposition techniques for film construction are well established, physisorbed polymers sometimes suffer from poor adhesion. Instead, grafting polymerization techniques have been widely applied into the preparation of polyamide films.<sup>7-10</sup> Grafting-to and grafting-from (surface-initiated polymerization) strategies result in linear polymers with a terminal group anchored to the surface.<sup>11-13</sup> The grafting-to approach enables the generation of well-defined polymer surfaces, but the surface grafting density is always limited by steric hindrance associated with tethering a large macromolecule to a surface.<sup>14</sup> Moreover, intermediate purification steps are often required. In contrast, the grafting-from or surface-initiated polymerization approach produces less well-defined polymers and is more vulnerable to trace impurities but often results in very high surface grafting density.<sup>15-17</sup> Both strategies have been investigated for surface modifications with polyamides.<sup>18</sup> Owing to ease of amino acid-derived N-carboxyanhydride (NCA) ring-opening polymerization (ROP) from amine initiators, the latter approach is more commonly used to afford polyamide brushes on metal oxides, polymer particles as well as silicon wafers.<sup>19-22</sup>

As mentioned in Chapter 1, redox-switchable polymerization catalysis can allow the temporal control of the desired polymerization reaction. To further achieve the spatial control, the direct attachment of the polymerization catalyst to the surface of TiO<sub>2</sub> nanoparticles and electrodes, and the resulting surface-initiated NCA polymerizations from the supported catalysts will be described in this chapter. An efficient cleavage strategy will be discussed that can allow the removal of polyamides from the surface of nanoparticles for quantitative characterization. As a result, understanding about the compositions and molecular weight properties of the surface-growth polyamides are obtainable. In addition, efforts will be shown to characterize the supported polymerization catalyst by an electrochemical measurement. Furthermore, kinetic studies about the surface-initiated NCA polymerizations will be described here by monitoring the monomer conversion versus time. The reactions are carried out in the batch and with the application of flow, which provides more insight about the polymerization mechanisms. The surface-initiated NCA polymerization system that will be demonstrated in this chapter is a good alternative to couple with NCA synthesis for integration of polyamide synthesis from amino acids and CO<sub>2</sub> for the future development.

## **2.2 Redox-switchable NCA Polymerization Catalyst**

As mentioned above, surface-initiated NCA polymerizations are mostly achieved using primary amine initiators, which always result in the formation of not well-defined polyamides in homogeneous polymerization reactions. So far, only a few studies have been reported to incorporate novel catalysts for the preparation of well-

defined polyamide thin films. Witte and Menzel exploited zerovalence nickel initiators to polymerize NCAs from high surface area polystyrene resins.<sup>23</sup> In 2011, Patton and coworkers applied similar attachment strategy to produce block copolyptide brushes from low surface area substrate (e.g., silicon wafer), which expanded the potential applications of these hybrid flat surfaces as biosensor platforms.<sup>24</sup> Nevertheless, tedious steps are required in order to attach nickel complexes on surfaces. Recently, Heise and coworkers employed light induced NCA polymerization on the surface of silicon wafer by attaching a photoamine generator to produce an amine as the polymerization catalyst upon exposure to light.<sup>25</sup> This strategy provides an alternative way to prepare spatiotemporally controlled surface patterning, however, the produced polyamide is limited to homopolymer. To achieve the spatiotemporal control for the preparation of polyamide thin films with an expanded scopes for polymer compositions, the redox-switchable polymerization will become a powerful tool when it is being applied to surfaces.

The Byers group has been investigating switchable ring-opening polymerization systems based on iron alkoxide complexes bearing bis(imino)pyridine (PDI) ligands.<sup>26-30</sup> Among this family of catalysts, the formally iron(I) monoalkoxide **2.1** was found to be active towards the polymerization of NCAs, such as  $\gamma$ -benzyl l-glutamate NCA (BLG-NCA) and sarcosine NCA (Sar-NCA). With the addition of the oxidant, ferrocenium, the formed iron(II) monoalkoxide **2.2** became dormant towards NCA polymerization. Instead, the complex **2.2** was active towards epoxide polymerization (Figure 2.1).<sup>30</sup> The switching of the orthogonal activity of iron

complexes **2.1** and **2.2** for polymerizations of NCA and epoxide makes the complex **2.1** a good candidate that can catalyze the NCA polymerization on surface under temporal control. The development of this unique iron complex system for homogeneous NCA and epoxide polymerization was found by the previous group member, Dr. Matthew Thompson. Herein, information about the homogeneous NCA polymerization catalyzed by the iron(I) complex **2.1** will be briefly discussed in this section since the focus of the thesis is to apply the iron(I)-initiated NCA polymerization on surface for integrated catalysis.

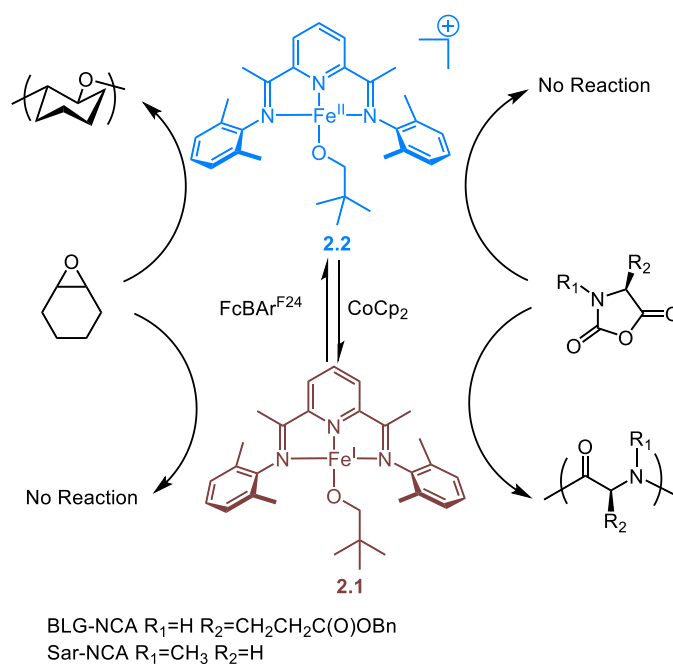


**Figure 2.1** Iron bis(iminopyridine) monoalkoxide complexes used in redox-switchable polymerizations of N-carboxyanhydride (NCAs) and cyclohexene oxide: iron(I) complex **2.1** is active to initiate polymerization of NCAs, such as BLG-NCA and Sar-NCA; after being oxidized, the formed iron(II) complex **2.2** is only active towards epoxide polymerization like the iron(II) bisalkoxide complex **1.2**. Recreated from Ref. 30.

Sequential addition of chemical redox reagents (ferrocenium and cobaltocene, respectively) provided a means to deactivate and reactivate the NCA polymerization. A surprising finding that resulted from catalyst development was an enhanced polymerization reaction rate and full monomer conversion. This phenomenon was observed upon catalyst reactivation with the addition of cobaltocene. Further studies revealed that the byproduct  $[\text{CoCp}_2][\text{BAR}_4^{\text{F}24}]$  was acting as a Lewis acidic co-catalyst for NCA polymerization.<sup>31</sup> Unlike most NCA polymerization reactions catalyzed by amines, where the mechanism is either the normal amine mechanism (NAM) or activated monomer mechanism (AMM), the mechanism for NCA polymerization with **2.1** was proposed to be a coordination-insertion mechanism (Figure 2.2). The precise role of the mild Lewis acid co-catalyst is not clear at this stage of understanding. The Lewis acid may bind to the NCA to activate its insertion to the iron alkoxide **2.1** or iron amide intermediates **2.4**. Additionally, after insertion of an NCA monomer and the decarboxylation, the amide carbonyl from the newly formed peptide **2.4** might form a five-membered ring chelate structure **2.5**. This chelated complex could prevent binding of the NCA monomer for insertion leading to product inhibition in the absence of a Lewis acid co-catalyst. In the presence of a Lewis acidic co-catalyst, the amide carbonyl **2.4** can interact with the Lewis acid instead of the iron center, which opens a coordination site on the metal to enable the subsequent NCA insertions.

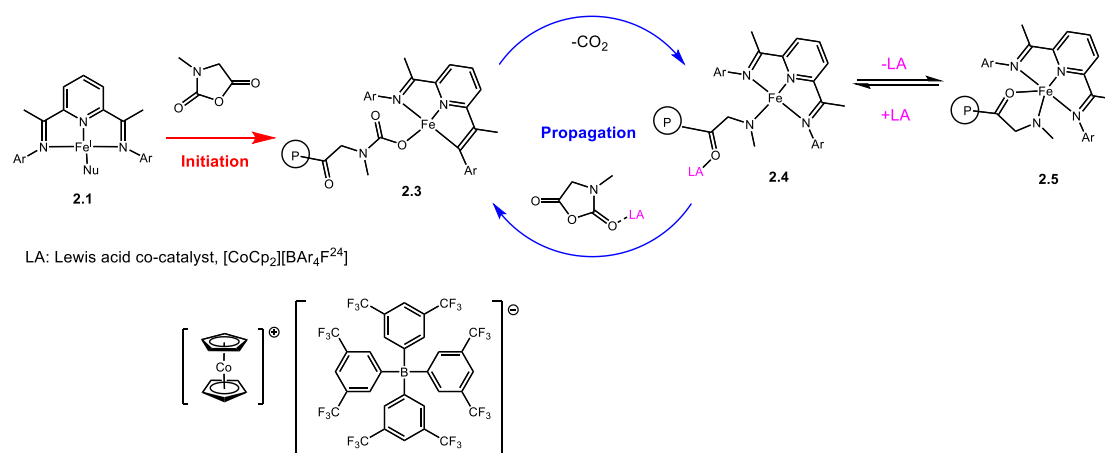


**Figure 2.2** Proposed coordination-insertion mechanism for Sar-NCA polymerization catalyzed by complex **2.1** and co-catalyzed by a Lewis acid co-catalyst,  $[\text{CoCp}_2][\text{BAR}_4\text{F}^{24}]$ . The Lewis acidic co-catalyst could serve two functions: to activate NCA for insertion and to prevent product inhibition. Recreated from Ref. 30.

### 2.3 Synthesis of the iron(I)-TiO<sub>2</sub> nanoparticles

To achieve the spatial control of polyamide synthesis, the redox-switchable NCA polymerization iron catalyst described above needs to be anchored on solid supports. In our previous study, the bis(imino)pyridine iron(II) bisalkyl complex **2.6** can be covalently immobilized onto titania nanoparticles or plates through protonolysis reaction utilizing Ti-OH groups on the surfaces to afford **2.6@TiO<sub>2</sub>**.<sup>32</sup> The immobilized Fe(II) **2.6@TiO<sub>2</sub>** like the molecular iron(II) alkoxide complex **1.1** is active for lactide polymerization. Similarly, the immobilized iron(III) complex after applying oxidized electrochemical potential to **2.6@TiO<sub>2</sub>** is only active for epoxide polymerization as observed for the molecular iron(III) alkoxide complex **1.2**.<sup>27</sup> Based on this strategy, a pattern of binary conducting channels was created by spatially controlling the polymerizations of lactide and epoxide on a TiO<sub>2</sub>-coated electrode

(Figure 2.3). To achieve immobilization of iron (I) complex on surface, the same anchoring strategy was explored for an analogous iron(I) mono(imino)pyridine alkyl complex **2.7** onto TiO<sub>2</sub> nanoparticles.

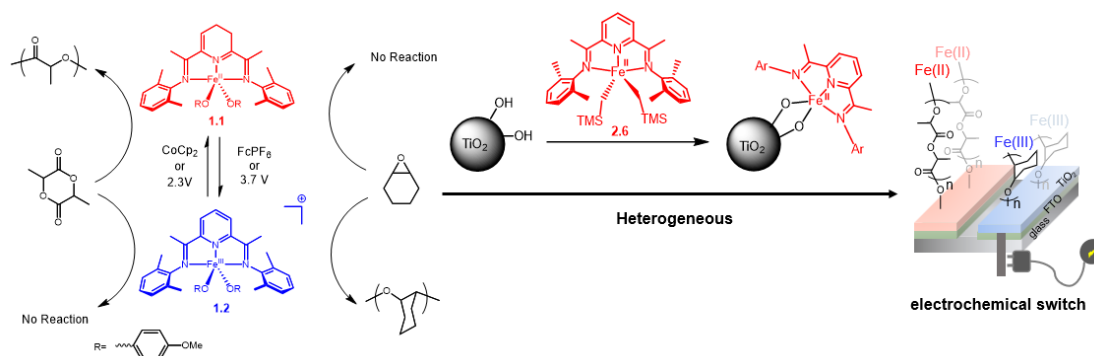
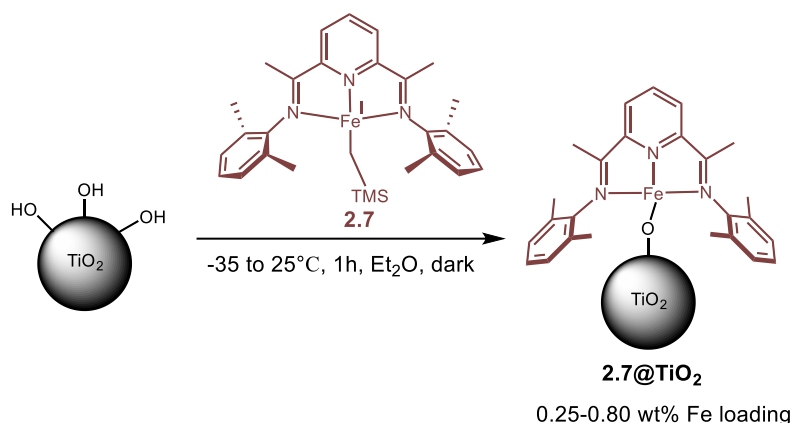


**Figure 2.3** Iron-based catalysts reported for the redox-switchable polymerization of lactide and epoxides are extended to the solid state by appending iron-based catalysts to titania nanoparticles through protonolysis reaction. Application of an electrochemical switch to a conducting substrate containing electrically isolated zones coated with these particles enables patterning of surfaces with two different polymer brushes. Recreated from Ref. 32.

TiO<sub>2</sub> nanoparticles P25 were first treated with UV light to introduce more surface hydroxyl groups followed by being heated under reduced pressure (10<sup>-2</sup> torr) at 130 °C for 2 days to remove physisorbed water completely. The drying temperature and time are important in order to avoid any reproducibility issues. The treated nanoparticles were then subjected to an iron monoalkyl precursor **2.7** at the optimal reaction conditions developed by Dr. Matthew Thompson in our group (Scheme 2.1).<sup>30</sup> The resulting iron containing titania nanoparticles **2.7@TiO<sub>2</sub>** were light blue. Analysis of this powder by inductively coupled plasma optical emission

spectrometry (ICP-OES) indicated the weight percent of iron was  $0.65 \pm 0.35$  wt%, which suggested that 25-50% of the surface hydroxyl groups were modified with iron(I) complex **2.7**. As a comparison, the iron content on **2.6@TiO<sub>2</sub>** was 2.1 wt% which was consistent with that all of the surface hydroxyl groups were modified by the iron(II) bisalkyl complex **2.6**. In addition, Mössbauer spectroscopy was also utilized to characterize the iron(II) complex of **2.6@TiO<sub>2</sub>**, where two iron-coating species were observed on the spectrum. The Mössbauer parameters from the major species (81%) are similar to those of the molecular iron(II) alkoxide complex **1.1**, which confirms the molecular identity of iron(II) complex was maintained when supported on the TiO<sub>2</sub> surface. For the surface immobilized iron(I), however, Mössbauer spectroscopy could not be utilized due to the low concentration of iron from **2.7@TiO<sub>2</sub>** powders. Noteworthy, **2.7@TiO<sub>2</sub>** should have twice as much iron content as **2.6@TiO<sub>2</sub>** considering the stoichiometry that the molecular iron(I) complex reacting with only one hydroxyl group while molecular iron(II) complex bridging two consecutive hydroxyl groups. The smaller iron content for **2.7@TiO<sub>2</sub>** might be attributed to potential inhibition for highly-dense surface hydroxyl groups to directly support the complex **2.7** with 1:1 ratio. Owing to the lack of powerful characterization tools, the reason for the low iron loading of **2.7@TiO<sub>2</sub>** still remains unclear without the aid of Mössbauer spectroscopy. This inherent limitation might be resolved by developing a different anchoring approach to enhance the surface iron loading, which will be discussed in Chapter 3.



**Scheme 2.1** Protonolysis reaction can allow the support of iron(I) complex **2.7** covalently on P25 titania nanoparticles to afford **2.7@TiO<sub>2</sub>**. The iron loading on the resulting **2.7@TiO<sub>2</sub>** sample was within 0.25-0.80 wt%.

#### 2.4 Polymerization of Sar-NCA with the iron(I) containing TiO<sub>2</sub> nanoparticles

To confirm the activity of supported iron(I) catalysts on TiO<sub>2</sub> nanoparticles, the **2.7@TiO<sub>2</sub>** nanoparticles were exposed to a 0.2 M THF solution of Sar-NCA containing the co-catalyst [CoCp<sub>2</sub>][BAR<sub>4</sub><sup>F24</sup>] and an internal standard 1,3,5-trimethoxybenzene (Figure 2.4 a). Herein, the co-catalyst was required for the surface-initiated NCA polymerization in order to enhance the monomer conversion based on previous studies done by Dr. Matthew Thompson.<sup>30</sup> Aliquots of the polymerization mixture were taken periodically, and the corresponding <sup>1</sup>H NMR spectra revealed that only Sar-NCA monomer was observed in the supernatants after centrifugation to remove the TiO<sub>2</sub> powders. Based on the NMR spectroscopy, NCA conversion from the surface of **2.7@TiO<sub>2</sub>** nanoparticles was determined by comparing the relative integration of the methylene peak of the remaining Sar-NCA monomer to the methine peak of the internal standard in the supernatant. After one week, 25 ± 5%

NCA conversion was obtained. The resulting poly(sarcosine)-coated TiO<sub>2</sub> nanoparticles was characterized by FT-IR, where the strong band at 1650 cm<sup>-1</sup> confirms the presence of secondary amide group that is from the surface-bound poly(sarcosine) (Figure 2.4 b).<sup>33</sup> Thermal gravity analysis (TGA) of the grafted poly(sarcosine)-TiO<sub>2</sub> nanoparticles showed a 15% weight loss at 215 °C, which is consistent with the conversion of the reaction and reported decomposition temperature of synthetic poly(sarcosine) (Figure 2.4 c).<sup>34</sup>

To analyze the resulting polyamide products with routine quantitative techniques used by polymer chemists (e.g., NMR, gel permeation chromatography (GPC), etc.), a facile cleavage method is required. Such a method should not involve harsh conditions, such as strongly acidic or basic conditions used commonly to cleave polyolefins from surface-initiated controlled radical polymerizations<sup>35</sup>. This is because the substrate surface can be easily damaged or the surface-bound polymers (e.g., polyesters, polyethers, polyamides etc.) generated from ring-opening polymerizations might be even degraded under these harsh circumstances. Previously, we found that the surface-grown poly(lactic acids) from **2.6@TiO<sub>2</sub>** could be cleaved efficiently from the nanoparticles by treating the particles with iodomethane.<sup>32</sup> Using this technique, polymer cleaved from the nanoparticle was methylated at the ester chain end only with the hydroxyl chain end remained unreacted. Since the hydrolysis of the iron complex at polymer chain end occurs spontaneously upon exposure to air, the cleavage reaction occurs selectively at the Ti-ester bond from the polymer chain.

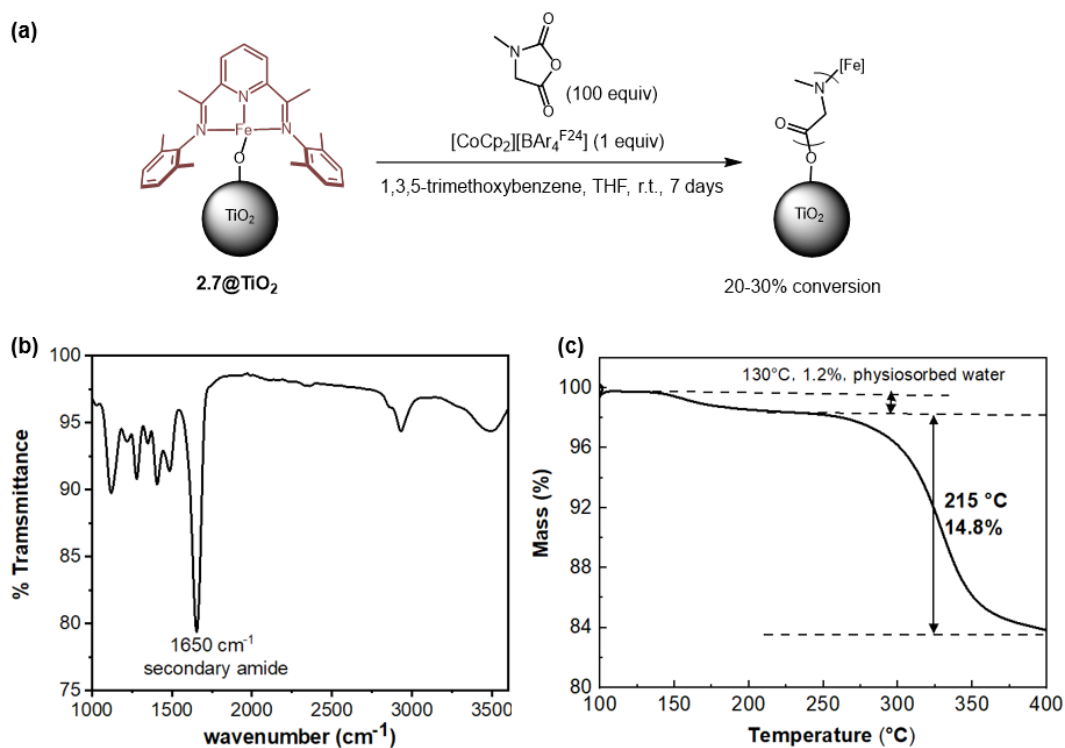


**Figure 2.4** Surface-initiated Sar-NCA polymerization from immobilized Fe(I) **2.7@TiO<sub>2</sub>** nanoparticles and Characterizations of the resulting poly(sarcosine)-coated TiO<sub>2</sub> nanoparticles. (a) Scheme for the surface-initiated Sar-NCA polymerization from **2.7@TiO<sub>2</sub>** powder; (b) FT-IR characterization of the poly(sarcosine)-coated TiO<sub>2</sub> nanoparticles; (c) TGA analysis of the poly(sarcosine)-coated TiO<sub>2</sub> nanoparticles.

A similar approach was explored for the cleavage of polyamides from the TiO<sub>2</sub> surfaces due to the presented existence of similar Ti-ester bond that covalently link the nanoparticles and polymers. Removal of poly(sarcosine) was achieved by subjecting the poly(sarcosine)-TiO<sub>2</sub> nanoparticles to iodomethane in a dichloromethane solution at room temperature overnight (Figure 2.5 a). TGA of the resulting nanoparticles after the cleavage experiment showed a 3.2% weight loss at the decomposition temperature of 215 °C, indicating that most (~80%) of the

polyamide was removed from the surface (Figure 2.5 b). The nanoparticles after cleavage were also characterized by FT-IR (Figure 2.5 c), where the amide stretching peak ( $1650\text{ cm}^{-1}$ ) was still observed, revealing that the poly(sarcosine) was not completely removed.

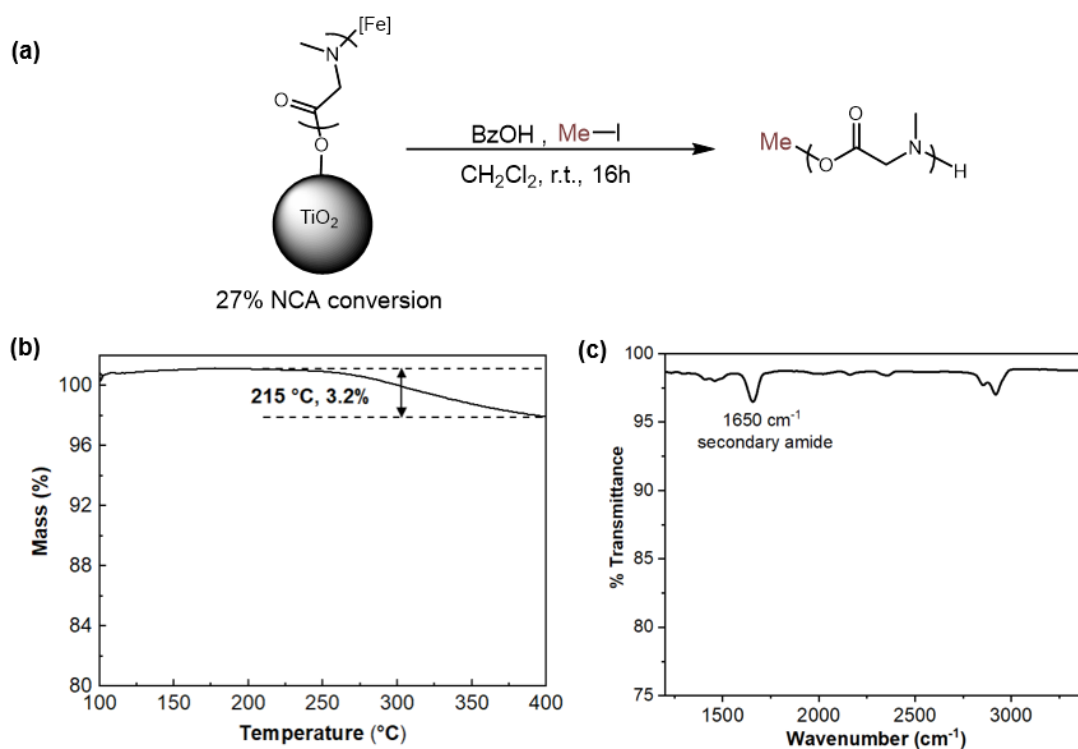


**Figure 2.5** Removal and characterizations of poly(sarcosine) cleaved from the  $\text{TiO}_2$  nanoparticles with iodomethane treatment. (a) Reaction scheme to cleave poly(sarcosine) from  $\text{TiO}_2$  powders; (b) TGA analysis of the cleaved  $\text{TiO}_2$  nanoparticles after iodomethane treatment; (c) FT-IR of the cleaved  $\text{TiO}_2$  nanoparticles after iodomethane treatment.

The cleavage strategy also allows the quantitative analysis for polyamides grown from the surface. Control experiments were conducted first by treating the poly(sarcosine) obtained from homogeneous NCA polymerization with iodomethane under similar condition. NMR and GPC analysis of the resulting poly(sarcosine)

showed that there was no change for the polymer properties after methyl iodide treatment, which verified that methyl iodide would not alkylate the polyamides leading to different polymer properties (Experimental Section). Thus, the cleaved poly(sarcosine) from nanoparticles was subjected for GPC analysis, which revealed a polymer with a trimodal molecular weight distributions (Figure 2.6 a). Analysis of each peak separately revealed  $M_n(\text{exp}) = 2.8 \text{ kg/mol}$ ,  $1.5 \text{ kg/mol}$  and  $0.77 \text{ kg/mol}$ , respectively. The corresponding molecular weight distributions  $M_w/M_n$  were 1.01, 1.01 and 1.02, respectively.  $^1\text{H}$  NMR spectroscopy was also utilized to characterize the composition of cleaved poly(sarcosine) (Figure 2.6 b), where the peaks agree well with those of the poly(sarcosine) obtained from the iron(I) alkoxide **2.1**-initiated Sar-NCA polymerization (Figure 2.6 c).

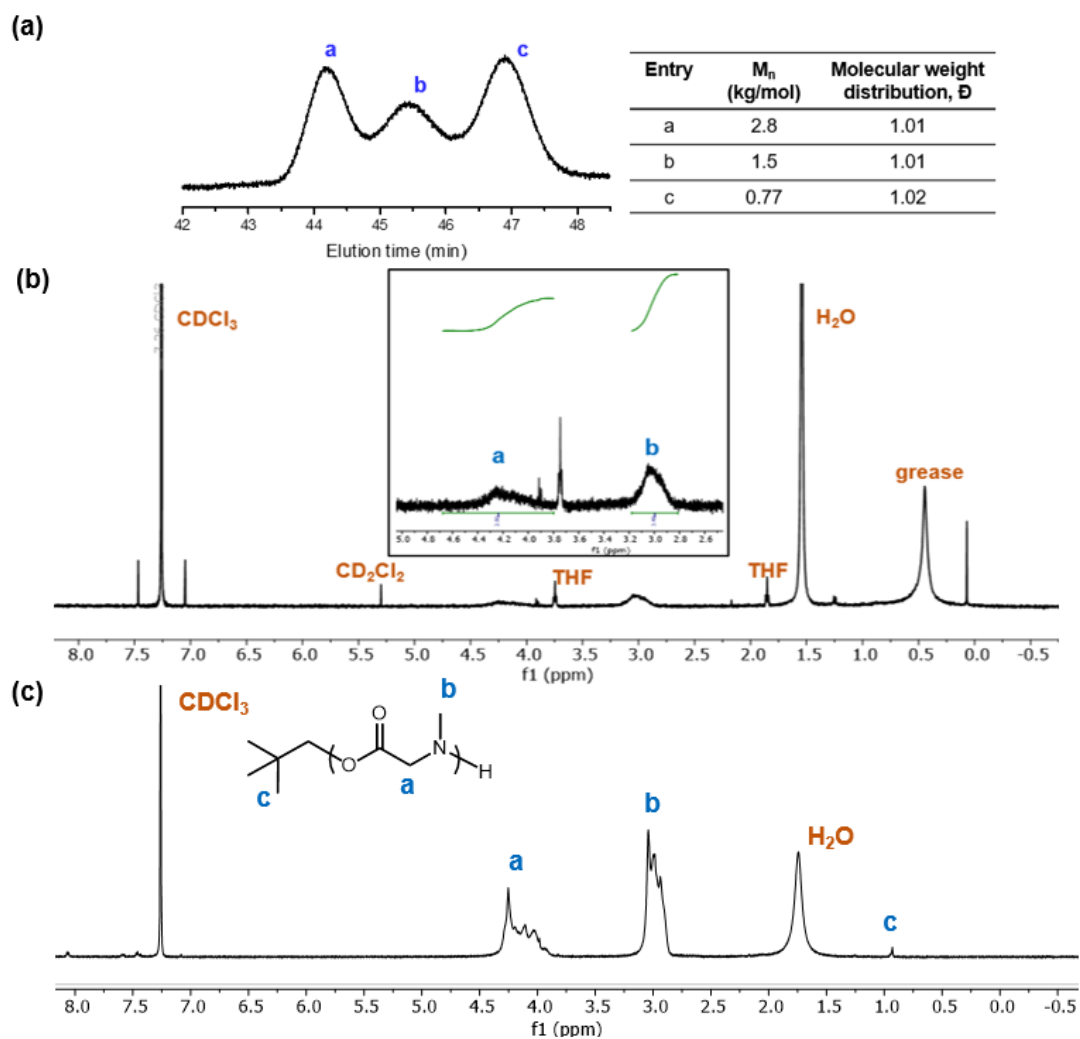


**Figure 2.6** Quantitative characterizations of the poly(sarcosine) cleaved from the surface of TiO<sub>2</sub> nanoparticles. (a) GPC analysis of the poly(sarcosine) cleaved off TiO<sub>2</sub> particles; (b) <sup>1</sup>H-NMR spectrum of poly(sarcosine) cleaved off TiO<sub>2</sub> particles; (c) <sup>1</sup>H-NMR spectrum of the poly(sarcosine) obtained from the iron (I) alkoxide **2.1** initiated Sar-NCA polymerization.

One of the polymer molecular weights agreed with the predicted molecular weight of 1.7 kg/mol, which was calculated based on the conversion of the reaction, the iron loading, and the assumption that each supported iron initiated one polymer chain via a living polymerization. The molecular weight results suggested that there

were three different catalytically active polymer species formed during the process of surface-initiated NCA polymerization from **2.7@TiO<sub>2</sub>** nanoparticles. This phenomenon is different than what we observed previously in the surface-initiated lactide polymerizations from **2.6@TiO<sub>2</sub>** nanoparticles.<sup>32</sup> Based on the time course investigation of surface-initiated lactide polymerization, a linear increase of molecular weight with conversion was observed, which demonstrated the living characteristics of this surface polymerization. A further kinetic study was examined to monitor the conversion versus reaction time, where the reaction rate was fast and followed first order reaction kinetics at low conversion (<40%). Molecular weight distributions were also relatively narrower than observed at the end of the reaction. At higher conversion, the reaction deviated from first order kinetics and the molecular weight distribution became broader (~1.6) as the reaction proceeded. The slower reaction rates and higher molecular weight distributions at high conversions revealed that the mass transport became more prominent as the polymerization proceeds. Noteworthy, the poly(lactide acids) were mono-dispersed during the polymerization process, that is different with the trimodal GPC curves obtained from the NCA polymerizations from **2.7@TiO<sub>2</sub>** nanoparticles with the addition of co-catalyst. Because both the lactide and NCA polymerizations are proposed to proceed in the coordination-insertion mechanisms, one possible explanation for the formation of three different polyamide species was attributed to the present co-catalyst in the NCA polymerization from **2.7@TiO<sub>2</sub>** nanoparticles. Since the co-catalyst would need to access the surface-bound iron amide intermediates to avoid product inhibition, its diffusion to various

positions of the supported iron catalysts could lead to different propagation rate and thus, polyamides with different molecular weights. Nevertheless, the effect of mass transport, a factor to consider in all heterogeneous reactions, cannot be ruled out at this stage for this surface-initiated NCA ROP system.

Overall, the cleavage method we developed to remove the surface-initiated polymers from the solid supports enables the quantitative identification of polymer composition and evaluation of polymer molecular weights, which is not commonly done in surface-initiated polymerization reactions.<sup>36,37</sup> The cleavage approach can be utilized as a mechanistic tool to obtain more understandings about the mechanisms of surface-initiated ring-opening polymerizations.

### **2.5 Direct attachment of iron(I) on spin-coated TiO<sub>2</sub> electrode and surface-initiated NCA polymerization from flat surface**

With the successful anchoring of the reactive iron(I) complex on the TiO<sub>2</sub> nanoparticles and the surface-initiated Sar-NCA polymerization from powders, we then moved to test the polymerization reactions on conductive flat surfaces in order to incorporate the electrochemical method for redox-switching of supported iron complex. To maximize the yield of surface grafted polymers and make the surfaces flat, we constructed an electrode by spin-coating a layer of P25 TiO<sub>2</sub> nanoparticles on the conductive fluorine-doped tin oxide (FTO) substrate.<sup>38</sup> Similar to the nanoparticles, anchoring of the iron complex onto the electrode was performed by immersing the pre-dried TiO<sub>2</sub> plate into a diethyl ether solution of bis(imino)pyridine iron(I) monoalkyl **2.7** in the dark at -35 °C for 1 h. The resulting plates turned to

green-bluish color and ICP-OES analysis showed an iron content that was  $0.030 \pm 0.01$   $\mu\text{mol}/\text{cm}^2$ . The obtained plate was then exposed to a 0.08 M Sar-NCA solution in THF at room temperature with a stirring rate of 1000 rpm. Similar to the surface-initiated NCA polymerization from **2.7@TiO<sub>2</sub>** nanoparticles, no polymer was observed in solution during the polymerization from the **2.7@TiO<sub>2</sub>** plate.  $15.0 \pm 5.0\%$  Sar-NCA was consumed after 48 h as evident by <sup>1</sup>H NMR spectroscopy (Figure 2.7).

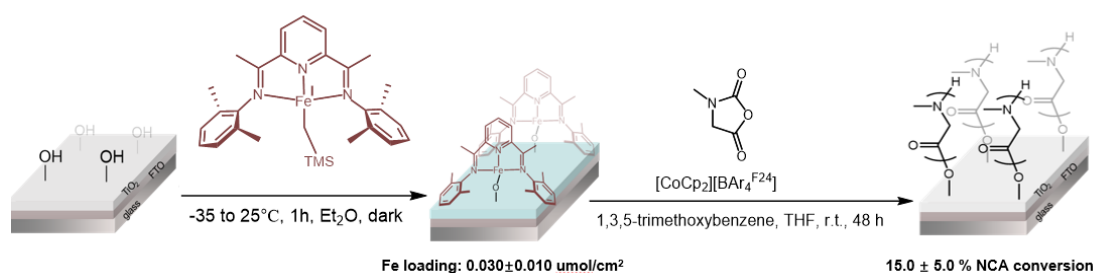


**Figure 2.7** Anchoring the iron(I) alkyl complex **2.7** onto the surface of spin-coated TiO<sub>2</sub> plate for surface-initiated Sar-NCA polymerization.

The plates obtained after NCA polymerization were further characterized by other surface qualitative techniques, such as FT-IR and XPS. Nitrogen from surface-coated polyamide was detected by XPS (Figure 2.8 a). In addition, the carbons from C=O and C-O groups were observed, which further confirmed the existence of poly(sarcosine) bound to the TiO<sub>2</sub> substrate (Figure 2.8 b). FT-IR analysis revealed a peak at  $1650\text{ cm}^{-1}$  that is consistent with secondary amide groups from poly(sarcosine) (Figure 2.8 c).<sup>39</sup> All the surface characterization results verified the successful formation of poly(sarcosine) thin film on the flat electrode (Figure 2.8).<sup>40</sup>

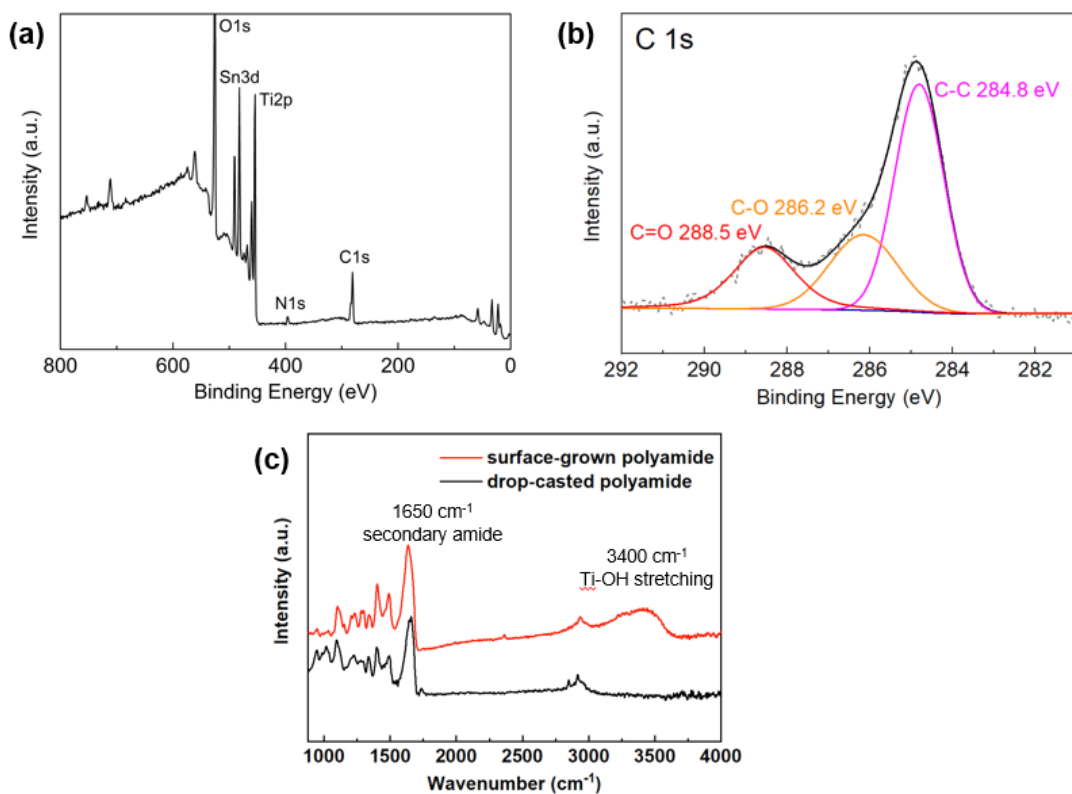


**Figure 2.8** XPS and ATR FT-IR and characterizations for the plate after Sar-NCA polymerization. (a) XPS survey scan spectra of poly(sarcosine)-plate; (b) C1s XPS spectra of poly(sarcosine)-plate; (c) FT-IR analysis of plate after surface-initiated NCA polymerization and a controlled plate that is prepared by drop casting a layer of pre-synthesized poly(sarcosine).

Cleavage of poly(sarcosine) from the TiO<sub>2</sub> plate succeeded as well using the same condition of iodomethane treatment as evident by <sup>1</sup>H NMR spectroscopy. Unlike the nanoparticles, however, not enough polymer solid was obtained from the plate for molecular weight analysis by GPC. The <sup>1</sup>H NMR of cleaved poly(sarcosine) confirmed its characteristics while additional peaks from the decomposed methyl iodide were observed due to the lack of the precipitation step that can purify the polymer product.

## 2.6 Redox behavior of surface-supported iron(I) towards the NCA polymerization

To enable temporal control of polyamide synthesis, we next wanted to study the redox behavior of the surface-bound iron(I) catalyst on the plate. We first explored using chemical redox reagents for this purpose. When an excess of oxidizing reagent  $\text{FcBAR}_4^{\text{F}24}$  was added to the supported iron(I)  $\mathbf{2.7@TiO}_2$  plate, the resulting oxidized plate lost its blue-green color. Upon immersing the plate into the NCA monomer solution, no NCA conversion was observed by  $^1\text{H}$  NMR spectroscopy under similar reaction conditions. Though the result demonstrates the specific activity of  $\mathbf{2.7@TiO}_2$  towards NCA polymerization can be turned off upon adding the chemical oxidant, however, the activity cannot be returned after the addition of a reducing agent,  $\text{CoCp}_2$ . Since the iron(I) complex  $\mathbf{1.1}$  is very sensitive to temperature, the relatively long reaction time is a concern. It is possible that the supported iron(I) complex from  $\mathbf{2.7@TiO}_2$  was destroyed rather than oxidized. More work needs to be done to allow the redox-switchable polymerization from the surface-attached iron(I) on  $\mathbf{2.7@TiO}_2$  tuned by chemical redox reagents.

In addition to exploring the activity of surface-attached iron(I)  $\mathbf{2.7@TiO}_2$  plate using chemical redox reagents, the electrochemical method was investigated. The  $\mathbf{2.7@TiO}_2$  plate was first utilized as the working electrode in a 0.1 M THF solution of  $^t\text{Bu}_4\text{PF}_6$  as the electrolyte for cyclic voltammetry (CV) measurement. However, an irreversible feature was observed during the electrochemical redox process, which was still attributed to the instability of iron(I) complex (Figure 2.9 a). To solve this

problem, the **2.7@TiO<sub>2</sub>** plate was subjected to the Sar-NCA monomer solution for 4 h with the insertion of a small amount of poly(sarcosine) (3% NCA conversion) between titania surface and terminal iron center. By doing that, we expected that the stability of the supported iron catalyst can be enhanced due to the formation of five-coordinated chelate structure, which was discussed in section 2.1. A CV measurement was performed by using the pre-polymerized **2.7@TiO<sub>2</sub>** plate as the working electrode. A reversible redox feature of the anchored Fe(I) was observed with the half-wave potential,  $E_{1/2}$ , of the poly(sarcosine)-stabilized Fe(I) being -0.77 V (vs.  $\text{Fc}^+/\text{Fc}$ ) (Figure 2.9 b). The 0.13 V positive shift relative to the molecular iron alkoxide complex ( $E_{1/2} = -0.90$  V) (Figure 2.9 c) showed that the iron center is more electron deficient when in contact with TiO<sub>2</sub>. This phenomenon is consistent with our previous observations for the surface-bound iron(II) **2.6@TiO<sub>2</sub>**. A 0.50 V positive shift was obtained for the surface-attached iron(II) **2.6@TiO<sub>2</sub>** ( $E_{1/2} = -0.40$  V, vs.  $\text{Fc}^+/\text{Fc}$ ) relative to the molecular iron(II) alkoxide complex measured in solution ( $E_{1/2} = -0.90$  V).<sup>32</sup> The **2.7@TiO<sub>2</sub>** plate after CV measurement was subjected again to the Sar-NCA polymerization. As expected, additional ~35% NCA conversion was consumed after another 6 days, indicating the activity of supported iron(I) catalysts still preserved after an electrochemical redox switching. Overall, the electrochemical measurement allows the characterization of the supported iron(I) **2.7@TiO<sub>2</sub>** with an insertion of a short-length polyamide to stabilize the unstable complex. The surface attached iron(I) catalyst will become a promising candidate to achieve spatial and temporal control for polyamide synthesis if its activity towards the NCA polymerization can be remained

after multi-electrochemical switches. By tuning on and off the surface-initiated NCA polymerization, the fidelity of polyamide chain ends might be able to be preserved, which could allow the further growth of polymers upon the addition of different NCAs. Future work will focus on the electrochemical switching studies with the collaborations of Wang group in the Chemistry Department of Boston College.

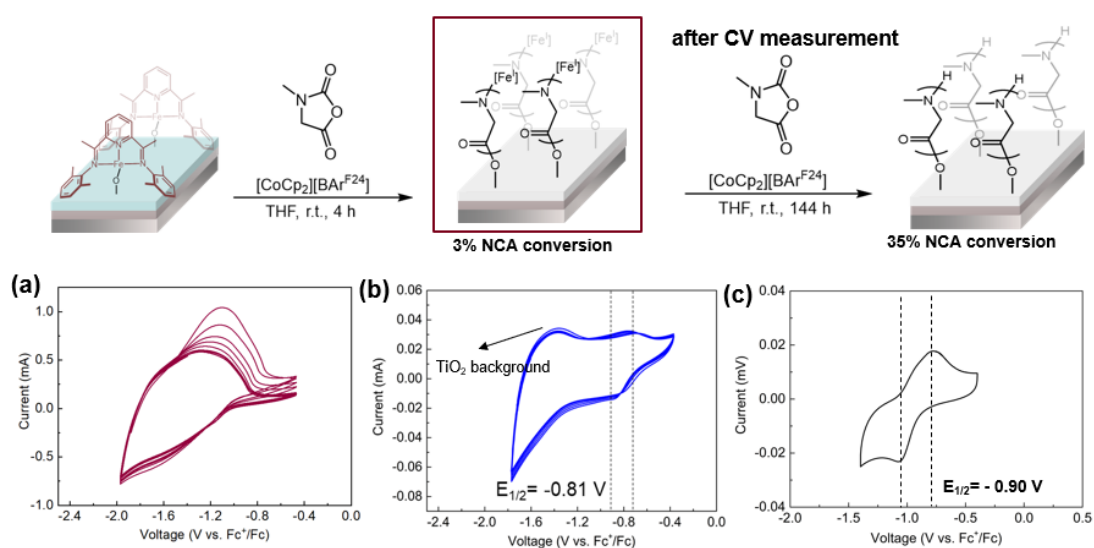


**Figure 2.9** Redox behavior of supported iron(I) catalyst **2.7@TiO<sub>2</sub>** towards NCA polymerization can be tuned by applying electrochemical potential (top); (a) Cyclic voltammetry (CV) curve for surface-anchored iron(I) **2.7@TiO<sub>2</sub>** plate; (b) CV measurement of surface-anchored iron(I) **2.7@TiO<sub>2</sub>** plate with the insertion of a small amount of poly(sarcosine) between the substrate and iron complex; c) CV curve for molecular iron(I) alkoxide complex **2.1**.<sup>30</sup> 0.1 M THF solution of Bu<sub>4</sub>PF<sub>6</sub> was used as the electrolyte; Working electrode: **2.7@TiO<sub>2</sub>** plate; Counter electrode: platinum wire, Reference electrode: lithium strip; Scan rate is 50 mV/s; The peak at about -1.4 V vs Fc<sup>+</sup>/Fc on Figure 2.9 (b) belongs to the TiO<sub>2</sub> background.

## 2.7 Kinetics of surface-initiated NCA polymerization from iron(I)-TiO<sub>2</sub> plate

Unlike the surface polymerization based on controlled radical polymerizations (such as atom transfer radical controlled polymerization, reversible addition–fragmentation chain-transfer polymerization, etc.)<sup>35,41</sup>, the mechanism for surface-initiated ring-opening polymerization has been hardly explored. Almost all previous studies have focused on using the polymer thin films obtained from surface-initiated ROP for specific applications, such as biomedical imaging<sup>9</sup>, drug delivery<sup>19</sup> and surface patterning<sup>21</sup>. Only two studies have been reported so far for surface-initiated ROP reactions that both monitored the kinetics based on the increased amount of polymer brushes. In 2009, Müller and coworkers monitored the kinetics of the surface-initiated ROP of caprolactone from multiwalled carbon nanotubes using TGA versus time.<sup>36</sup> In 2012, Carlmark and coworkers applied the quartz crystal microbalance technique into the surface-initiated ROP of caprolactone on a, which allow them to monitor the formation of polymer brushes from surfaces in real time.<sup>37</sup> Nevertheless, the amount of polymer brushes is not a direct indicator, and the latter work requires the specific cellulose substrate and experimental setup.<sup>42</sup> The lack of understandings regarding the nature of the surface-initiated polymerizations is likely due to insufficient characterization methods and tools to monitor the polymerization or due to slow rates of the heterogeneous reactions that make such studies tedious. It is possible to monitor the polymerizations occur in solution, along with the surface polymerization by different characterization techniques assuming the polymerizations occur in solution and on the surface follow the similar mechanisms.<sup>43</sup> However, this

assumption may not be true for all reactions especially for the transition metal-catalyzed ROP. To fill the gap, we wanted to better understand why surface polymerization reactions were slower and always produced polymers with broader molecular weight distributions. Therefore, we decided to investigate the kinetics of the surface-initiated ROP from surface-bound iron(I) complex **2.7@TiO<sub>2</sub>** described above. By utilizing this polymerization reaction as a model, we could take advantage of facile cleavage method we have developed for quantitative analysis between polymer brushes and titania surfaces.

To begin with, the surface-initiated NCA polymerizations were conducted by soaking the **2.7@TiO<sub>2</sub>** plate in a 0.08 M THF solution of Sar-NCA with stirring at 1000 rpm. Similarly, the monomer conversions consumed on surface were determined by <sup>1</sup>H NMR analysis of the aliquots taken from the supernatants at different time points (Table 2.1). The NCA conversion on **2.7@TiO<sub>2</sub>** was 8.5±4.5%, 13.4±2.5% and 26.6±5.0% after 24 h, 48 h and 168 h, respectively (Figure 2.10).

**Table 2.1** Kinetics of Fe(I)-catalyzed Sar-NCA polymerization from TiO<sub>2</sub> plate carried out in the batch.

Entry	Reaction time (h)	Conversion %	$k_b$ (cm·s <sup>-1</sup> )
1	24	8.5±4.5	2.4 x 10 <sup>-6</sup>
2	48	13.4±2.5	2.0 x 10 <sup>-6</sup>
3	168	26.6±5.0	1.4 x 10 <sup>-6</sup>

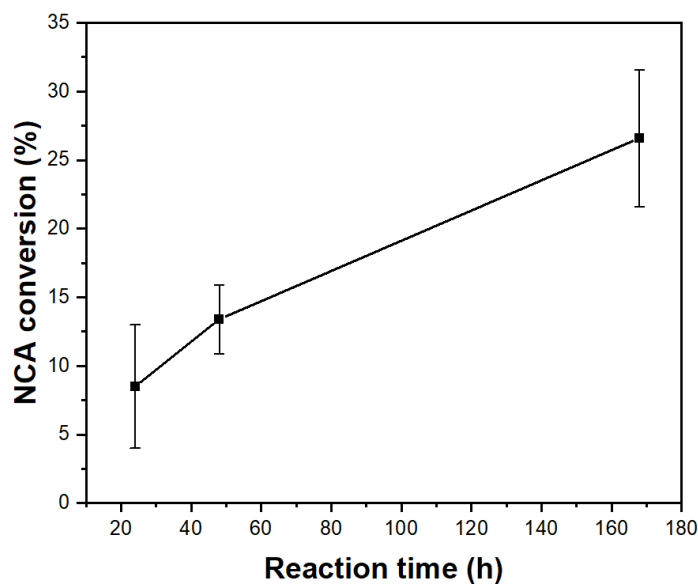


**Figure 2.10** Evolution of NCA conversion versus reaction time for NCA polymerizations on **2.7@TiO<sub>2</sub>** plates carried out in the batch with stirring at 1000 rpm.

The apparent rate constant  $k_b$  was normalized by the surface areas of the spin-coated plates (0.3 x 1.2 inches) used in the batch and can be calculated based on the equation (7). The mathematical work to obtain equation (7) was derived by our collaborators, Brandon Jolly and Prof. Chong Liu at UCLA.

The polymerization rate follows equation (1)

$$r_{poly} = \frac{-d[NCA]}{dt} = k_b[NCA] \quad (1)$$

To normalize different sizes of the plates, surface area ( $SA$ ) was included on the right-hand side of the equation (2). To make the unit of left-hand side similar to that of right-hand side, volume of NCA solution ( $V$ ) was added on the left-hand side of equation (2).

$$\frac{dV[NCA]}{dt} = -SA * k_b[NCA] \quad (2)$$

$$[NCA]_t = [NCA]_{t=0} \exp\left[-\frac{SA}{V}k_b t\right] \quad (3)$$

The NCA conversion consumed from **2.7@TiO<sub>2</sub>** plate is

$$Conversion = \frac{[NCA]_0 - [NCA]_t}{[NCA]_0} = 1 - \frac{[NCA]_t}{[NCA]_0} \quad (4)$$

The equation (3) can be modified to afford equation (5) and (6)

$$\frac{[NCA]_t}{[NCA]_0} = \exp \left[ -\frac{SA}{V} k_b t \right] \quad (5)$$

$$\ln \left( \frac{[NCA]_t}{[NCA]_0} \right) = -\frac{SA}{V} k_b t \quad (6)$$

By incorporating equation (4) into equation (6), the apparent rate constant for the batch reaction  $k_b$  is

$$k_b = \frac{\ln(-Conversion + 1) V}{-SA * t} \quad (7)$$

As summarized in Table 2.1, the rate constants for the surface-initiated NCA polymerizations from **2.7@TiO<sub>2</sub>** were obtained at different reaction times based on equation (7). Small reaction rates were obtained for the heterogeneous polymerization carried out in the batch, and a small decrease of reaction rate was observed with extended reaction time. There are two possible reasons for the low reaction rates: one is due to the mass transport limitation, and the other is due to the low iron loading on the **2.7@TiO<sub>2</sub>** plate. To identify the role of mass transport plays in the surface-initiated polymerizations, we attempted to utilize continuous flow for the heterogeneous reactions.

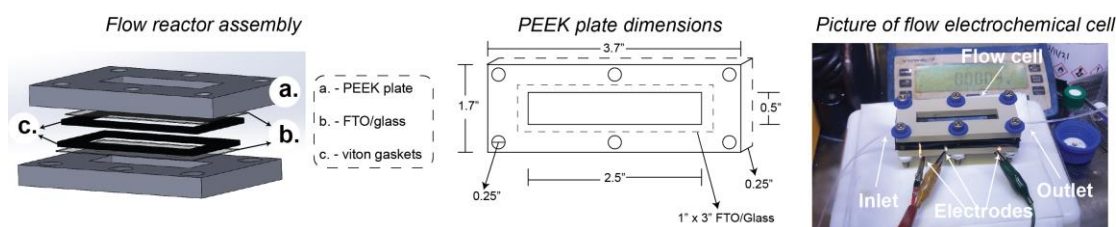


**Figure 2.11** Design of the microfluidic cell used for the heterogeneous surface-initiated Sar-NCA polymerization from **2.7@TiO<sub>2</sub>** plate.

The flow cell used for the model surface-initiated NCA polymerization was designed by Brandon Jolly and Prof. Chong Liu at UCLA. Figure 2.11 shows the design of the parallel cell, which is composed of polyetheretherketone (PEEK) plates spaced by viton gaskets to allow the position of a TiO<sub>2</sub> plate in the middle. The dimension of the TiO<sub>2</sub> spin-coated FTO plate used for the flow cell is 0.5 x 2 inches, which is different than what was being used in the batch. The iron(I) catalyst **2.7** was anchored on the larger plate by similar preparation we have developed and the resulting **2.7@TiO<sub>2</sub>** plate was put in the flow cell. A 0.08 M Sar-NCA solution in THF was flowed in and out of the cell under different flow rates and resident time ( $t_r$ ) to achieve surface-initiated NCA polymerizations. The corresponding monomer conversions were determined by <sup>1</sup>H NMR analysis of the aliquots taken at different times from the outlet of the microfluidic cell by Brandon, and summarized in Table 2.2.

**Table 2.2** Kinetics of the NCA polymerization from **2.7@TiO<sub>2</sub>** plate carried out in the microfluidic cell under different flow rate and residence time<sup>a</sup> of the Sar-NCA solution via a single cycle<sup>b</sup>.

Entry	NCA flow rate (mL/min)	$t_r$ (min)	Conversion %	$k_f$ (cm·s <sup>-1</sup> )
1	0.07	~14	3	$3.2 \times 10^{-3}$
2	0.12	~8	4	$4.0 \times 10^{-3}$
3	0.25	~4	5	$4.4 \times 10^{-3}$
4	0.50	~2	13	$1.3 \times 10^{-2}$

<sup>a</sup> The time for the NCA monomer solution to pass through the surface of **2.7@TiO<sub>2</sub>** plate.

<sup>b</sup> The overall time for monomer solution to flow in and out of the cell is 1 h in a single cycle.

With applying flow to the surface-initiated NCA polymerization reactions, rates were much improved compared with that obtained from the batch reactions. When the flow rate of NCA monomer solution is 0.07 mL/min and the residence time is 14 min, the corresponding monomer conversion was 3% (entry 1, Table 2.2). When increasing the flow rate of NCA monomer solution, monomer conversions increased to 4%, 5% and 13% at residence time  $t_r$  of 8 min, 4 min and 2 min, respectively (Table 2.2). The apparent rate constant for the reaction carried out in the microfluidic cell  $k_f$  was determined as well after normalization of the surface areas of TiO<sub>2</sub> plates used in the flow cell. The mathematical work derived by Brandon and Prof. Liu was summarized below.

At steady state, the monomer NCA concentration at the outlet (M),  $[NCA]_{out}$ , is a constant. At low conversions, the amount of NCA consumed is assumed to be approximately equal to the amount replenished under flow leading to equation (8), where  $Q$  (mL/min) is the flow rate, and  $[NCA]_{in}$  (M) is NCA concentration at the inlet of the microfluidic cell.

$$([NCA]_{in} - [NCA]_{out})\Delta t * Q = SA * k_f \left( \frac{[NCA]_{in} - [NCA]_{out}}{2} \right) \Delta t \quad (8)$$

The equation (8) can be modified to afford equation (9)

$$\left( 1 - \frac{[NCA]_{out}}{[NCA]_{in}} \right) Q = SA * k_f * \frac{1}{2} \left( 1 + \frac{[NCA]_{out}}{[NCA]_{in}} \right) \quad (9)$$

Analogous to equation (4), conversion in flow cell can be defined as

$$Conversion = 1 - \frac{[NCA]_{out}}{[NCA]_{in}} \quad (10)$$

To replace all concentration terms with conversion in equation (9), the parenthetical

term on the right-hand side can be re-written as:

$$1 + \frac{[NCA]_{out}}{[NCA]_{in}} = -Conversion + 2 \quad (11)$$

Inputting equation (10) and (11) into equation (9), the following expression for apparent rate constant in flow  $k_f$  can be expressed as:

$$k_f = \frac{2 * Conversion * Q}{SA(Conversion + 2)} \quad (12)$$

As shown in Table 2.2, the rate constant  $k_f$  was calculated to be  $3.2 \times 10^{-3}$  cm/s when flow rate was 0.07 mL/min. When the flow rate increased or the residence time decreased, the corresponding rate constant increased with  $k_f$  equaling to  $4.0 \times 10^{-3}$  cm/s,  $4.4 \times 10^{-3}$  cm/s and  $1.3 \times 10^{-2}$  cm/s (entry 2-4 in Table 2.2). The monomer conversion or apparent rate constant is proportional to the flow rate (Figure 2.12). Noteworthy, a monomer conversion of 14% can be achieved at  $t_r$  of 1 min in the flow cell, however, two days are required for the reaction carried out in the batch to obtain the comparable conversion. These results demonstrate that the mass transport is the significant limitation for surface-initiated NCA polymerization. Unlike the slow rate of surface-initiated NCA polymerization carried out in the batch, applying flow alleviates the mass transport problem and greatly enhance the rate of this heterogeneous polymerization reaction. Until now, only one work has demonstrated the combination of flow and a heterogeneous polymerization catalyst, Pd/C.<sup>44</sup> However, it was used for polycondensations to synthesize conjugated copolymers. To the best of our knowledge, the work shown here is the first example to apply continuous flow into the heterogeneous chain-growth polymerizations. We anticipate that the surface-initiated ROP system we have developed will enable quantitative

determination of molecular weight properties of the polymer brushes and thus, provide mechanistic understandings about the heterogeneous ROP.

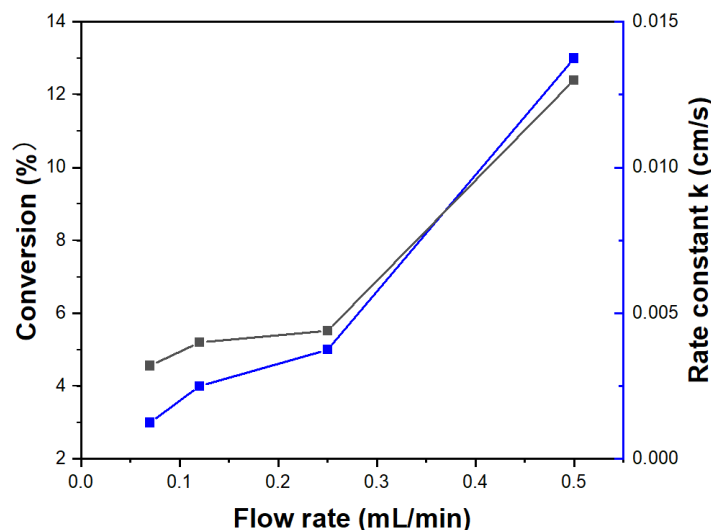


**Figure 2.12** Plots for NCA conversion and rate constant versus flow rate for NCA polymerizations on **2.7@TiO<sub>2</sub>** plates carried out in the microfluidic cell.

## 2.8 Conclusions

In this chapter, we demonstrated the support of an iron(I) complex **2.7** to a titania nanoparticle **2.7@TiO<sub>2</sub>** directly via protonolysis reaction. Like the molecular iron(I) catalyst, the anchored complex on **2.7@TiO<sub>2</sub>** remains its polymerization activities towards the Sar-NCA polymerization. In addition, an electrode with a porous TiO<sub>2</sub> layer spin-coated on conducting FTO support was constructed as a flat substrate for supporting iron(I) catalyst **2.7** and initiating Sar-NCA polymerization. The anchored catalyst on **2.7@TiO<sub>2</sub>** plate was characterized by employing the electrochemical method. As expected, the surface-attached catalyst exhibited its redox features during CV measurement and still retained its polymerization activity after a CV measurement. TGA, FT-IR and XPS were used to determine the chemical

compositions of polyamides grown from the surface of nanoparticles and plates. Efficient removal of the surface-bound poly(sarcosine) from nanoparticles was achieved by treating the surfaces with iodomethane. The cleaved polyamide was characterized by  $^1\text{H}$  NMR spectroscopy and GPC. Unlike the homogenous reaction, several different polymer species were formed on the surfaces of titania nanoparticles based on GPC. Possible explanations are the existence of several different active sites on surfaces or the diffusions of co-catalyst towards the surface-bound polymer might lead to different polymerization processes. To obtain more mechanistic insights about surface-initiated polymerization, kinetic studies were carried out by monitoring the NCA monomer conversion versus time using the polymerization initiated from the plate as the model reaction. When being conducted in the batch, the rate of the polymerization reaction was slow compared to reactions carried out in solutions. The application of flow could alleviate the mass transport limitation and greatly enhance the rate of this heterogeneous polymerization reaction. Comparable monomer conversion was achieved only in minute when applying flow compared with two days required for the reactions conducted in the batch.

With the improvement of reaction rate of the model heterogeneous polymerization by applying flow, our next step is to see whether the properties of surface-grown polymer will change or not. It will be interesting if the polymer growth is more under control under flow. To answer that question, cleavage will be tried to remove the polyamides from the plates after polymerization in the flow cell. As mentioned above, the remaining challenge for achieving the removal of polymers

from the plates carried out in solutions is the small amount of polymer products which is attributed to the relatively small plates and low monomer conversions observed. Since applying flow can improve the polymerization rate, the amount of polymers obtained on the plate can also be enhanced. Compared with the plate obtained from batch polymerization reaction, the larger amount of polymer solids that can be obtained from the plate in the microfluidic cell will enable the analysis of them by quantitative characterizations. This benefit will allow the determination of polymer molecular weight properties, and more importantly, mechanistic understandings of the heterogeneous polymerization reaction. These cleavage experiments are the subject of ongoing investigations.

Overall, we demonstrated here how redox-switchable ring-opening polymerization catalysis can be used under spatial control for polyamide synthesis. Specifically, an alternative way to synthesize polyamides is provided which is to synthesize polyamides on flat surface via applying flow followed by the removal of the polymer films. Sophisticated polyamide structures with controlled molecular weight properties might be accessible via the spatiotemporal control utilizing electrochemically redox-switchable polymerizations. Unlike the commonly used SSPS and normal NCA polymerization strategies discussed in Chapter 1 that both have their limitations, this efficient and mild method will fill the gap by enabling the synthesis of sequence-defined polyamide materials in a large scale.

## **Experimental Section**

**General Considerations.** Unless stated otherwise, all reactions were carried out in

oven-dried glassware in a nitrogen-filled glove box. Solvents (diethyl ether, tetrahydrofuran, toluene, etc) were used after passage through a solvent purification system under a blanket of argon and then degassed briefly by exposure to vacuum.<sup>45</sup> Iodomethane was purchased from Fisher Scientific and used without further purification. Titania P<sub>25</sub> nanoparticles were purchased from Sigma-Aldrich. Sarcosine amino acid was purchased from Acros Organics and used as received. Triphosgene was purchased from Chem-Impex International Inc. and used as received. use. Glassy carbon obtained from CHIInstrument was used as the working electrode for the electrochemical experiment. Platinum wire, lithium strip and tetrabutylammonium hexafluorophosphate (<sup>t</sup>Bu<sub>4</sub>PF<sub>6</sub>) (>99%) were purchased from Aldrich. Iron(I) monoalkyl complex **2.7** complex was synthesized as described previously.<sup>29</sup> FcBArF<sup>24</sup> was synthesized according to literature procedures.<sup>46</sup>

**Equipment and Analytical Methods.** Nuclear magnetic resonance (NMR) spectra were recorded at ambient temperature on either a Varian Gemini-600 (600 MHz) or Varian Inova-500 (500 MHz) NMR spectrometer. Centrifugation was carried out for purifications of polymers or nanoparticles using the Sorvall Legend X1 Centrifuge (Thermo Fisher, Germany.) at 10000 RPM operating for 10 minutes. Size exclusion chromatography (SEC) was carried out with a Tosoh's high-performance SEC system HLC-8320GPC containing TSKgel Alpha-M columns at 50 °C and a flow rate of 0.6 mL/min. The eluent used was HPLC grade N,N-Dimethylformamide (DMF) with 0.01 M LiBr. Polystyrene standards (ReadyCal Kit, Sigma-Aldrich #81434) were used to determine the molecular weight and molecular weight distribution of the polymers.

Prior to injection, the polymers were dissolved in DMF and filtered through a 0.20  $\mu\text{m}$  polytetrafluoroethylene (PTFE) filter. UV-irradiation of the  $\text{TiO}_2$  nanoparticles and plates were processed using the Model 42 UVO-Cleaner (Jelight Company Inc.). Preparation of  $\text{TiO}_2$ -FTO plate was carried out following a previously reported method using the spin-coater (Laurell WS-400E).<sup>38</sup> X-ray photoelectron spectroscopy (XPS) was measured on a Thermo Scientific K-Alpha+ X-ray photoelectron spectrometer. ATR FT-IR spectra were recorded using a Bruker Vertex 70 FTIR spectrometer (Billerica, MA) equipped with an MCT detector (FTIR-16; Infrared Associates; Stuart, FL). Inductively coupled plasma optical emission spectrometry (ICP-OES) was performed on an Agilent 5100 instrument that was calibrated using known concentrations of standard solutions to quantify Fe. 1000 ppm Fe standard solution was purchased from Sigma-Aldrich. Thermal gravimetric analysis (TGA) was carried out on an STA 449 F1 Jupiter  $\text{\textcircled{R}}$  from NETZSCH (NETZSCH- Gerätebau GmbH Wittelsbacherstraße 42 95100 Selb Germany) under a constant flow of nitrogen (40 mL/min) and a heating rate of 5  $^\circ\text{C}/\text{min}$ . Samples were prepared in  $\text{Al}_2\text{O}_3$  crucibles, heated from ambient temperatures to 120  $^\circ\text{C}$  and held at 120  $^\circ\text{C}$  for 30 min to remove any solvent or water residues and then were further ramped to 500  $^\circ\text{C}$ .

**Synthesis of Sar-NCA.** Sar-NCA was synthesized based on modified procedures reported from the literature.<sup>47</sup> Phosgene detector strips were placed near the working areas to indicate the formation of any toxic phosgene. Sarcosine (1.16 g, 13.0 mmol) was weighed in a two-neck flask equipped with a condenser and dried *in vacuo* for 1 hour. Triphosgene (2.32 g, 7.81 mmol) was dissolved in 50 ml of anhydrous THF and

added to the sarcosine suspension. The suspension was allowed to stir under active nitrogen flow into a bottle of concentrated sodium hydroxide to quench any phosgene decomposed from the excess of triphosgene. The reaction was heated at 50 °C for 4 h until the suspension became homogeneous and clear. THF was removed *in vacuo* to give a brown oil and then further dried at 50 °C to obtain an amorphous solid. The solid was re-dissolved in 5 mL of THF at 50 °C and precipitated into 20 mL of hexane. The crude solid was collected by vacuum filtration and dried *in vacuo* overnight. Sublimation of the solid was carried out under high vacuum at 80-85 °C to leave a fine white powder (Sar-NCA, 49%). The product was collected from the sublimation apparatus in a nitrogen-filled glove box and stored in the freezer. <sup>1</sup>H NMR (500 MHz, CDCl<sub>3</sub>)<sup>47</sup>: δ (ppm) = 2.86 (s, 3H, NH-CH<sub>3</sub>), 4.22 (s, 2H, NH-CH<sub>2</sub>-CO).

**Procedure for anchoring the iron complex onto P25 TiO<sub>2</sub> powder.** Before bringing into the nitrogen-filled glovebox, the P25 TiO<sub>2</sub> powder was heated under reduced pressure (10<sup>-2</sup> torr) at 130 °C for 1 day with stirring to remove any physically bound water on the surface. In a nitrogen-filled glove box, iron bis(imino)pyridine alkyl **1** (25.0 mg, 0.05 mmol) was dissolved in 4 ml of diethyl ether at -35°C. The solution was added to P25 TiO<sub>2</sub> (150 mg) in the dark and allowed to stir at room temperature for 1 hour. The suspension was centrifuged and washed with diethyl ether (2 ml × 3) and tetrahydrofuran (2 ml) until the supernatant was colorless. The final **2.7@TiO<sub>2</sub>** powder was light blue in color. The powder was soaked in 20 mL 1% nitric acid solution overnight to digest iron complex from **2.7@TiO<sub>2</sub>**. The solution was then subjected to centrifugation and used for ICP-OES characterization which shows that

the iron concentration on TiO<sub>2</sub> powder is  $0.50 \pm 0.25$  wt%.

**Representative procedure for the surface-initiated polymerization of Sar-NCA on the 2.7@TiO<sub>2</sub> powder.** In a nitrogen-filled glove box, 2.7@TiO<sub>2</sub> nanoparticles (30.0 mg, 0.390 wt% Fe, 2.64  $\mu$ mol Fe) was suspended in a solution of Sar-NCA (30.4 mg, 264  $\mu$ mol), CoBAR<sup>F24</sup> (2.78 mg, 2.64  $\mu$ mol) and 1,3,5-trimethoxy benzene (13.0 mg, 77.3  $\mu$ mol) dissolved in THF (1.42 mL). The mixture was allowed to stir vigorously at room temperature. Aliquots were taken periodically, quenched with a small amount of benzoic acid, and the solvent was removed *in vacuo*. The mixture was centrifuged to separate the powder from the supernatant. Monomer conversion was tracked by comparing the relative integration of the methylene peaks of the remaining Sar-NCA (s, 4.1 ppm) to the methine peaks of the internal standard (s, 6.1 ppm) in the supernatant by <sup>1</sup>H NMR. The powder was washed with THF (5 mL) and each wash was followed by centrifugation with  $120 \pm 20$  mg 2.7@TiO<sub>2</sub> nanoparticles being recovered.

**Removing poly(sarcosine) from the surface of Fe(I)-TiO<sub>2</sub> nanoparticles.** On the bench in air, the nanoparticles (15.0 mg) obtained from the surface-initiated polymerization of Sar-NCA were suspended in dichloromethane (5.00 mL) in a 7- mL vial. Iodomethane (0.100 mL, 0.230 g, 1.60 mmol) was added to the suspension of the TiO<sub>2</sub> powder dropwise. The reaction mixture was allowed to stir at room temperature for 16 hours. The solvent was removed under vacuum. The remaining solid was then washed 3 times with dichloromethane (10.0 mL), following each wash with centrifugation. The supernatant and washes were combined, and the solvent was

removed *in vacuo*. The resulting solid was redissolved with a minimum amount of chloroform (0.600 mL) and precipitated in diethyl ether (5.00 mL). The polymer solid (1.00 mg) was collected after centrifugation and dried under vacuum for further analysis by  $^1\text{H}$  NMR and GPC to get polymer composition and molecular weight properties, respectively.

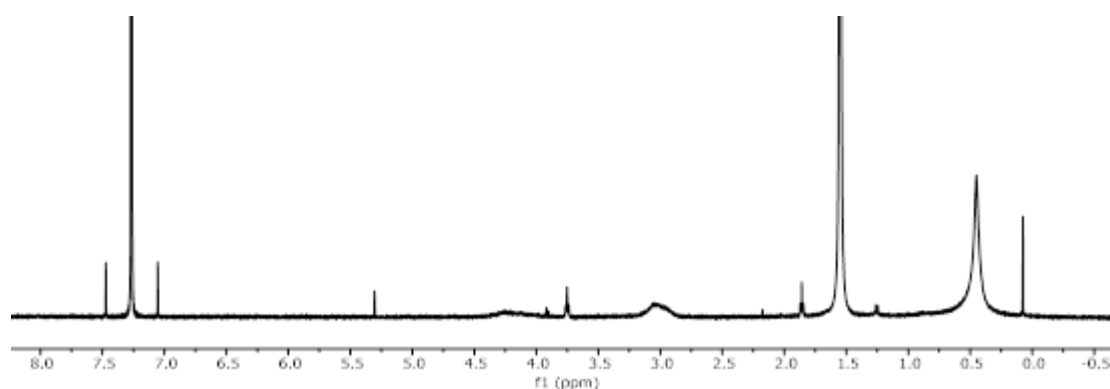


**Figure S 2.1** Original  $^1\text{H}$  NMR of the cleaved poly(sarcosine) in  $\text{CDCl}_3$ .

Specific analysis is shown in Figure 2.6 (b).

**Representative procedure for anchoring iron(I) complex on the spin-coated  $\text{TiO}_2$  plate.** Prior to bring the spin-coated plates into the glovebox, the plates were first treated with UV/ozone for 30 min to enhance the -OH density and then heated under reduced pressure (lower than  $10^{-2}$  torr) at  $130\text{ }^\circ\text{C}$  for 2 days to remove the surface bound water. The plates were soaked into a solution of bis(imino)pyridine iron monoalkyl complex **1** (25.0 mg, 50.0  $\mu\text{mol}$ ) in diethyl ether (10.0 mL) at  $-35\text{ }^\circ\text{C}$  in the dark in a 20-mL vial for 1 h. The supernatant was dried *in vacuo* and analyzed by  $^1\text{H}$  NMR in  $\text{C}_6\text{D}_6$ . The plates were washed with diethyl ether (2.00 mL  $\times$  3) and THF (2.00 mL) until the washing was colorless. The resulting Fe(I)- $\text{TiO}_2$  plate was soaked in 20 mL 1% nitric acid solution overnight to digest iron complex. The solution was

then subjected to centrifugation and used for ICP-OES characterization which shows that the iron loading on spin-coated TiO<sub>2</sub> plate is within the range of 0.02±0.005 umol/cm<sup>2</sup>.

**Representative procedure for the surface-initiated polymerization of Sar-NCA on the Fe(I)-TiO<sub>2</sub> plate carried out in batch.** In a nitrogen-filled glovebox, Fe(I)-TiO<sub>2</sub> plate was soaked in a THF (5.00 mL) solution of Sar-NCA (50.0 mg, 0.430 mmol), CoBAR<sup>F24</sup> (4.60 mg, 4.30 umol) and 1,3,5-trimethoxy benzene (33.0 mg, 0.200 mmol) in a 7-mL vial stirring at 1000 rpm in the dark. Aliquots were taken periodically for sampling, quenched with a small amount of benzoic acid and the solvent was removed *in vacuo*. Conversion was determined by comparing the ratio of methine signal of 1,3,5-trimethoxybenzene to the methine polymer and monomer signals for Sar-NCA on <sup>1</sup>H NMR.

**Representative procedure for CV measurements of surface-bound Fe(I)-catalyst.** In an argon-filled glovebox, the cyclic voltammetry (CV) measurement of surface-bound Fe(I) was conducted using a three-electrode configuration, where the Fe(I)-modified TiO<sub>2</sub>-FTO plate was used as the working electrode, and the platinum wire served as the counter electrode and the lithium strip was used as the reference electrode. A 0.1 M solution of Bu<sub>4</sub>PF<sub>6</sub> in THF was used as the electrolyte. Measurements were taken with a scan rate of 50 mV/s. Electrochemical potentials were calibrated relative to a ferrocenium/ferrocene redox potential in another control experiment.

**Homogeneous polymerization of Sar-NCA.** In a nitrogen-filled glove box, Sar-NCA

(25.0 mg, 0.220 mmol) was dissolved in THF (0.750 ml) in a 7 mL-vial. Iron(I) neopentyl alkoxide complex (1.10 mg, 2.20  $\mu\text{mol}$ ) was dissolved in 0.25 ml of THF and  $\text{CoBAR}^{\text{F24}}$  (2.32 mg, 2.20  $\mu\text{mol}$ ) was dissolved in 0.25 mL of THF. The three solutions were combined together and stirred at room temperature for 10 min. Reaction was terminated with benzoic acid and dried *in vacuo* to afford a brown solid. The solid was then dissolved in chloroform (0.6 mL) and precipitated into diethyl ether (5 mL). The poly(sarcosine) was isolated by centrifugation and further dried *in vacuo*. Due to the overlap of monomer and polymer signals for Sar-NCA by  $^1\text{H}$  NMR, conversion was instead determined based on the mass of the collected poly(sarcosine).

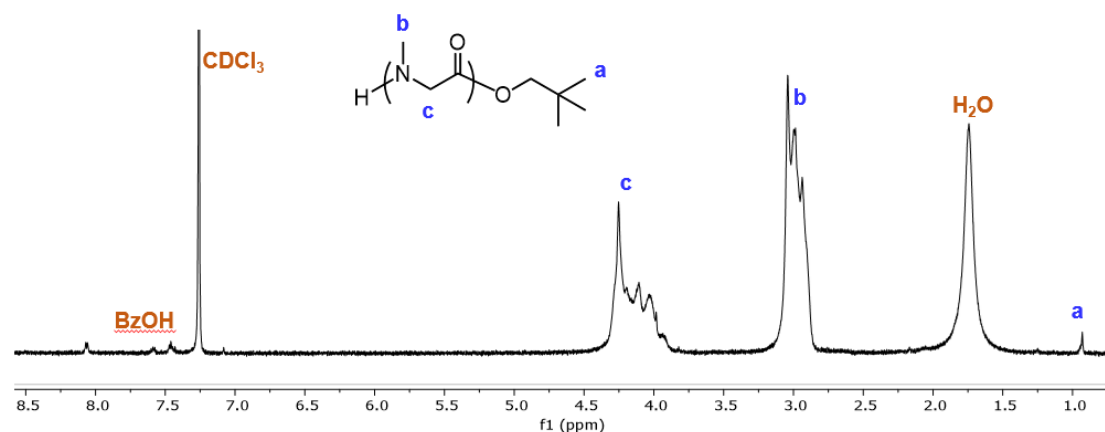


**Figure S 2.2**  $^1\text{H}$  NMR of precipitated homogeneous poly(sarcosine) in  $\text{CDCl}_3$ .

**Treatment of iodomethane for homogeneous poly(sarcosine).** Poly(sarcosine) (5.00 mg) was dissolved in 5 mL  $\text{CH}_2\text{Cl}_2$  in a 7-mL vial. Methyl iodide (100  $\mu\text{L}$ ) was added dropwise to the polymer solution and the solution was allowed to stir overnight at room temperature. After that, the solution was dried *in vacuo* to afford a yellow solid. The solid was redissolved by chloroform (0.6 mL) and the solution was added to diethyl ether (5 mL) to precipitate out the poly(sarcosine). The polymer product was

washed by diethyl ether (5 mL x3) followed by the centrifugation. The final product (3 mg) was collected after being dried *in vacuo*.

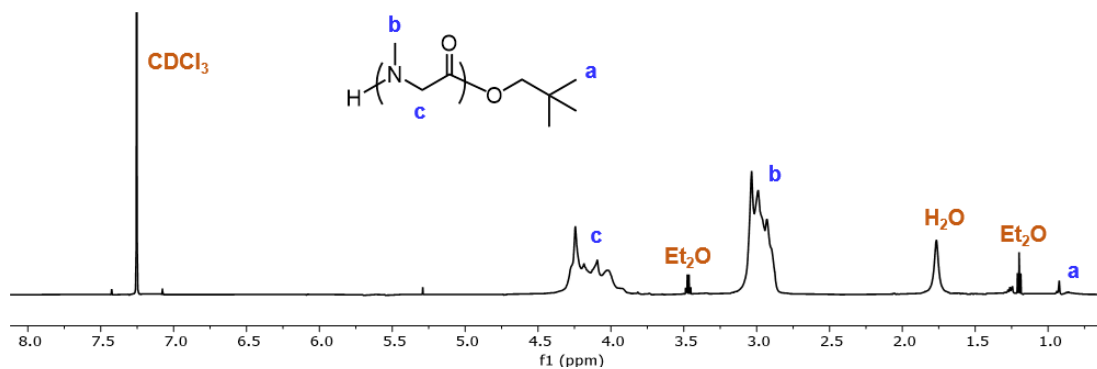


**Figure S 2.3** <sup>1</sup>H NMR of the homogeneous poly(sarcosine) after the iodomethane treatment in CDCl<sub>3</sub>.

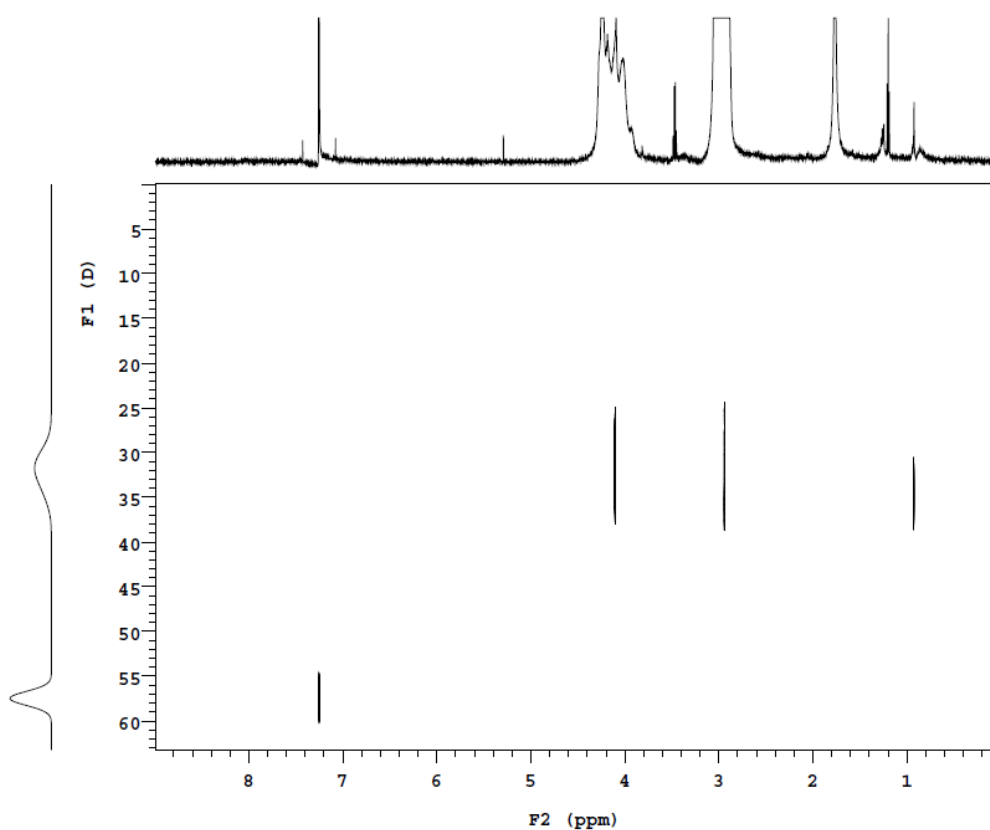


**Figure S 2.4** Diffusion ordered spectroscopy (DOSY) of the homogeneous poly(sarcosine) after iodomethane treatment. Only single polymer species existed after the methyl iodide treatment.

## References

- (1) Bozokalfa, G.; Akbulut, H.; Demir, B.; Guler, E.; Gumus, Z. P.; Odaci Demirkol, D.; Aldemir, E.; Yamada, S.; Endo, T.; Coskunol, H.; Timur, S.; Yagci, Y. Polypeptide Functional Surface for the Aptamer Immobilization: Electrochemical Cocaine Biosensing. *Anal. Chem.* **2016**, *88* (7), 4161–4167. DOI: 10.1021/acs.analchem.6b00760
- (2) Demir, B.; Yilmaz, T.; Guler, E.; Gumus, Z. P.; Akbulut, H.; Aldemir, E.; Coskunol, H.; Colak, D. G.; Cianga, I.; Yamada, S.; Timur, S.; Endo, T.; Yagci, Y. Polypeptide with Electroactive Endgroups as Sensing Platform for the Abused Drug ‘Methamphetamine’ by Bioelectrochemical Method. *Talanta* **2016**, *161*, 789–796. DOI: 0.1016/j.talanta.2016.09.042.
- (3) Park, K.; Jeong, H.; Tanum, J.; Yoo, J. C.; Hong, J. Poly-l-Lysine/Poly-l-Glutamic Acid-Based Layer-by-Layer Self-Assembled Multilayer Film for Nitric Oxide Gas Delivery. *J. Ind. Eng. Chem.* **2019**, *69*, 263–268. DOI: 10.1016/j.jiec.2018.09.005
- (4) Jiang, B.; Defusco, E.; Li, B. Polypeptide Multilayer Film Co-Delivers Oppositely-Charged Drug Molecules in Sustained Manners. *Biomacromolecules* **2010**, *11* (12), 3630–3637. DOI: 10.1021/bm1010855
- (5) Gao, Q.; Yu, M.; Su, Y.; Xie, M.; Zhao, X.; Li, P.; Ma, P. X. Rationally Designed Dual Functional Block Copolymers for Bottlebrush-like Coatings: In Vitro and in Vivo Antimicrobial, Antibiofilm, and Antifouling Properties. *Acta Biomater.* **2017**, *51*, 112–124. DOI: 10.1016/j.actbio.2017.01.061.

- (6) Yuran, S.; Dolid, A.; Reches, M. Resisting Bacteria and Attracting Cells: Spontaneous Formation of a Bifunctional Peptide-Based Coating by On-Surface Assembly Approach. *ACS Biomater. Sci. Eng.* **2018**, *4* (12), 4051–4061. DOI: 10.1021/acsbiomaterials.8b00885.
- (7) Chang, Y. C.; Frank, C. W. Grafting of Poly( $\gamma$ -Benzyl-L-Glutamate) on Chemically Modified Silicon Oxide Surfaces. *Langmuir* **1996**, *12* (24), 5824–5829. DOI:10.1021/LA950686M.
- (8) Heise, A.; Menzel, H.; Yim, H.; Foster, M. D.; Wieringa, R. H.; Schouten, A. J.; Erb, V.; Stamm, M. Grafting of Polypeptides on Solid Substrates by Initiation of N-Carboxyanhydride Polymerization by Amino-Terminated Self-Assembled Monolayers. *Langmuir* **1997**, *13* (4), 723–728. DOI: 10.1021/LA960467G.
- (9) Audouin, F.; Fox, M.; Larragy, R.; Clarke, P.; Huang, J.; O'Connor, B.; Heise, A. Polypeptide-Grafted Macroporous PolyHIPE by Surface-Initiated N-Carboxyanhydride (NCA) Polymerization as a Platform for Bioconjugation. *Macromolecules* **2012**, *45* (15), 6127–6135. DOI: 10.1021/ma3010263
- (10) Zhang, C.; Yuan, J.; Lu, J.; Hou, Y.; Xiong, W.; Lu, H. From Neutral to Zwitterionic Poly( $\alpha$ -Amino Acid) Nonfouling Surfaces: Effects of Helical Conformation and Anchoring Orientation. *Biomaterials* **2018**, *178*, 728–737. DOI: 10.1016/j.biomaterials.2018.01.052.
- (11) Uyama, Y.; Kato, K.; Ikada, Y. Surface Modification of Polymers by Grafting. *Adv. Polym. Sci.* **1998**, *137*, 1–39. DOI:10.1007/3-540-69685-7\_1
- (12) Kato, K.; Uchida, E.; Kang, E. T.; Uyama, Y.; Ikada, Y. Polymer Surface with

- Graft Chains. *Prog. Polym. Sci.* **2003**, *28* (2), 209–259. DOI:10.1016/S0079-6700(02)00032-1.
- (13) Minko, S. Grafting on Solid Surfaces: “Grafting to” and “Grafting from” Methods. *Polym. Surfaces Interfaces Charact. Modif. Appl.* **2008**, 215–234. DOI:10.1007/978-3-540-73865-7\_11.
- (14) Zdyrko, B.; Luzinov, I. Polymer Brushes by the “Grafting to” Method. *Macromol. Rapid Commun.* **2011**, *32* (12), 859–869. DOI:10.1002/MARC.201100162.
- (15) Edmondson, S.; Osborne, V. L.; Huck, W. T. S. Polymer Brushes via Surface-Initiated Polymerizations. *Chem. Soc. Rev.* **2004**, *33* (1), 14–22. DOI: 10.1039/B210143M.
- (16) Rowe-Konopacki, M. D.; Boyes, S. G. Synthesis of Surface Initiated Diblock Copolymer Brushes from Flat Silicon Substrates Utilizing the RAFT Polymerization Technique. *Macromolecules* **2007**, *40* (4), 879–888. DOI: 10.1021/ma0623340.
- (17) Chen, W. L.; Cordero, R.; Tran, H.; Ober, C. K. 50th Anniversary Perspective: Polymer Brushes: Novel Surfaces for Future Materials. *Macromolecules* **2017**, *50* (11), 4089–4113. DOI: 10.1021/acs.macromol.7b00450.
- (18) Wibowo, S. H.; Sulistio, A.; Wong, E. H. H.; Blencowe, A.; Qiao, G. G. Polypeptide Films via N-Carboxyanhydride Ring-Opening Polymerization (NCA-ROP): Past, Present and Future. *Chem. Commun.* **2014**, *50* (39), 4971–4988. DOI: 10.1039/C4CC00293H.

- (19) Xu, Z.; Feng, Y.; Liu, X.; Guan, M.; Zhao, C.; Zhang, H. Synthesis and Characterization of Fe<sub>3</sub>O<sub>4</sub>@SiO<sub>2</sub>@poly-L-Alanine, Peptide Brush–Magnetic Microspheres through NCA Chemistry for Drug Delivery and Enrichment of BSA. *Colloids Surfaces B Biointerfaces* **2010**, *81* (2), 503–507. DOI: 10.1016/j.colsurfb.2010.07.048.
- (20) Shen, Y.; Li, Z.; Klok, H. A. Polypeptide Brushes Grown via Surface-Initiated Ring-Opening Polymerization of  $\alpha$ -Amino Acid N-Carboxyanhydrides. *Chinese J. Polym. Sci.* **2015**, *33* (7), 931–946. DOI: 10.1007/s10118-015-1654-7.
- (21) Lu, L.; Lahasky, S. H.; McCandless, G. T.; Zhang, D.; Garno, J. C. Thermoresponsive Behavior of Polypeptoid Nanostructures Investigated with Heated Atomic Force Microscopy: Implications toward the Development of Smart Coatings for Surface-Based Sensors. *ACS Appl. Nano Mater.* **2019**, *2* (12), 7617–7625. DOI: 10.1021/acsanm.9b01715.
- (22) Yang, C.; Shi, Z.; Feng, C.; Li, R.; Luo, S.; Li, X.; Ruan, L.; Yang, C.; Shi, Z.; Li, R.; Luo, S.; Ruan, L.; Feng, C.; Li, X. An Adjustable PH-Responsive Drug Delivery System Based on Self-Assembly Polypeptide-Modified Mesoporous Silica. *Macromol. Biosci.* **2020**, *20* (6), 2000034. DOI: 10.1002/mabi.202000034.
- (23) Witte, P.; Menzel, H. Nickel-Mediated Surface Grafting from Polymerization of  $\alpha$ -Amino Acid-N-Carboxyanhydrides. *Macromol. Chem. Phys.* **2004**, *205* (13), 1735–1743. DOI: 10.1002/macp.200400100.

- (24) Sparks, B. J.; Ray, J. G.; Savin, D. A.; Stafford, C. M.; Patton, D. L. Synthesis of Thiol-Clickable and Block Copolypeptide Brushes Via Nickel-Mediated Surface Initiated Polymerization of  $\alpha$ -Amino Acid N-Carboxyanhydrides (NCAs). *Chem. Commun.* **2011**, 47 (22), 6245–6247. DOI: 10.1039/C1CC11534K.
- (25) Stukenkemper, T.; Paquez, X.; Verhoeven, M. W. G. M.; Hensen, E. J. M.; Dias, A. A.; Brougham, D. F.; Heise, A. Polypeptide Polymer Brushes by Light-Induced Surface Polymerization of Amino Acid N-Carboxyanhydrides. *Macromol. Rapid Commun.* **2018**, 39 (7). DOI: 10.1002/marc.201700743.
- (26) Biernesser, A. B.; Li, B.; Byers, J. A. Redox-Controlled Polymerization of Lactide Catalyzed by Bis(Imino)Pyridine Iron Bis(Alkoxide) Complexes. *J. Am. Chem. Soc.* **2013**, 135 (44), 16553–16560. DOI:10.1021/ja407920d.
- (27) Biernesser, A. B.; Chiaie, K. R. D.; Curley, J. B.; Byers, J. A. Block Copolymerization of Lactide and an Epoxide Facilitated by a Redox Switchable Iron-Based Catalyst. *Angew. Chemie Int. Ed.* **2016**, 55 (17), 5251–5254. DOI:10.1002/ANIE.201511793.
- (28) Qi, M.; Dong, Q.; Wang, D.; Byers, J. A. Electrochemically Switchable Ring-Opening Polymerization of Lactide and Cyclohexene Oxide. *J. Am. Chem. Soc.* **2018**, 140 (17), 5686–5690. DOI: 10.1021/jacs.8b02171.
- (29) Delle Chiaie, K. R.; Biernesser, A. B.; Ortuño, M. A.; Dereli, B.; Iovan, D. A.; Wilding, M. J. T.; Li, B.; Cramer, C. J.; Byers, J. A. The Role of Ligand Redox Non-Innocence in Ring-Opening Polymerization Reactions Catalysed by

- Bis(Imino)Pyridine Iron Alkoxide Complexes. *Dalt. Trans.* **2017**, *46* (38), 12971–12980. DOI:10.1039/C7DT03067C.
- (30) Thompson, M. S. Redox-Switchable Copolymerization: Transforming Underutilized Monomer Feedstocks to Complex Copolymers, Ph.D. Dissertation, Boston College, Boston, MA, 2021.
- (31) Yan, Y.; Pageni, P.; Kabir, M. P.; Tang, C. Metallocenium Chemistry and Its Emerging Impact on Synthetic Macromolecular Chemistry. *Synlett* **2016**, *27*, 984–1005. DOI: 10.1055/s-0035-1561504.
- (32) Qi, M.; Zhang, H.; Dong, Q.; Li, J.; Musgrave, R. A.; Zhao, Y.; Dulock, N.; Wang, D.; Byers, J. A. Electrochemically Switchable Polymerization from Surface-Anchored Molecular Catalysts. *Chem. Sci.* **2021**, *12* (26), 9042–9052. DOI:10.1039/D1SC02163J.
- (33) Zhu, H.; Chen, Y.; Yan, F. J.; Chen, J.; Tao, X. F.; Ling, J.; Yang, B.; He, Q. J.; Mao, Z. W. Polysarcosine Brush Stabilized Gold Nanorods for in Vivo Near-Infrared Photothermal Tumor Therapy. *Acta Biomater.* **2017**, *50*, 534–545. DOI:10.1016/J.ACTBIO.2016.12.050.
- (34) Fetsch, C.; Luxenhofer, R. Thermal Properties of Aliphatic Polypeptoids. *Polymers.* **2013**, *5* (1), 112-127. DOI: 10.3390/polym5010112.
- (35) Zoppe, J. O.; Ataman, N. C.; Mocny, P.; Wang, J.; Moraes, J.; Klok, H. A. Surface-Initiated Controlled Radical Polymerization: State-of-the-Art, Opportunities, and Challenges in Surface and Interface Engineering with Polymer Brushes. *Chem. Rev.* **2017**, *117* (3), 1105–1318. DOI:

- 10.1021/acs.chemrev.6b00314.
- (36) Priftis, D.; Sakellariou, G.; Hadjichristidis, N.; Penott, E. K.; Lorenzo, A. T.; Müller, A. J. Surface Modification of Multiwalled Carbon Nanotubes with Biocompatible Polymers via Ring Opening and Living Anionic Surface Initiated Polymerization. Kinetics and Crystallization Behavior. *J. Polym. Sci. A Polym. Chem.* **2009**, *47* (17), 4379–4390. DOI: DOI:10.1002/POLA.23491.
- (37) Carlsson, L.; Utsel, S.; Wågberg, L.; Malmström, E.; Carlmark, A. Surface-Initiated Ring-Opening Polymerization from Cellulose Model Surfaces Monitored by a Quartz Crystal Microbalance. *Soft Matter* **2011**, *8* (2), 512–517. DOI:10.1039/C1SM06121F.
- (38) Hoertz, P. G.; Chen, Z.; Kent, C. A.; Meyer, T. J. Application of High Surface Area Tin-Doped Indium Oxide Nanoparticle Films as Transparent Conducting Electrodes. *Inorg. Chem.* **2010**, *49* (18), 8179–8181. DOI: 10.1021/ic100719r.
- (39) Yu, H.; Ingram, N.; Rowley, J. V.; Parkinson, S.; Green, D. C.; Warren, N. J.; Thornton, P. D. Thermoresponsive Polysarcosine-Based Nanoparticles. *J. Mater. Chem. B* **2019**, *7* (26), 4217–4223. DOI: 10.1039/C9TB00588A.
- (40) Birke, A.; Ling, J.; Barz, M. Polysarcosine-Containing Copolymers: Synthesis, Characterization, Self-Assembly, and Applications. *Prog. Polym. Sci.* **2018**, *81*, 163–208. DOI: 10.1016/j.progpolymsci.2018.01.002
- (41) Zoppe, J. O.; Ataman, N. C.; Mocny, P.; Wang, J.; Moraes, J.; Klok, H.-A. Correction to Surface-Initiated Controlled Radical Polymerization: State-of-the-Art, Opportunities, and Challenges in Surface and Interface Engineering

- with Polymer Brushes. *Chem. Rev.* **2017**, *117* (5), 4667.  
DOI:10.1021/ACS.CHEMREV.7B00093.
- (42) Marx, K. A. Quartz Crystal Microbalance: A Useful Tool for Studying Thin Polymer Films and Complex Biomolecular Systems at the Solution - Surface Interface. *Biomacromolecules* **2003**, *4* (5), 1099–1120. DOI: 10.1021/bm020116i.
- (43) Husseman, M.; Malmström, E. E.; McNamara, M.; Mate, M.; Mecerreyes, D.; Benoit, D. G.; Hedrick, J. L.; Mansky, P.; Huang, E.; Russell, T. P.; Hawker, C. J. Controlled Synthesis of Polymer Brushes by “Living” Free Radical Polymerization Techniques. *Macromolecules* **1999**, *32* (5), 1424–1431. DOI:10.1021/MA981290V.
- (44) Jin, S. H.; Ko, W.; Lee, S.; Hwang, Y. J. Combining Flow Synthesis and Heterogenous Catalysis for the Preparation of Conjugated Polymers. *Polym. Chem.*, **2022**, *13*, 3171-3178. DOI: 10.1039/D2PY00362G.
- (45) Pangborn, A. B.; Giardello, M. A.; Grubbs, R. H.; Rosen, R. K.; Timmers, F. J. Safe and Convenient Procedure for Solvent Purification. *Organometallics* **1996**, *15* (5), 1518–1520. DOI: 10.1021/om9503712.
- (46) Le Bras, J.; Jiao, H.; Meyer, W. E.; Hampel, F.; Gladysz, J. A. Synthesis, Crystal Structure, and Reactions of the 17-Valence-Electron Rhenium Methyl Complex  $[(\text{H}5\text{-C}5\text{Me}5)\text{Re}(\text{NO})(\text{P}(\text{4-C}6\text{H}4\text{CH}3)_3)(\text{CH}3)]^+ \text{B}(\text{3,5-C}6\text{H}3(\text{CF}3)_2)_4^-$ : Experimental and Computational Bonding Comparisons with 18-Electron Methyl and Methylidene Complexes. *J. Organometallic. Chem.*

2000, 616 (1–2), 54–66. DOI: 10.1016/S0022-328X(00)00531-3.

- (47) Klinker, K.; Schäfer, O.; Huesmann, D.; Bauer, T.; Capelôa, L.; Braun, L.; Stergiou, N.; Schinnerer, M.; Dirisala, A.; Miyata, K.; Osada, K.; Cabral, H.; Kataoka, K.; Barz, M. Secondary-Structure-Driven Self-Assembly of Reactive Polypept(o)ides: Controlling Size, Shape, and Function of Core Cross-Linked Nanostructures. *Angew. Chem. Int. Ed.* **2017**, *56* (32), 9608–9613. DOI: 10.1002/anie.201702624.

## Chapter 3. Efforts towards Integrated Catalysis of Polyamide Synthesis

### 3.1 Introduction

As mentioned in Chapter 1, our eventual goal is to achieve the integrated catalysis of polyamide synthesis from amino acids and CO<sub>2</sub> via the NCA formation and its in-situ polymerization. In that regard, incompatibilities between the two separate reaction systems need to be solved which requires more delicate design of the method(s) to anchor catalysts and additional compatibility tests for all the additives involved in the two systems.

In Chapter 2, we developed a facile approach to directly support the polymerization catalyst on a surface for surface-initiated polymerization of NCA. However, its inherent and potential drawbacks limit the future development towards integration. First, the pK<sub>a</sub> of Ti-OH is more similar to phenols (pK<sub>a</sub> < 10) than aliphatic alcohols, while the homogeneous NCA polymerization is normally initiated from iron(I) neopentyl alkoxide **2.1** based on the previous study.<sup>1</sup> In addition, the polymer density is always limited by using this attachment method, which has been confirmed by the small water contact-angles (within the range of 15-20°) in our previous study compared with those for drop-casted polyesters/polyethers.<sup>2</sup> More importantly, this anchoring method to immobilize iron catalyst on surface through its iron center is not the optimal way to allow the spatiotemporal control of polyamide synthesis: (1) the distance between surface and iron center will be increasing that could lower the switching rate caused by the slow charge transfer as polymerization proceeds; (2) The iron catalysts, which are located at the polymer chain ends, will be

removed after cleaving the surface-bound polyamides from solid support (Figure 3.1, a). To resolve these limitations, another attachment method, which will rely on immobilizing catalysts through their ligands, is required. With applying this anchoring strategy, the distance between the solid surface and iron centers will remain constant during the polymerization process, which can facilitate the ability to recycle the supported catalysts (Figure 3.1 b).

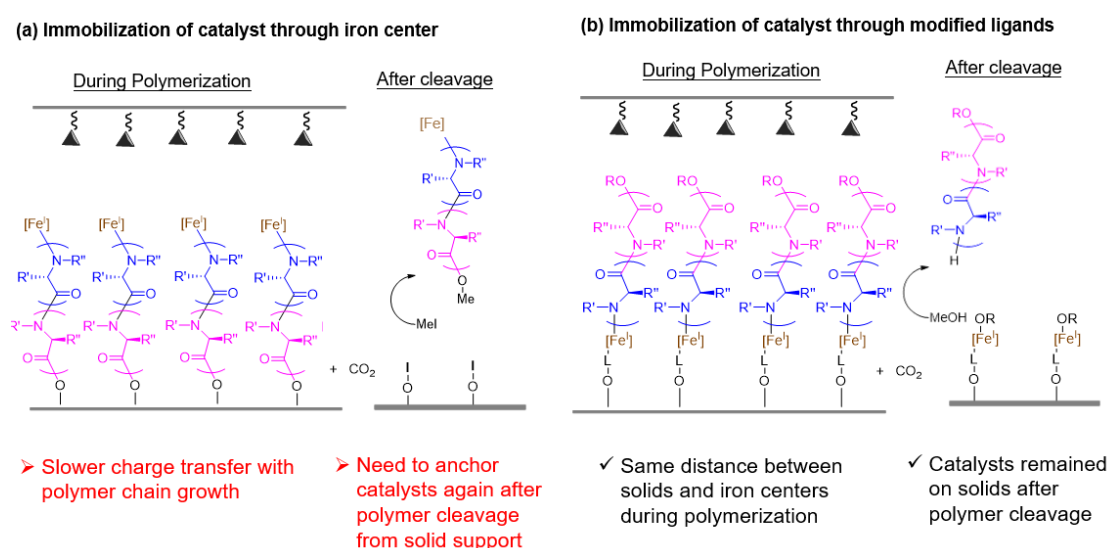


**Figure 3.1** Drawbacks of attaching catalyst through iron center ((a), method described in Chapter 2) versus advantages of anchoring catalyst through modified ligands ((b), method discussed in Chapter 3).

In this chapter, efforts towards investigating this anchoring method to support polymerization catalysts on a surface through their ancillary ligands and compatibility tests for integration with NCA synthesis will be discussed, respectively.

### 3.2 Different attachment methods of polymerization catalyst on surface

Self-assembled monolayer (SAM) is a structural assembly that can provide

well-ordered and densely packed films of functional molecules on surfaces.<sup>3,4</sup> Synthesis of SAM is a powerful strategy through either a silane linker or a phosphate linker on the surface of metal oxides,<sup>5-8</sup> or a thiol linker on the surface of gold nanoparticles<sup>9,10</sup> to introduce organic residues on inorganic substrates. The functional group-modified surfaces have been used widely to support organic compounds through a variety of organic reactions, such as nucleophilic substitutions<sup>11-17</sup>, “click” chemistry<sup>18-22</sup>, and photochemical reactions<sup>23-29</sup>. These modified organic-inorganic surfaces have been widely applied in organic solar cells<sup>30</sup>, electron transfer<sup>31,32</sup> and surface patterning<sup>33,34</sup>. By synthesizing SAMs on the surfaces, therefore, we expect to introduce terminal functional groups on the substrates that can be linked covalently with the modified bis(imino)pyridine (PDI) ligands. In addition, surface density of the supported catalyst can also be adjusted by tuning the density of surface functional groups, which could accommodate the conformations of organometallic complexes and make the system more reproducible.

### **3.2.1 Preparation of modified surface as the substrate**

Since the attachment of iron catalyst **2.7** on the surface has been achieved utilizing the protonolysis reaction on titania, our initial attempt is to introduce aliphatic alcohol groups on SAM to replace with the surface hydroxyl groups from titania. SAMs of organosilanes have been successfully used to tailor material surfaces to obtain control over the molecular composition which is normally achieved via in-situ modifications of functional groups on the exposed SAM surface. There have been numerous examples for surface functionalizations with the formation of SAMs using

organosilanes.<sup>35,36</sup> However, only one method has been reported to prepare the hydroxyl-terminated organosilane monolayers, which might be due to the readily aggregated silanols. This approach was developed by Whitesides and coworkers in 1989 and relied on hydroboration oxidation reaction to convert terminal vinyl groups on SAMs to alcohol groups.<sup>37</sup> Nevertheless, this method requires three steps to obtain the hydroxyl-terminated SAMs and the required vinyl-functionalized silane linker needs to be synthesized particularly as well. Owing to the time-consuming process to generate the hydroxyl-functionalized SAM surfaces, we proposed to develop an efficient approach based on the halide substitution reaction that can convert the halide groups to alcohol groups on SAMs in only one step.

SAMs with terminal -Cl and -Br groups were successfully introduced on the TiO<sub>2</sub> nanoparticles and spin-coated TiO<sub>2</sub>-FTO plates according to the reported procedures in literature with some modifications.<sup>38</sup> The TiO<sub>2</sub> substrates were first treated by UV-ozone for 30 min to improve surface -OH density, and then exposed to an anhydrous toluene solution of (3-chloropropyl)trimethoxysilane (CPTMS) at 120 °C for 3 days to give Cl-terminated SAM TiO<sub>2</sub> substrates (Figure 3.2 a). Similarly, Br-terminated substrates can also be obtained after immersing the TiO<sub>2</sub> plates into a solution of (3-bromopropyl)trimethoxysilane (BPTMS) in the anhydrous toluene at 80 °C for 3 days (Figure 3.2 b). The resulting Cl-terminated and Br-terminated plates were confirmed by surface contact angle measurements and XPS spectroscopy, respectively. Moreover, the introduction of terminal -Br groups on surface was also demonstrated utilizing 11-bromoundecyltrichlorosilane (BUTCS) (Figure 3.2 c).

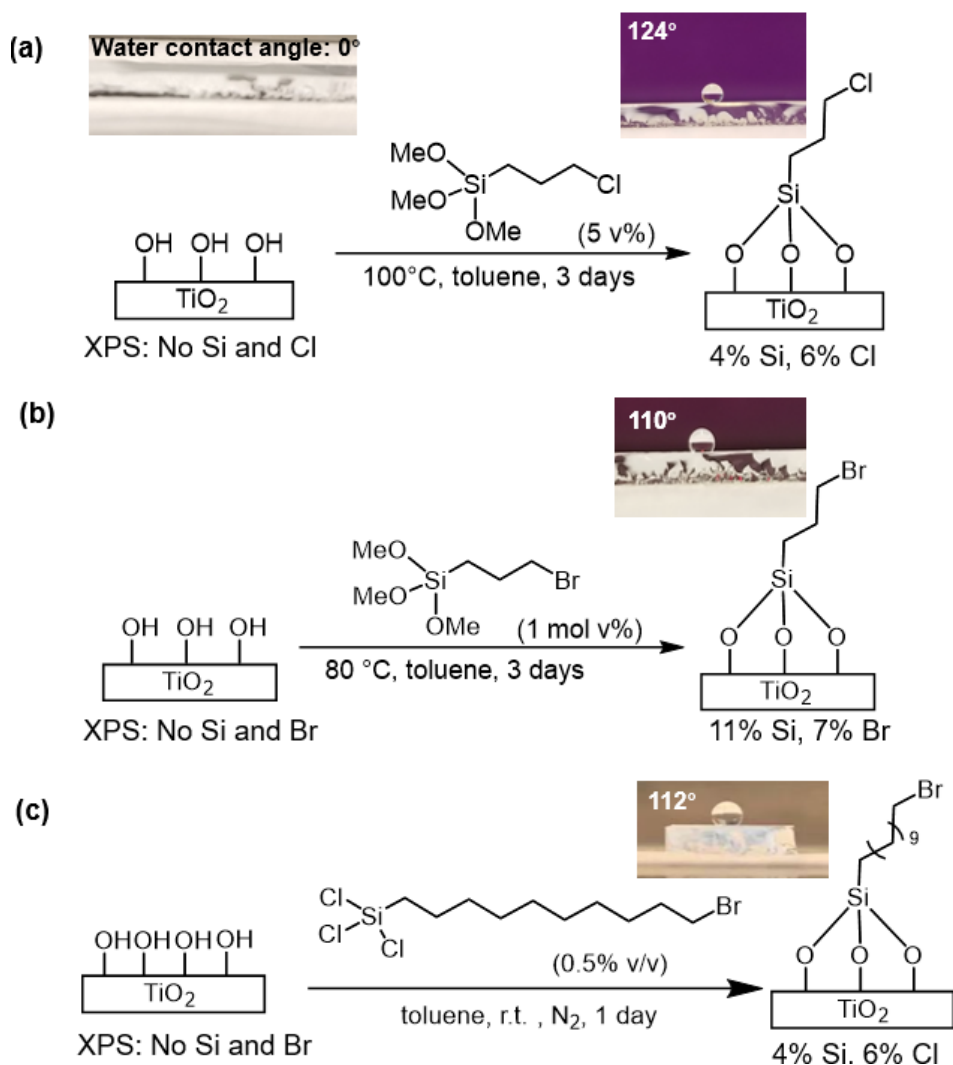


**Figure 3.2** Formation of halide-terminated SAMs on the TiO<sub>2</sub> plate that was prepared by spin-coating a layer of TiO<sub>2</sub> P25 nanoparticles on an FTO-glass slide. (a) Cl-terminated SAM on spin-coated TiO<sub>2</sub> plate using (3-chloropropyl)trimethoxysilane (CPTMS); (b) Br-terminated SAM on spin-coated TiO<sub>2</sub> plate using (3-bromopropyl)trimethoxysilane (BPTMS); (c) Br-terminated SAM on spin-coated TiO<sub>2</sub> plate using 11-bromoundecyltrichlorosilane (BUTCS); Water contact angles and XPS were used as the characterizations for the plates to confirm the successful introduction of halide elements on their hydrophobic surfaces.

With the formation of halide-terminated SAMs on TiO<sub>2</sub> surfaces, the hydrolysis reaction was carried out for halide substitution to form alcohol groups. Since SAMs formed by organosilanes are vulnerable to strong acidic or basic conditions,<sup>39</sup> mild reaction condition is required to achieve nucleophilic substitutions of halides on surfaces. Various hydrolysis conditions were screened that did not require strong acid or base catalysts (Table 3.1). With the help of XPS analysis, desired conditions that allow the conversion of halides to alcohols with maintaining the SAMs could be determined. We first followed the procedures that were developed to convert chloride to hydroxyl groups on the organic-inorganic hybrid polyhedral oligomeric silsesquioxane (POSS), a nanoscale polyhedral cluster containing silicon and oxygen.<sup>40</sup> In the attempt, Ag<sub>2</sub>O was suspended in 10 ml of THF/deionized water (3:7) mixture. The spin-coated Cl-SAM TiO<sub>2</sub> plates (entry 1, Table 3.1) were immersed in the mixture and heated at 80 °C in the dark for 4 days (entry 2, Table 3.1). The XPS analysis revealed a large decrease of the content of Cl element meaning the hydrolysis reaction occurred. However, the reaction was not complete due to the existence of 0.9% Cl. More importantly, a silver solid was formed and precipitated on the surfaces of the plates that cannot be removed with the applications of sulfuric acid aqueous solutions (pH 1-3). Therefore, we then moved on to test other mild conditions that have been reported in literature to achieve the homogeneous hydrolysis reaction.<sup>41</sup> The spin-coated Cl-SAM TiO<sub>2</sub> plates obtained from entry 1 were immersed in different aqueous mixtures of aprotic polar solvents, such as dimethyl sulfoxide (DMSO), N,N-Dimethylformamide (DMF), acetic acid and 1,4-

dioxane. These mixtures were allowed to heat at 80 °C for 4 days, respectively (entry 3-6, Table 3.1). Owing to the existence of remaining Cl element, the hydrolysis reaction using acetic acid and water mixture did not achieve the completion on the TiO<sub>2</sub> plate as shown in entry 5. On the other hand, complete disappearance of Cl and the presence of remaining Si was observed on the plates under the reaction conditions shown in entry 3, 4 and 6, respectively. The aqueous mixture with aprotic polar solvents (DMSO, DMF and 1,4-dioxane) facilitates the hydrolysis of halide on SAM under these mild conditions. Besides applying the aqueous mixture with aprotic polar solvents discussed above, a 15% (v/v) aqueous solution of hexamethylphosphoramide (HMPA) was applied to the Cl-terminated SAM TiO<sub>2</sub> plates at 100 °C for 4 days (entry 7, Table 3.1). The reaction condition was used previously to convert primary halides to alcohols according to the literature.<sup>42</sup> Nevertheless, an incomplete reaction was observed as evident by the remaining Cl element on XPS analysis of the plates. In addition, another efficient method for preparations of alcohols through the hydrolysis of organohalides in the presence of copper salts in aqueous DMSO was applied to organohalide-modified SAM TiO<sub>2</sub> plates.<sup>43</sup> The reaction was allowed to be heated at 100 °C for 4 days. However, the XPS analysis showed that the SAM was removed after the reaction as shown in entry 8. Overall, the reaction conditions shown in entry 3, 4 and 6 were determined to achieve the complete hydrolysis by converting terminal halide groups to alcohols on SAMs. The hydrolysis reaction was further optimized with the addition of a small amount of triethylamine (NEt<sub>3</sub>) (20.0 uL) to drive the reaction equilibrium (entry 9, Table 3.1). As a result, the reaction efficiency was much

improved by decreasing the reaction time from 4 days to 1 day. Besides the XPS characterization, the hydrophilicity of the resulting OH-terminated surface was confirmed based on the small surface contact angle (Figure 3.3 a).

**Table 3.1** Reaction conditions for hydrolysis of terminal -Cl groups on SAMs and the corresponding XPS characterization results.<sup>a</sup>

Entry	Condition	O (%)	Si (%)	Cl (%)
1 <sup>b</sup>	Cl-terminated TiO <sub>2</sub> plate	51.4	3.90	7.00
2	Ag <sub>2</sub> O, THF/ H <sub>2</sub> O (3:7), 80 °C, 4 days	44.5	11.1	0.90
3	DMSO/H <sub>2</sub> O (3:7), 80 °C, 4 days	57.3	4.00	0
4	DMF/ H <sub>2</sub> O (3:7), 80 °C, 4 days	58.5	2.60	0
5	Acetic acid/ H <sub>2</sub> O (3:7), 80 °C, 4 days	54.5	2.10	1.50
6	1,4-Dioxane/ H <sub>2</sub> O (3:7), 80 °C, 4 days	57.8	3.50	0
7 <sup>c</sup>	15% aqueous HMPA, 100 °C, 4 days	54.0	15.5	0.70
8	CuSO <sub>4</sub> , DMSO/ H <sub>2</sub> O (1:2.4), 100 °C, 4 days	56.3	0	0.70
9	NEt <sub>3</sub> , 1,4-dioxane/H <sub>2</sub> O (3:7), 80 °C, 1 day	56.0	5.50	0

<sup>a</sup> C element was not included since it was dependent on environment for the measurement.

<sup>b</sup> original Cl-terminated TiO<sub>2</sub> substrate used before hydrolysis reaction.

Overall, a mild and efficient methodology was developed to introduce -OH functionality on SAM-modified surface of a TiO<sub>2</sub> electrode. This strategy is reliable and can also be applied to form OH-terminated SAMs when using silane linker with longer alkyl chain, e.g., 11-bromoundecyltrichlorosilane, as shown in Figure 3.3 b. With these OH-modified surfaces in hand, our next step is to support the modified PDI ligands that have desired functional groups for catalyst attachment.

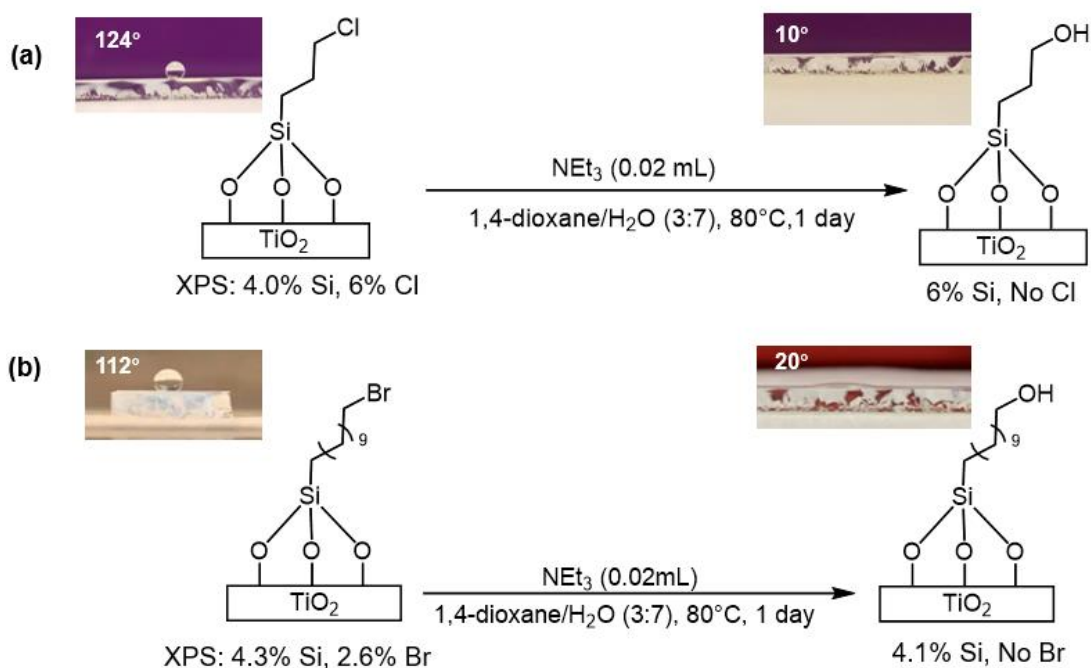
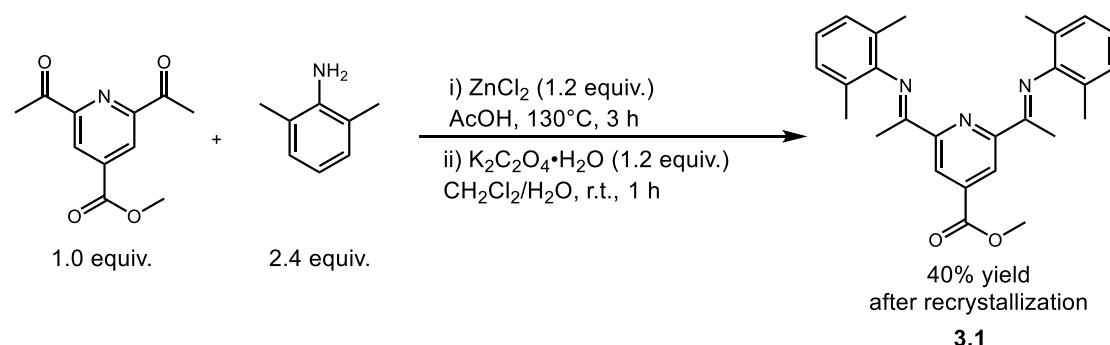


**Figure 3.3** Preparations of OH-terminated SAMs of different lengths from (a) the Cl-terminated propylorganosilane-modified spin-coated  $\text{TiO}_2$  plate or (b) Br-terminated undecylorganosilane-modified spin-coated  $\text{TiO}_2$  plate using the hydrolysis reaction condition shown in entry 9 of Table 3.1. XPS analysis and water contact angles are included.

### 3.2.2 Attempts to introduce functionalized ligands on modified substrates

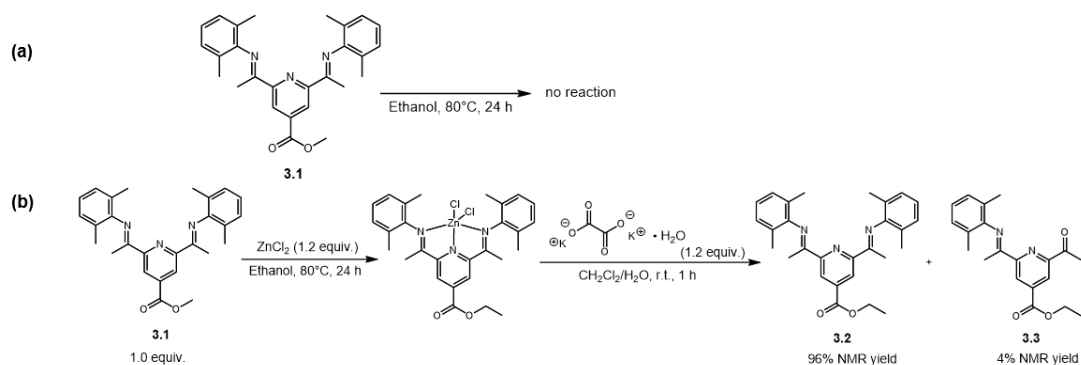
Previously, Christine Vo, Carolina Battle and Connor Gallin from the Byers group synthesized the methyl ester-functionalized bis(imino)pyridine **3.1** (2,6-(2,6-Me<sub>2</sub>-C<sub>6</sub>H<sub>3</sub>N=CMe)<sub>2</sub>C<sub>5</sub>H<sub>2</sub>COOCH<sub>3</sub>N, COOMe-PDI) from 2,6-diacetyl methyl ester-functionalized pyridine and 2,6-dimethylaniline with the addition of zinc dichloride ( $\text{ZnCl}_2$ ) in glacial acetic acid (Scheme 3.1). When using ethanol as the solvent, the transesterification was found to occur unintentionally on the ligand backbone. To gain more insight about this reaction and its potential application in catalyst

immobilization on surfaces, the methyl ester-functionalized PDI ligand **3.1** was utilized as the substrate to understand the condition of its transesterification reaction.



**Scheme 3.1** Reaction scheme for the synthesis of methyl ester-functionalized bis(imino)pyridine (PDI) ligand **3.1**.

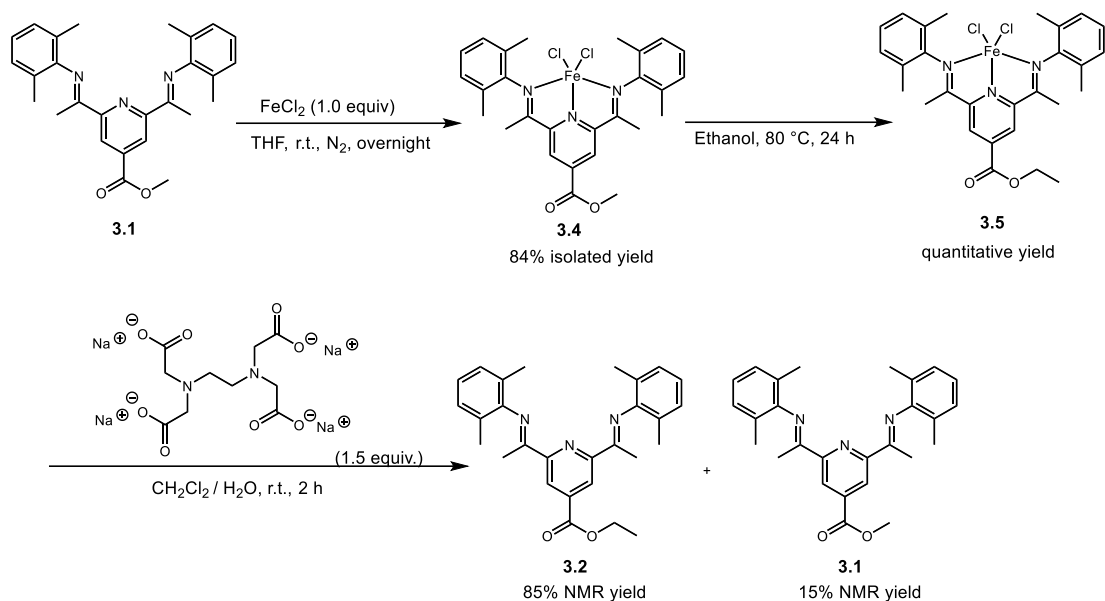
Initial attempts were carried out by refluxing the ligand **3.1** in ethanol for 1 day. Analysis of the reaction mixture by  $^1\text{H}$  NMR spectroscopy indicated that no reaction occurred without the zinc chloride ( $\text{ZnCl}_2$ ) (Scheme 3.2 a). With the help of Lewis acid additive, transesterification reaction occurred on the ligand backbone. Removal of zinc was achieved by treating the crude reaction mixture with a potassium oxalate aqueous solution.<sup>44</sup> Based on the  $^1\text{H}$  NMR spectroscopy, a COOEt-PDI compound **3.2** was obtained in the crude with 4% of the mono-substituted ketone molecule **3.3** being observed as the byproduct due to the side hydrolysis of diimine (Scheme 3.2 b).



**Scheme 3.2** Transesterification reaction of methyl ester-functionalized PDI ligand **3.1** in ethanol (a) without and (b) with the addition of  $\text{ZnCl}_2$ . With adding  $\text{ZnCl}_2$ , the reaction afforded 96% of an ethyl ester-functionalized PDI compound **3.2** and a small amount (4%) of the mono-substituted ketone byproduct **3.3** as evident by  $^1\text{H}$  NMR spectroscopy.

Iron dichloride ( $\text{FeCl}_2$ ) was also tried as the Lewis acid additive for this reaction. After mixing PDI ligand **3.1** with  $\text{FeCl}_2$  in ethanol, the suspension was headed to reflux for 1 day. A green-blue colored iron complex was produced. The paramagnetic iron complex made it difficult to assess whether transesterification had occurred. To address this complication, another trial was conducted by refluxing the premade iron(COOMe-PDI)dichloride complex **3.4** in ethanol for one day to afford an iron complex **3.5** (Scheme 3.3). However, no obvious change between the two complexes was observed by  $^1\text{H}$  NMR, which might be due to the challenge of using paramagnetic NMR spectra for the identification of iron complexes. Therefore, a hydrolysis reaction was carried out to remove iron species by treating the dichloromethane solution of iron complex **3.5** with a 0.05 M aqueous solution of ethylenediaminetetraacetic acid disodium salt (EDTA) at ambient temperature for 2 h.

Based on the  $^1\text{H}$  NMR spectroscopy, the resulting yellow solid was determined to be a mixture of mainly the ethyl ester-functionalized PDI ligand **3.2** and the methyl ester-functionalized PDI ligand **3.1** (~15%). Incomplete conversion from methyl ester to ethyl ester group on ligand backbone was observed, which can likely be solved by conducting the transesterification reaction in ethanol with longer time at elevated temperature. Optimization of the reaction conditions is in demand and will be the focus of future work. Overall, the result shown here indicates that the  $\text{FeCl}_2$  can also be utilized as the acid additive to facilitate the transesterification on PDI ligand backbone, which allows the conversion from methyl ester to ethyl ester group. Since the iron dichloride complex is an intermediate to synthesize the Fe(I) alkoxide catalyst **2.1** used for NCA polymerization reactions,<sup>45</sup>  $\text{Fe}(\text{COOMe-PDI})\text{Cl}_2$  complex **3.4** might be the optimal substrate that may react with the heterogeneous alcohol groups on SAMs directly. If so, the surface-bound Fe(I) catalyst can be formed efficiently in a short-step synthesis process.

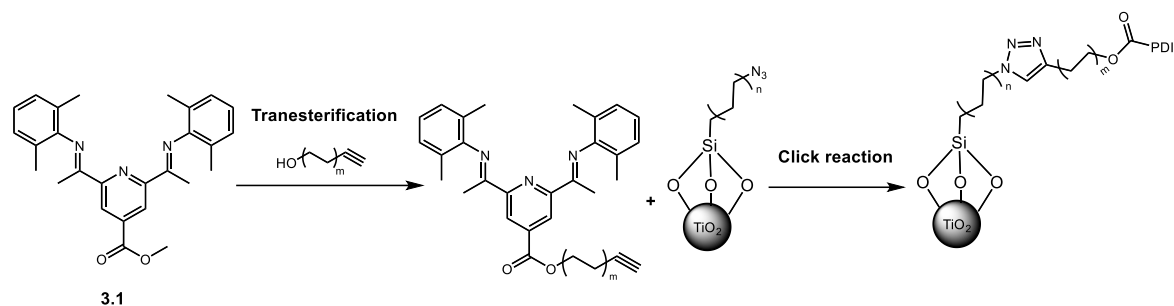


**Scheme 3.3** Transesterification reaction of methyl ester-functionalized PDI ligand **3.2** with ethanol in the presence of  $\text{FeCl}_2$ . Upon removal of iron species, 85% of the ethyl ester-functionalized PDI ligand **3.2** and 15% of the methyl ester-functionalized PDI ligand **3.1** (~15%) were obtained as evident by  $^1\text{H}$  NMR spectroscopy.

To test whether the heterogeneous transesterification could occur, some initial studies were conducted by mixing the PDI ligand **3.1** with  $\text{TiO}_2$  nanoparticles owing to their high surface areas. The yellow ligand **3.1** (50 mg) and white  $\text{TiO}_2$  nanoparticles (20 mg) were suspended in 5 mL of anhydrous toluene at ambient temperature for 1 day in the initial attempt. Colorless titania nanoparticles were obtained after three washes with toluene followed by centrifugation. FT-IR was utilized for the characterization of resulting  $\text{TiO}_2$  nanoparticles. Compared with the FT-IR of molecular PDI ligand **3.1**, the IR spectrum of these  $\text{TiO}_2$  nanoparticles did not have any feature from the ligand **3.1**. Further trial was carried out by Connor

Gallin, where the reaction time was extended to 2 days. Based on FT-IR of the resulting nanoparticles, only the presence of IR band from carboxyl group was observed with the peaks from pyridine not shown. We hypothesized that the failures of the heterogeneous transesterification between might be due to the Lewis acid additive which was not added into the system. The usage of Lewis acid additive might be necessary in order to make the carbonyl group on ligand backbone more electrophilic for the nucleophilic attack from alcohols. In addition, compared with ethanol used as the solvent, the heterogeneous -OH groups might not be nucleophilic enough for the transesterification to occur. To apply the similar strategy into the heterogeneous system, the density of terminal -OH groups on nanoparticles needs to be high and the distance between the terminal alcohol groups might need to be adjusted. Since the OH-terminated SAM modified TiO<sub>2</sub> nanoparticles have larger surface areas and organized surface structure,<sup>36</sup> they might work as a better solid substrate to achieve the goal. The experiments to replace the homogeneous alcohols with heterogeneous alcohol groups on SAMs will be explored. Moreover, instead of relying on transesterification reaction, a different attachment strategy we would like to try is the click reaction that has been widely applied in surface chemistry.<sup>18-22</sup> The proposal is depicted in Scheme 3.4. By taking advantage of the transesterification reaction we have developed, alkyne group could be installed on the ligand backbone through the reaction between ligand **3.1** and an alkyne-functionalized alcohol. The introduced alkyne functionality will provide great opportunities for enabling the attachment of PDI ligands by reacting with azide-terminated SAM surfaces. The

experiments discussed here are the subject of ongoing investigations.



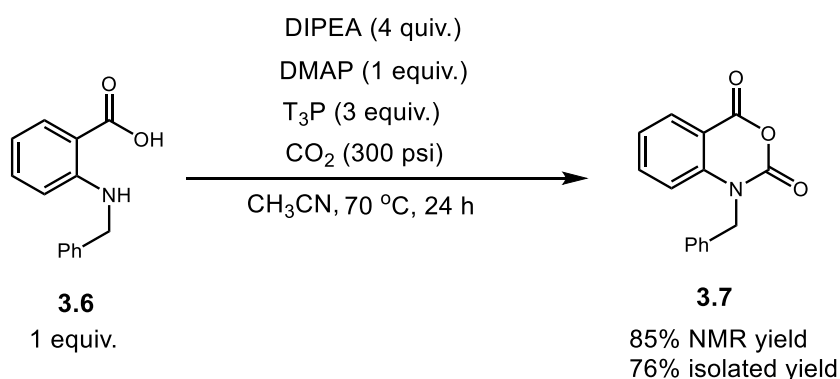
**Scheme 3.4** Proposal to attach PDI ligand on titania substrate through (i) transesterification reaction to introduce alkyne group on ligand backbone followed by (ii) a click reaction between the ligand on azide-terminated SAM surface.

### 3.3 Compatibility tests for integration of NCA synthesis and its polymerization

#### 3.3.1 A new NCA synthesis methodology from amino acids and CO<sub>2</sub>

In order to enable the integrated catalysis for polypeptide synthesis as described in Chapter 1, one essential aspect is to develop a methodology for NCA synthesis that utilizes CO<sub>2</sub>. The advantage of this method is not only it can avoid the usage of toxic phosgene derivatives but also enables the recycling of C1 source-CO<sub>2</sub> released from the NCA polymerization. A methodology has been developed recently to allow the synthesis of 6-membered ring NCA from  $\beta$ -amino acid and CO<sub>2</sub> directly by our collaborators, Dr. Thi Tran from Prof. Do's group at University of Houston and Yi Shen from Prof. Diaconescu's group at UCLA, respectively (Scheme 3.5). Owing to the poor solubility of  $\alpha$ -amino acids in organic solvents and the lower stability of 5-membered ring NCAs, they instead focused on the anthranilic acid **3.6** as the model substrate in this unpublished work. The  $\beta$ -amino acid dissolves well in common solvents and would afford chemically stable 6-membered ring NCA as the product.

After extensive studies, Dr. Tran and Yi determined the optimal reaction conditions for the synthesis of benzylisatoic anhydride **3.7**. A one-pot combination of anthralinic acid **3.6** under 300 psi of CO<sub>2</sub> with propanephosphonic acid anhydride (T<sub>3</sub>P) (3 equiv.) as the coupling agent and addition of 4 equivalence of N,N-diisopropylethylamine (DIPEA) and 1 equivalence of 4-dimethylaminopyridine (DMAP) in acetonitrile at 70 °C for 24 h afforded 76% isolated yield (85% yield determined by <sup>1</sup>H NMR spectroscopy) of the desired NCA **3.7** (Scheme 3.4). The conversion of the reaction was determined to be 100% as evident by <sup>1</sup>H NMR spectroscopy.



**Scheme 3.5** Optimal conditions for the synthesis of benzylisatoic anhydride from unprotected β-amino acid and CO<sub>2</sub> directly in one-pot; 1 equivalence of anthralinic acid under 300 psi of CO<sub>2</sub> with T<sub>3</sub>P (3 equivalence), DIPEA (4 equivalence) and DMAP (1 equivalence) in acetonitrile at 70 °C for 24 h.

In conclusion, Dr. Tran and Yi have developed a mild, nonacidic process for synthesizing a 6-membered ring NCA from unprotected β-amino acid and CO<sub>2</sub> directly using T<sub>3</sub>P as an activating reagent. The process is safe and generates nontoxic, easy-to-remove byproducts. The final product can be recovered easily in a good yield

and at an excellent level of purity. Ongoing studies are being explored to elucidate mechanistic understanding about the reaction.

### 3.3.2 Polymerizations of 6-membered ring NCA by iron catalysts

Although the methodology is efficient and mild, the resulting 6-membered ring N-benzylisatoic anhydride **3.7** is uncommon and more stable that cannot readily undergo ring opening process compared with the 5-membered ring NCAs derived from natural  $\alpha$ -amino acids. To explore the possibility of integrating NCA synthesis and its further polymerization, we would like to know whether the benzylisatoic anhydride **3.7** can be polymerized by surface-attached iron(I) complex **2.7@TiO<sub>2</sub>** we have synthesized. Therefore, efforts were dedicated by us to carrying out the polymerizations of benzylisatoic anhydride **3.7** in the presence of homogeneous iron complexes while expansion of substrate scope towards 5-membered ring NCAs was being studied by Dr. Tran and Yi.

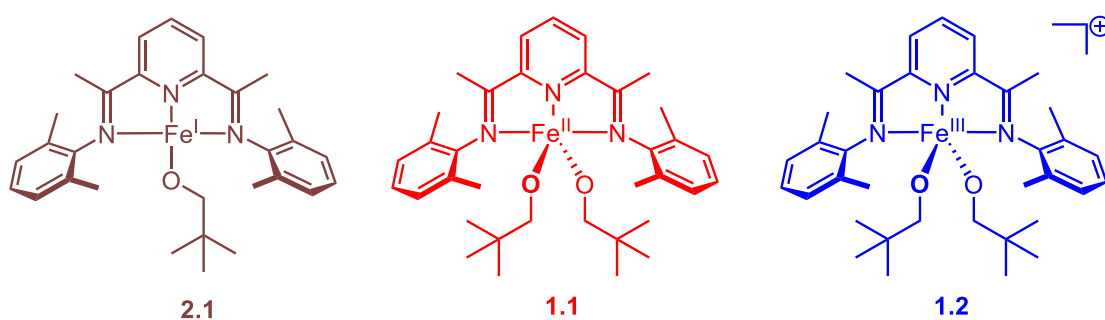


**Figure 3.4** Iron complexes used for the NCA polymerization studies.

Polymerization reaction trials were first carried out under the normal conditions used for Sar-NCA polymerization where THF was the reaction solvent. The reaction was allowed to heat at 80 °C for 1 day (entry 1, Table 3.2). Unlike the fast polymerization of 5-membered ring Sar-NCA initiated by the Fe(I) alkoxide

complex **2.1** in THF,<sup>1</sup> low activity was observed. After precipitation of the resulting polymer in diethyl ether, only a small amount of solid (<1 mg) was collected. Noteworthy, owing to the rigid polymer backbone, the resulting polymer was only soluble in very polar solvent (such as trifluoroacetic acid). Therefore, yield based on the mass of the collected solid product, instead of the conversion, was used as the indicator to reflect the progress of polymerization. As shown in entry 1 of Table 3.2, around 4.8 % yield was obtained when THF was utilized as solvent and the iron(I) complex **2.1** was the initiator. Since the NCA synthesis method developed by our collaborators did not work in THF due to the poor solubilities of all reagents in THF, incomparability issue needs to be resolved in order to perform NCA synthesis and NCA polymerization in one pot. We then moved on to test propylene carbonate (PC) or a mixture of PC and THF as the polymerization solvent in which the benzylisatoic anhydride **3.7** could be synthesized. After applying similar polymerization condition except the solvent, comparable yields were obtained from the polymerization catalyzed by the iron(I) complex **2.1** (entry 2 and 3, Table 3.2). In conclusion, the system or the condition that normally works for the Sar-NCA polymerization cannot be directly applied when using 6-membered ring NCA **3.6** as the monomer even at an elevated temperature.

Besides the iron(I) alkoxide catalyst **2.1**, we tested other iron catalysts for the polymerization of N-benzylisatoic anhydride **3.7**. Similar to the iron(I) monoalkoxide complex **2.1**, the iron(II) bisalkoxide complex **1.1** and iron(III) bisalkoxide complex **1.2** were previously found to be also capable of polymerizing Sar-NCA based on Dr.

Thompson's dissertation work (Figure 3.4).<sup>1</sup> Owing to the coordination-insertion mechanism of the NCA polymerization by iron catalyst discussed in Chapter 2 (Scheme 2.2), the coordination might be easier between more Lewis acidic iron center and NCA monomer, which could facilitate the insertion of NCA into the catalyst and the polymerization to proceed. With that expectation, polymerization trials were conducted using the complex **1.1** or complex **1.2** as the catalyst, respectively. Specifically, the polymerization reactions were conducted in THF at 80 °C for 1 day. However, comparable yields were still observed with the catalyst as iron(I) complex **2.1**. About 4.7 % and 2.9 % yield was obtained when complex **1.1** and **1.2** was utilized as the polymerization catalyst, respectively (entry 4 and 5, Table 3.2). Overall, the results indicated the limited polymerization activities of the complexes towards the readily stable 6-membered ring NCA even with more acidic iron centers.

**Table 3.2** Polymerization of 6-membered ring N-benzylisatoic anhydride by different iron complexes.<sup>a</sup>

Entry	Catalyst	Solvent	Yield (%)
1 <sup>b</sup>	<b>2.1</b>	THF	4.8
2 <sup>b</sup>	<b>2.1</b>	propylene carbonate (PC)	3.0
3 <sup>b</sup>	<b>2.1</b>	PC: THF=3:7	4.3
4	<b>1.1</b>	THF	4.7
5	<b>1.2</b>	THF	2.9

<sup>a</sup> [NCA]:[Fe]=100:1; heated at 80 °C in a sealed vessel filled with N<sub>2</sub>.

<sup>b</sup> with the addition of 1mol% [CoCp<sub>2</sub>][BAr<sub>4</sub><sup>F24</sup>]

### 3.3.3 Polymerization of 5-membered ring NCA by iron(I) complex 2.1

Since the 6-membered ring NCA cannot be polymerized by any of the iron complexes shown in Figure 3.4, the NCA required for integration is limited to a 5-membered ring NCA if an iron-based catalyst is to be used. Some challenges still remain in the NCA synthesis methodology developed by our collaborators. For example, additional organic groups need to be introduced to the NCA in order to alleviate the solubility problem. Thus, the N-benzyl glycine N-carboxyanhydride (N-Bn Gly-NCA) was chosen as the substrate due to its characteristics of owning a 5-membered ring structure and a hydrophobic benzyl substituent. Polymerizations of N-Bn Gly-NCA were first carried out using iron (I) complex **2.1** as the catalyst with and without the addition of cocatalyst,  $[\text{CoCp}_2][\text{BAr}_4\text{F}^{24}]$ , in THF at ambient temperature. The formed polymer was known to be only soluble in trifluoroacetic acid because of the aromatic substitutes in its polymer structures.<sup>46</sup> For easy operational purpose, internal standard (1,3,5-trimethoxybenzene) was added to allow the monitoring of NCA conversion versus time by  $^1\text{H}$  NMR spectroscopy. The conversion with and without the addition of co-catalyst after 48 hours achieved ~6% and ~10%, respectively (Table 3.3). Nevertheless, the polymerization solution changed its color after 48 h from purple to green, which indicated that the catalyst might decompose at that stage. Control studies and further purification of NCA monomer ruled out the possibilities that any impurity residues existed in the system which would decompose iron catalysts.

**Table 3.3** N-Bn Gly-NCA polymerizations catalyzed by iron(I) complex **2.1**

with or without the addition of co-catalyst. <sup>a</sup>

Entry	Co-catalyst	Solvent	Conversion <sup>b</sup> (%)
1	-	THF	10.2
2	1 mol%	PC	6.2

<sup>a</sup> [NCA]:[Fe]=100:1, 25 °C, reaction was performed in a sealed vessel in a N<sub>2</sub>-filled glove box;

<sup>b</sup> conversion was calculated after 48 h.

Noteworthy, this color change was also observed in the polymerization studies of 6-membered ring NCA **3.7**. One possible explanation is that the CO<sub>2</sub> generated from the NCA polymerization reaction could lead to the decomposition of the air-sensitive iron complex **2.1**. Since the released CO<sub>2</sub> could affect the kinetics of primary amine-initiated NCA polymerizations,<sup>47-49</sup> the CO<sub>2</sub> effect might also exist in the iron-catalyzed NCA polymerization system we have developed. Future work will be conducted by carrying out the polymerization reactions under reduced pressure or dynamic N<sub>2</sub> atmosphere to remove the released CO<sub>2</sub>.

### 3.4 Conclusions

In this chapter, efforts towards the integration of NCA synthesis and its polymerization were demonstrated. To help the integration, a different attachment approach was studied by SAM formation. Compared with attaching the polymerization catalyst through the protonolysis, catalyst immobilized from the ligand can not only facilitate charge transfer from the substrate to the supported catalyst and enable the recycling of attached catalyst after cleavage of polymer chains. Progress towards this goal included the development of an efficient and mild

approach to introduce -OH groups on the SAMs through the hydrolysis of alkyl halides. Based on this methodology, the modified titania surfaces with short and long silane linkers can be formed, as evident by XPS and water contact angle measurements. In addition, transesterification on the PDI ligand backbone was achieved in the presence of a Lewis acid additive, such as ZnCl<sub>2</sub> or FeCl<sub>2</sub>. Conversion of methyl ester to ethyl ester group on the ligand backbone can also occur directly on the iron dichloride complex **3.4** in ethanol. With the success of using homogeneous alcohol (ethanol) for transesterification reaction with modified PDI ligand **3.1**, our future focus will be the application of similar reaction to surfaces through the usage of heterogeneous alcohol groups on the modified substrate. By doing that, we hope the iron dichloride complex **3.4** can be attached on the modified substrate under optimal conditions. Moreover, introduction of alkyne functionality on ligand backbone will also be explored in the future in order to achieve the attachment of ligand through robust and efficient click reaction on surfaces. Another aspect in this chapter was to focus on testing the substrate limitations that might exist in the two separate reactions: NCA synthesis from unprotected amino acids and CO<sub>2</sub> and surface-initiated NCA polymerization catalyzed by different iron complexes. Polymerizations initiated by the redox-switchable iron complexes were carried out towards the uncommon 6-membered ring NCA that can be readily synthesized from the NCA approach developed by our collaborators. Unlike the normal 5-membered ring NCAs derived from natural amino acids, the 6-membered ring N-benzylisatoic anhydride is too stable to be polymerized by different iron catalysts even with more acid iron centers at

elevated temperature. N-Bn Gly-NCA was also used as the monomer for polymerization tests due to its structural similarity to Sar-NCA and relative availability from the NCA synthesis methodology our collaborators have developed. However, low NCA conversion was obtained even after two days. The catalyst decomposition was a concern due to the obvious color change of polymerization solutions. One possible explanation is the CO<sub>2</sub> generated from the NCA polymerization could cause the decomposition of catalyst or product inhibition, which was mentioned before in the system of primary amine-catalyzed NCA polymerization reactions. Future work will be continued optimization of the polymerization reaction conditions, such as carrying out polymerizations under dynamic N<sub>2</sub> atmosphere to remove the released CO<sub>2</sub>.

## **Experimental Section**

**General Considerations.** Unless stated otherwise, all reactions were carried out in oven-dried glassware in a nitrogen-filled glove box. Solvents (toluene, 1,4-dioxane, etc) were used after passage through a solvent purification system under a blanket of argon and then degassed briefly by exposure to vacuum.<sup>50</sup> Titania P<sub>25</sub> nanoparticles were purchased from Sigma-Aldrich. N-benzyl glycine was purchased from Thermo Scientific™ used as received. Anhydrous dimethyl sulfoxide (DMSO) and N,N-Dimethylformamide (DMF) packaged under Argon in resealable bottles were purchased from Alfa Aesar and used as received. N-benzylisatoic anhydride **3.6** was purchased from VWR and used after recrystallization in toluene. Triphosgene was purchased from Chem-Impex International Inc. and used as received. (3-

chloropropyl)trimethoxysilane (CPTMS) and (3-bromopropyl)trimethoxysilane (BPTMS) were purchased from Fisher and stored in the glove box. 11-bromoundecyltrichlorosilane (BUTCS) was purchased from Gelest, Inc. and stored in the glove box. Copper (II) sulfate pentahydrate was purchased from Fisher and used as received. Hexamethylphosphoramide (HMPA) was purchased from Oakwood and used as received. Iron (I) neopentyl monoalkoxide complex **2.1**, iron(II) neopentyl bisalkoxide complex **1.1** and iron(III) neopentyl bisalkoxide complex **1.2** were synthesized as described previously.<sup>45,51,52</sup> The methoxy-functionalized PDI ligand **3.1** and Fe(COOMe-PDI)Cl<sub>2</sub> complex **3.3** used here were received from Connor Gallin and Christine Vo in the Byers group.

**Equipment and Analytical Methods.** Nuclear magnetic resonance (NMR) spectra were recorded at ambient temperature on either a Varian Gemini-600 (600 MHz) or Varian Inova-500 (500 MHz) NMR spectrometer. High-resolution mass spectra (HRMS) were obtained at the Boston College Mass Spectrometry Facility on a JEOL AccuTOF DART instrument. Centrifugation used for nanoparticle purification was carried out polymer purification was carried out using the Sorvall Legend X1 Centrifuge (Thermo Fisher, Germany.) at 10000 RPM operating for 10 minutes for each run. Preparation of TiO<sub>2</sub>-FTO plate was conducted following a previously reported method using the spin-coater (Laurell WS-400E).<sup>53</sup> X-ray photoelectron spectroscopy (XPS) was measured on a Thermo Scientific K-Alpha+ X-ray photoelectron spectrometer. Water contact angle measurements were simply carried out by adding a drop of deionized water (0.2 uL) on the surface of plate and then

taking a picture by a cellphone.

**Representative procedure for formation of halide-terminated SAM on spin-coated TiO<sub>2</sub> plates.** This synthesis was carried out based on literature procedures after modification.<sup>38</sup> Spin-coated TiO<sub>2</sub> plates were treated by UV-ozone for 30 min to improve -OH density. The plates were brought into the glovebox and then immediately immersed in a BPTMS (0.5 mL) solution in anhydrous toluene (10 mL) at 80 °C for 3 days. The plates were then washed with fresh toluene (5 mL) to remove excess silanes followed by being rinsed with methanol (3 x 5 mL) and isopropanol (3 x 5 mL). The plates were dried in a vacuum oven at 80 °C overnight to generate Br-terminated SAMs on TiO<sub>2</sub> plates. For the preparation of Cl-terminated plates, an anhydrous toluene solution (10 mL) of CPTMS (0.5 mL) was used to soak the spin-coated TiO<sub>2</sub> plates and the reaction was heated at 100 °C for 3 days. For the synthesis of Br-terminated SAM on plates that have longer chains, the spin-coated TiO<sub>2</sub> plates were immersed in a 0.2 umol toluene solution of BUTCS at ambient temperature for 1 day.

**Synthesis of Cl-terminated SAM on TiO<sub>2</sub> nanoparticles.** This synthesis was carried out based on literature procedures after modification.<sup>38</sup> P25 TiO<sub>2</sub> nanoparticles were treated by UV-ozone for 30 min first to improve -OH density. The nanoparticles were heated under reduced pressure (lower than 10<sup>-2</sup> torr) at 130 °C for 1 day and were brought into a nitrogen-filled glovebox. The nanoparticles (200 mg) were suspended in a solution of CPTMS (1 mL) in anhydrous toluene (20 mL) and heated at 100 °C for 3 days with stirring. The resulting nanoparticles were collected by centrifugation.

The resulting nanoparticles were further washed by toluene and methanol to remove excess silanes followed by centrifugation. The Cl-terminated TiO<sub>2</sub> nanoparticles were dried in a vacuum oven at 80 °C overnight before the XPS characterization.

**Procedures for synthesis of OH-terminated SAM on spin-coated TiO<sub>2</sub> plates using silver oxide (entry 2, Table 3.2).** This synthesis was carried out based on literature procedures after modification.<sup>40</sup> On the bench, silver oxide (Ag<sub>2</sub>O) (465 mg, 2.00 mmol) was suspended in a mixture (10 mL) of THF and deionized water (3:7). The dried Cl-terminated plates were immersed in the mixture. The reaction was allowed to heat at 80 °C in the dark for 4 days. The resulting plates were washed with THF (3 x 10 mL) and deionized water (3 x 10 mL). The plates were dried in a vacuum oven at 80 °C overnight before any characterizations.

**Representative procedures for synthesis of OH-terminated SAM on spin-coated TiO<sub>2</sub> plates using aprotic polar solvents (entry 3-6, Table 3.2).** This synthesis was carried out based on literature procedures after modification.<sup>41</sup> On the bench, the dried Cl-terminated TiO<sub>2</sub> plates were soaked in an aqueous mixture (10 mL) of DMSO, DMF, acetic acid or 1,4-dioxane (aprotic polar solvent: H<sub>2</sub>O=3:7). The mixture was allowed to heat at 80 °C for 4 days. The resulting plates were washed with the corresponding aprotic polar solvent (3 x 10 mL) first followed by the deionized water (3 x 10 mL). The plates were dried in a vacuum oven at 80 °C overnight before any characterizations.

**Procedures for synthesis of OH-terminated SAM on spin-coated TiO<sub>2</sub> plates using HMPA (entry 7, Table 3.2).** This synthesis was carried out based on literature

procedures after modification.<sup>42</sup> On the bench, the dried Cl-terminated TiO<sub>2</sub> plates were immersed in a 15% (v/v) aqueous mixture (10 mL) of HMPA. The mixture was allowed to heat at 100 °C for 4 days. The resulting plates were washed with the deionized water (3 x 10 mL). The plates were dried in a vacuum oven at 80 °C overnight before any characterizations.

**Procedures for synthesis of OH-terminated SAM on spin-coated TiO<sub>2</sub> plates using copper salts (entry 8, Table 3.2).** This synthesis was carried out based on literature procedures after modification.<sup>43</sup> On the bench, copper (II) sulfate pentahydrate (CuSO<sub>4</sub>·5H<sub>2</sub>O) (0.50 g, 2.0 mmol) was dissolved in an aqueous mixture (10 mL) of DMSO (molar ratio of CuSO<sub>4</sub>·5H<sub>2</sub>O: DMSO: H<sub>2</sub>O =1:10:12). The Cl-terminated TiO<sub>2</sub> plates were immersed in the mixture and heated at 100 °C for 4 days. The resulting plates were washed with deionized water (3 x 10 mL) and dried in a vacuum oven at 80 °C overnight before any characterizations.

**Representative procedures for synthesis of OH-terminated SAM on spin-coated TiO<sub>2</sub> plates under the optimal condition (entry 9, Table 3.2).** On the bench, the dried halide-terminated plates were soaked in a mixture (10 mL) of dioxane and H<sub>2</sub>O (3:7) with the addition of 0.02 mL NEt<sub>3</sub>. The mixture was allowed to heat at 80 °C for 1 day. The resulting plates were washed with ultrapure water (3 x 10 mL) and then dried in a vacuum oven at 80 °C overnight.

**Representative procedures for preparation of OH-terminated SAM on TiO<sub>2</sub> nanoparticles.** On the bench in air, 30 mg dried Cl-terminated SAM TiO<sub>2</sub> nanoparticles were suspended in 5 mL dioxane/H<sub>2</sub>O (3:7) mixture in a 7-mL vial. 0.02

mL  $\text{NEt}_3$  was added dropwise into the suspension. The mixture was heated at 80 °C for 1 day with stirring and the resulting nanoparticles were collected by centrifugation. The nanoparticles were further washed by ultrapure water (3 x 10 mL) followed by centrifugation to remove excess  $\text{NEt}_3$ . The OH-terminated  $\text{TiO}_2$  nanoparticles were dried in a vacuum oven at 80 °C overnight for XPS analysis.

**Representative procedure of homogeneous polymerization of N-benzylisatoic anhydride 3.6 by iron(I) complex 2.1.** In a nitrogen-filled glove box, benzylisatoic anhydride **3.6** (25.4 mg, 0.100 mmol) and iron(I) neopentyl alkoxide complex **2.1** (0.51 mg, 1.00  $\mu\text{mol}$ ) was dissolved in 0.15 ml of THF.  $\text{CoBAr}_4^{\text{F}24}$  (1.1 mg, 1.00  $\mu\text{mol}$ ) was dissolved in 0.15 mL of THF and transferred to the other THF solution. The reaction was allowed to heat at 80 °C for two days and was terminated after being exposed upon air. The polymerization solution was precipitated into diethyl ether and dried to leave a solid after centrifugation. Due to the limited solubility of this kind of rigid polyamide dissolved in  $\text{CDCl}_3$ , yield was determined based on the mass of the collected polymer solid.

**Representative procedure of homogeneous polymerization of N-benzylisatoic anhydride 3.6 by iron(II) complex 1.1 or iron(III) complex 1.2.** In a nitrogen-filled glove box, benzylisatoic anhydride **3.6** (25.4 mg, 0.100 mmol) was dissolved in 0.15 ml of THF. Iron(II) neopentyl alkoxide complex **1.1** (0.6 mg, 1.00  $\mu\text{mol}$ ) was dissolved in 0.15 mL of THF and added to the NCA monomer solution. The reaction was allowed to heat at 80°C for two days. Outside of the glove box, the polymerization solution was precipitated into diethyl ether and dried to leave a solid

after centrifugation. Due to the limited solubility of this kind of rigid polyamide dissolved in  $\text{CDCl}_3$ , yield was determined based on the mass of the collected solid.

**Synthesis of N-Bn Gly-NCA.** N-benzyl glycine (1.50 g, 9.09 mmol) was weighed in a two-neck flask equipped with a condenser and dried *in vacuo* for 1 hour. Triphosgene (1.62 g, 5.45 mmol) was dissolved in 50 ml of dry THF and added to the Sarcosine. The suspension was allowed to stir under active nitrogen flow into a wash bottle of concentrated sodium hydroxide. The reaction was heated at 50 °C with a water bath until the suspension became homogeneous and clear after 4 h. THF was removed *in vacuo* to give a yellow/brown oil and then further dried at 50 °C to obtain an amorphous solid. The solid was redissolved in minimal THF at 50 °C and precipitated into hexanes immediately. Solid was collected by filtration and dried *in vacuo* overnight. Recrystallization in THF/pentane afforded a fine white powder (1.25 g, 72%).  $^1\text{H}$  NMR (500 MHz;  $\text{CDCl}_3$ ):  $\delta$  (ppm) = 3.95 (2 H, s, CO-CH<sub>2</sub>-N-), 4.5 (2 H, s, C<sub>6</sub>H<sub>5</sub>-CH<sub>2</sub>-), 7.3 (5 H, m, C<sub>6</sub>H<sub>5</sub>-CH<sub>2</sub>-). The  $^1\text{H}$  NMR results matched the values reported in the literature.<sup>22</sup>

**Representative procedure of homogeneous polymerization of N-Bn Gly-NCA.** In a nitrogen-filled glove box, N-Bn glycine N-carboxyanhydride (N-Bn Gly-NCA) (28.0 mg, 0.146 mmol) and iron(I) neopentyl alkoxide complex **2.1** (0.75 mg, 1.46  $\mu\text{mol}$ ) was dissolved in 0.15 ml of THF.  $\text{CoBAr}_4^{\text{F}24}$  (1.54 mg, 1.46  $\mu\text{mol}$ ) and 1,3,5-trimethoxybenzene (12.3 mg, 73.2  $\mu\text{mol}$ ) were dissolved in 0.15 mL of THF. The two solutions are mixed and was allowed to heat at 80 °C. The reaction was terminated after being exposed to air. Conversion was determined by comparing the relative

integration of the methylene peaks of the remaining N-Bn Gly-NCA (s, 4.5 ppm) to the methine peaks of the internal standard (s, 6.1 ppm) in the supernatants by  $^1\text{H}$  NMR spectroscopy. The NMR solution was precipitated into diethyl ether and dried to leave a solid after centrifugation.

### **Synthesis of ethyl ester-functionalized PDI ligand 3.2 with the addition of $\text{ZnCl}_2$ .**

In a nitrogen-filled glovebox, methyl methoxy-functionalized PDI ligand **3.1** (10.0 mg, 23.4  $\mu\text{mol}$ ) and zinc dichloride (6.00 mg, 44.00  $\mu\text{mol}$ ) was dissolved in 1 mL anhydrous ethanol in a sealed 7-mL vial. After being reflux at 80 °C for 1 day outside of the glovebox, the suspension was dried *in vacuo* to afford a dark yellow solid. The solid was then suspended in dichloromethane (5 mL) and mixed with an aqueous solution (2 mL) of potassium oxalate monohydrate (50.0 mg, 271  $\mu\text{mol}$ ). The mixture was stirred vigorously for 30 min and the aqueous layer was washed with dichloromethane (3 x 10 mL). The combined organic layer was dried *in vacuo* to obtain a yellow solid which was determined to be the ethyl ester-functionalized PDI ligand **3.2** with 4% of the mono-substituted ketone byproduct **3.3** being obtained (calculated based on the methyl ketone peak at 2.80 ppm).  $^1\text{H}$  NMR (600 MHz,  $\text{CDCl}_3$ ):  $\delta$  (ppm) = 1.44 (t, 3H,  $\text{COOCH}_2\text{CH}_3$ ), 2.07 (s, 12H,  $\text{Ph-CH}_3$ ), 2.26 (s, 6H,  $\text{N=C(CH}_3\text{)}$ ), 4.48 (q, 2H,  $\text{COOCH}_2\text{CH}_3$ ), 6.96(t, 2H,  $\text{Ph}_p\text{-H}$ ), 7.09(d, 4H,  $\text{Ph}_m\text{-H}$ ), 9.00 (s, 2H,  $\text{py}_m\text{-H}$ ).  $^{13}\text{C}$  NMR (151 MHz,  $\text{CDCl}_3$ ):  $\delta$  (ppm) = 14.46 ( $\text{COOCH}_2\text{CH}_3$ ), 16.76 ( $\text{N=C(CH}_3\text{)}$ ), 18.12 ( $\text{Ph-CH}_3$ ), 62.14 ( $\text{COOCH}_2\text{CH}_3$ ), 121.71 ( $\text{Ar-CH}$ ), 123.37 ( $\text{Ar-CH}$ ), 125.48 ( $\text{Ar-CH}$ ), 128.09 ( $\text{Ar-CH}$ ), 139.45 (py), 148.68 (py), 156.36 (py), 165.31 ( $\text{COOCH}_2\text{CH}_3$ ), 167.78(py). FT-IR (neat,  $\text{cm}^{-1}$ ): 2975, 2916, 1730, 1645, 1593,

1560, 1467, 1438, 1365, 1238, 1204, 1129, 1093, 1022, 921, 815, 766, 737. HRMS-DART (m/z): [M + H]<sup>+</sup> calculated for C<sub>28</sub>H<sub>32</sub>N<sub>3</sub>O<sub>2</sub>, and 442.56; found, 442.25.

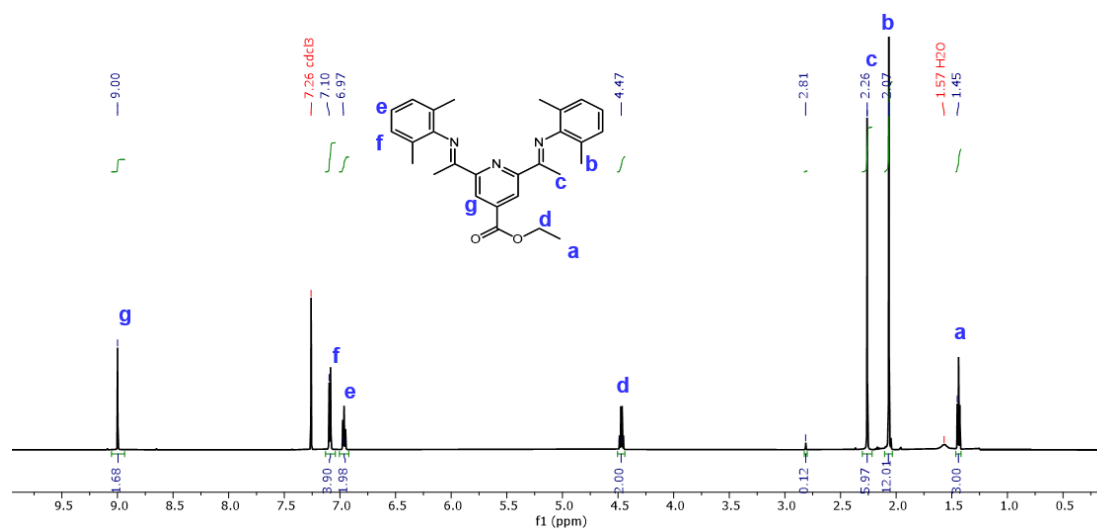


Figure S 3.1 <sup>1</sup>H NMR of ethyl ester-functionalized PDI ligand 3.2 in CDCl<sub>3</sub>.

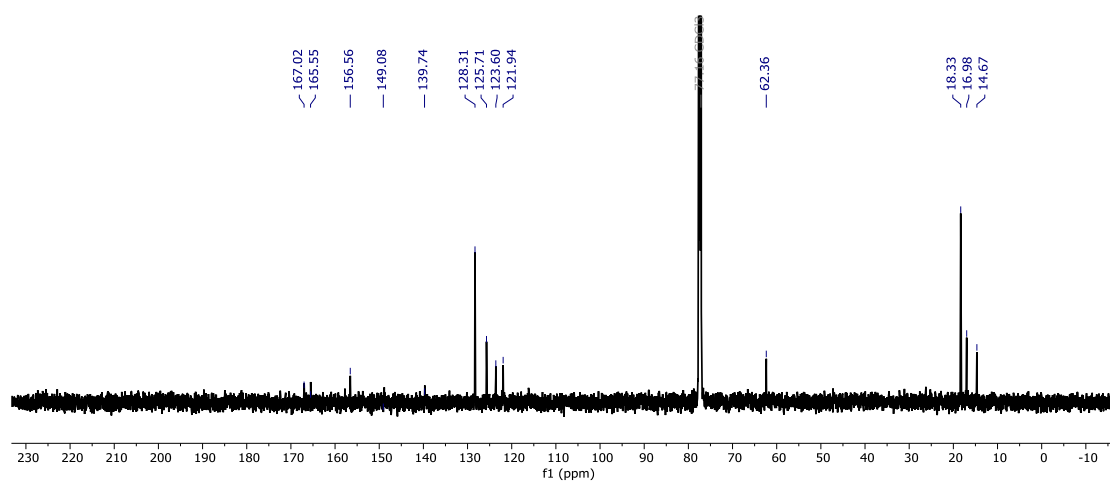
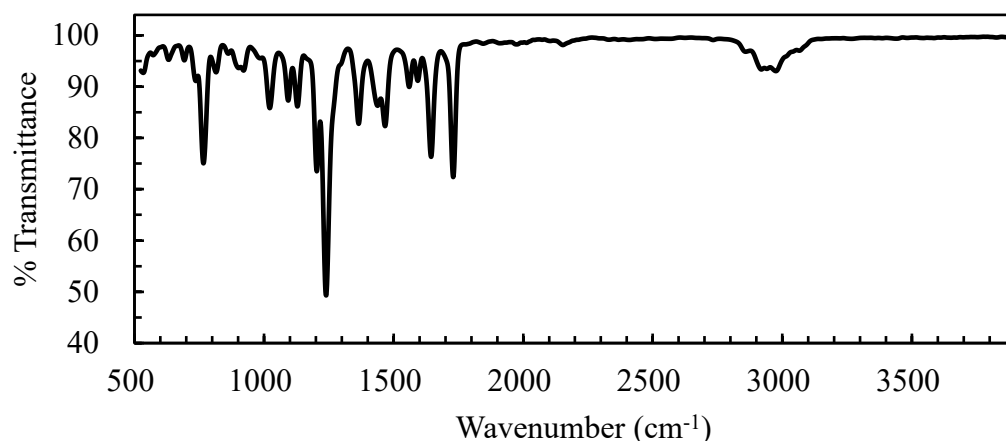
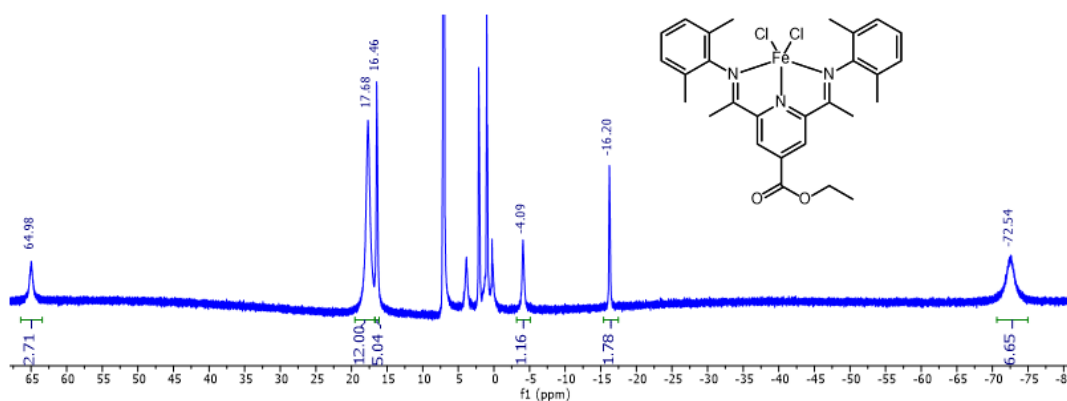


Figure S 3.2 <sup>13</sup>C NMR of ethyl ester-functionalized PDI ligand 3.2 in CDCl<sub>3</sub>.



**Figure S 3.3** FT-IR of ethyl ester-functionalized PDI ligand **3.2**.

**Transesterification of Fe(COOMe-PDI)Cl<sub>2</sub> complex 3.4 in ethanol.** In a N<sub>2</sub>-filled glovebox, Fe(COOMe-PDI)Cl<sub>2</sub> complex **3.4** (14.8 mg, 26.70 μmol) was suspended in 0.5 mL ethanol in a sealed 7-mL vial. The suspension changed to green-blue color immediately and was heated at 80 °C for 1 day outside of the glove box. The suspension was then dried *in vacuo* in the glove box resulting in a green-blue complex **3.5**. <sup>1</sup>H NMR (500 MHz, C<sub>6</sub>D<sub>6</sub>): δ (ppm)= -72.54 (7H), -16.20 (2H), -4.09 (1H), 16.46 (5H), 17.68 (12H), 64.98(3H). FT-IR (neat, cm<sup>-1</sup>): 2949, 1724, 1598, 1444, 1370, 1262, 1095, 982, 774. HRMS-DART (m/z): [M + H]<sup>+</sup> calculated for C<sub>28</sub>H<sub>31</sub>N<sub>3</sub>O<sub>2</sub>Cl<sub>2</sub>Fe, and 568.31; found, 567.11.



**Figure S 3.4** Paramagnetic  $^1\text{H}$  NMR of iron dichloride complex **3.5** in  $\text{C}_6\text{D}_6$ .

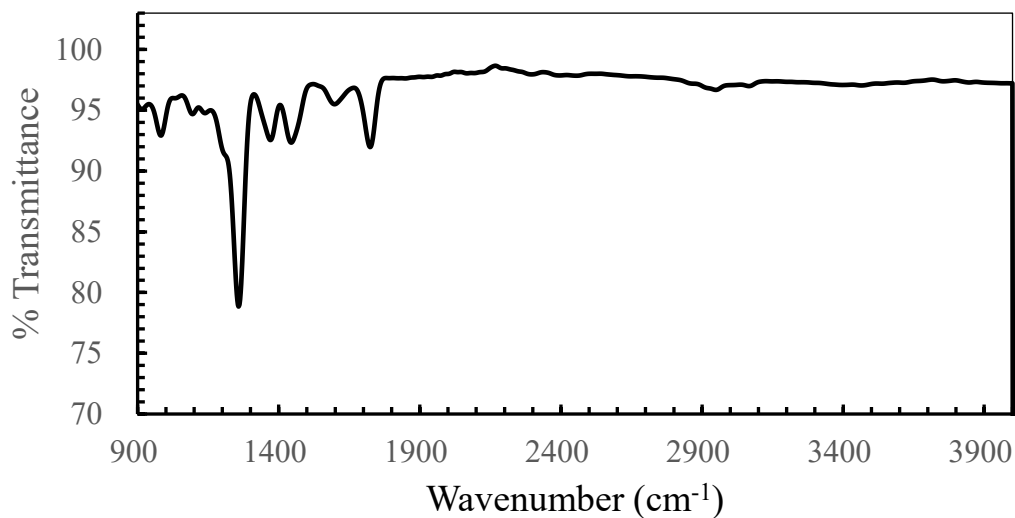


**Figure S 3.5** FT-IR of ethyl ester-functionalized iron dichloride complex **3.5**.

**Hydrolysis of iron complex 3.5 to remove iron species.** On the bench top, the iron complex **3.5** (10 mg) was dissolved in dichloromethane (5 mL). Ethylenediaminetetraacetic acid disodium salt (EDTA) (0.17 mmol, 64 mg) was dissolved in a saturated NaCl aqueous solution (3 mL). The two solutions were combined together, and the resulting mixture was allowed to stir vigorously at ambient temperature for 2 h. The aqueous layer was washed with dichloromethane (3 x 5 mL). The combined organic layer was dried *in vacuo* to obtain a yellow solid which was mainly the ethyl ester-functionalized PDI ligand **3.2** with 15% of the methyl ester-functionalized PDI ligand **3.1** being observed (calculated based on the methyl group peak at 4.00 ppm).  $^1\text{H}$  NMR (600 MHz,  $\text{CDCl}_3$ ):  $\delta$  (ppm) = 1.44 (t, 3H), 2.07 (s, 12H), 2.26 (s, 6H), 4.00 (s, 3H), 4.48 (q, 2H), 6.96(t, 2H), 7.09(d, 4H), 9.00 (s, 2H), 9.01 (s, 2H).

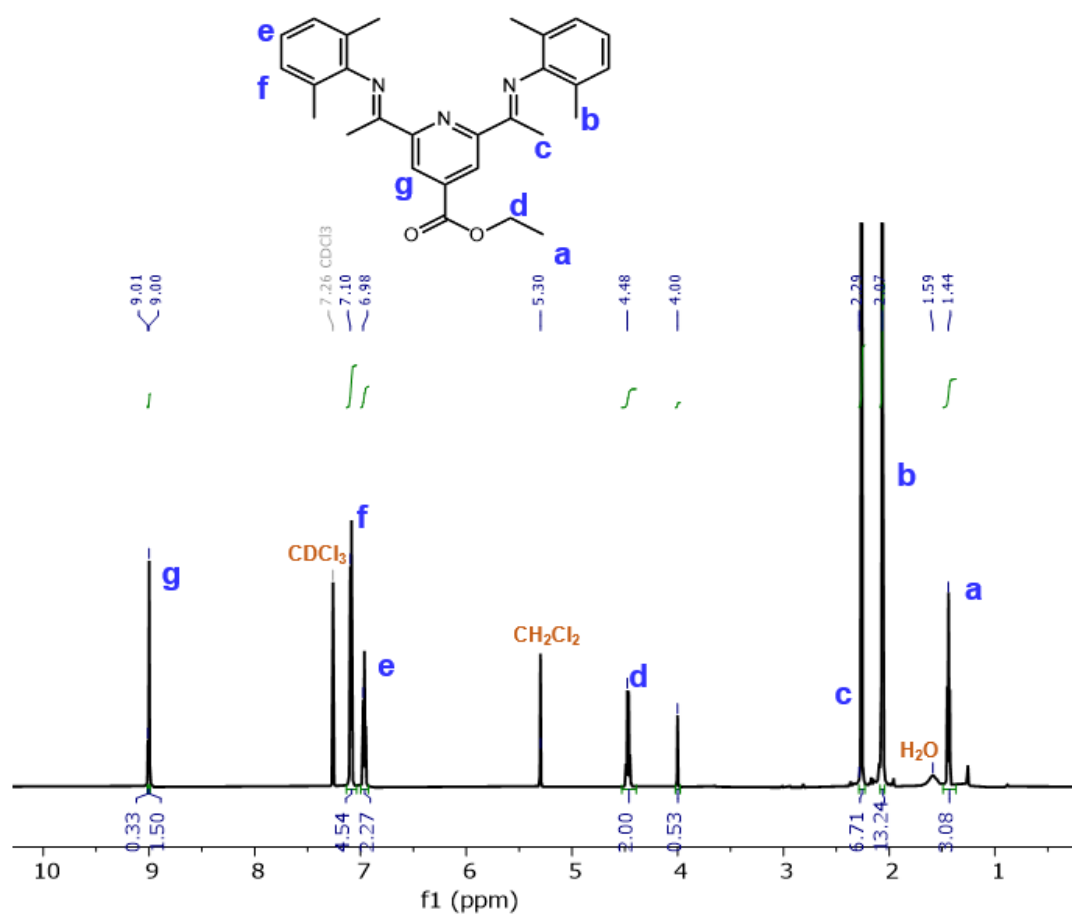


**Figure S 3.6** <sup>1</sup>H NMR after hydrolysis and removal of iron from complex **3.5**.

## References

- (1) Thompson, M. S. Redox-Switchable Copolymerization: Transforming Underutilized Monomer Feedstocks to Complex Copolymers, Ph.D. Dissertation, Boston College, Boston, MA, 2021.
- (2) Qi, M.; Zhang, H.; Dong, Q.; Li, J.; Musgrave, R. A.; Zhao, Y.; Dulock, N.; Wang, D.; Byers, J. A. Electrochemically Switchable Polymerization from Surface-Anchored Molecular Catalysts. *Chem. Sci.* **2021**, *12* (26), 9042–9052. DOI: 10.1039/D1SC02163J.
- (3) Barlow, S. M.; Raval, R. Complex Organic Molecules at Metal Surfaces: Bonding, Organisation and Chirality. *Surf. Sci. Rep.* **2003**, *50* (6–8), 201–341. DOI: 10.1016/S0167-5729(03)00015-3.
- (4) Love, J. C.; Estroff, L. A.; Kriebel, J. K.; Nuzzo, R. G.; Whitesides, G. M. Self-Assembled Monolayers of Thiolates on Metals as a Form of Nanotechnology. *Chem. Rev.* **2005**, *105* (4), 1103–1169. DOI: 10.1021/CR0300789.
- (5) Kango, S.; Kalia, S.; Celli, A.; Njuguna, J.; Habibi, Y.; Kumar, R. Surface Modification of Inorganic Nanoparticles for Development of Organic-Inorganic Nanocomposites - A Review. *Prog. Polym. Sci.* **2013**, *38* (8), 1232–1261. DOI: 10.1016/j.progpolymsci.2013.02.003.
- (6) Mutin, P. H.; Guerrero, G.; Vioux, A. Hybrid Materials from Organophosphorus Coupling Molecules. *J. Mater. Chem.* **2005**, *15* (35–36), 3761–3768. DOI:10.1039/B505422B.
- (7) Chourifa, H.; Bouloussa, H.; Migonney, V.; Falentin-Daudré, C. Review of

- Titanium Surface Modification Techniques and Coatings for Antibacterial Applications. *Acta Biomater.* **2019**, *83*, 37–54. DOI: 10.1016/j.actbio.2018.10.036.
- (8) Paniagua, S. A.; Giordano, A. J.; Smith, O. L.; Barlow, S.; Li, H.; Armstrong, N. R.; Pemberton, J. E.; Brédas, J. L.; Ginger, D.; Marder, S. R. Phosphonic Acids for Interfacial Engineering of Transparent Conductive Oxides. *Chem. Rev.* **2016**, *116* (12), 7117–7158. DOI: 10.1021/acs.chemrev.6b00061.
- (9) Liu, Y. F.; Lee, Y. L. Adsorption Characteristics of OH-Terminated Alkanethiol and Arenethiol on Au(111) Surfaces. *Nanoscale* **2012**, *4* (6), 2093–2100. DOI: 10.1039/C2NR11495J.
- (10) Colangelo, E.; Comenge, J.; Paramelle, D.; Volk, M.; Chen, Q.; Lévy, R. Characterizing Self-Assembled Monolayers on Gold Nanoparticles. *Bioconjug. Chem.* **2017**, *28* (1), 11–22. DOI: 10.1021/acs.bioconjchem.6b00587.
- (11) Haensch, C.; Ott, C.; Hoeppener, S.; Schubert, U.S. Combination of Different Chemical Surface Reactions for the Fabrication of Chemically Versatile Building Blocks onto Silicon Surfaces *Langmuir*, **2008**, *24*, 10222-10227. DOI: 10.1021/la8016744.
- (12) Lee, Y. W.; Reed-Mundell, J.; Zull, J. E.; Sukenik, C. N. Electrophilic siloxane-based self-assembled monolayers for thiol-mediated anchoring of peptides and proteins. *Langmuir*, **1993**, *9*, 3009-3014. DOI: 10.1021/la00035a045.
- (13) Fryxell, G. E.; Rieke, P. C.; Wood, L. L.; Engelhard, M. H.; Williford, R. E.; Graff, G. L.; Campbell, A. A.; Wiacek, R. J.; Lee, L.; Halverson, A.

- Nucleophilic Displacements in Mixed Self-Assembled Monolayers. *Langmuir*, **1996**, *12*, 5064-5075. DOI: 10.1021/la9506842.
- (14) Flink, S.; van Veggel, F. C. J. M.; Reinhoudt, D. N. Functionalization of self-assembled monolayers on glass and oxidized silicon wafers by surface reactions. *J. Phys. Org. Chem.*, **2001**, *14*, 407-415. DOI: 10.1002/poc.372.
- (15) Crivillers, N.; Mas-Torrent, M.; Perruchas, S.; Roques, N.; Vidal-Gancedo, J.; Veciana, J.; Rovira, C.; Basabe-Desmonts, L.; Ravoo, B. J.; Crego-Calama, M.; Reinhoudt, D. N. Self-Assembled Monolayers of a Multifunctional Organic Radical. *Angew. Chem., Int. Ed.*, **2007**, *46*, 2215-2219. DOI: 10.1002/anie.200603599.
- (16) Duan, X.; Sadhu, V. B.; Perl, A.; M. Peter, M.; Reinhoudt, D.N.; Huskens, J. Bifunctional, Chemically Patterned Flat Stamps for Microcontact Printing of Polar Inks. *Langmuir*, **2008**, *24*, 3621-3627. DOI: 10.1021/la702975q.
- (17) La, Y.-H.; Jung, Y. J.; Kim, H. J.; Kang, T.-H.; Ihm, K.; Kim, K.-J.; Kim, B.; Park, J. W. Sub-100-nm Pattern Formation through Selective Chemical Transformation of Self-Assembled Monolayers by Soft X-ray Irradiation. *Langmuir*, **2003**, *19*, 4390-4395. DOI: 10.1021/la026815y.
- (18) Rozkiewicz, D. I.; Janczewski, D.; Verboom, W.; Ravoo, B. J.; Reinhoudt, D. N. "Click" Chemistry by Microcontact Printing. *Angew. Chem., Int. Ed.*, **2006**, *45*, 5292-5296. DOI: 10.1002/anie.200601090.
- (19) Michel, O.; Ravoo, B. J. Carbohydrate Microarrays by Microcontact "Click" Chemistry. *Langmuir*, **2008**, *24*, 12116-12118. DOI: 10.1021/la802304w.

- (20) Ku, S.-Y.; Wong, K.-T.; Bard, A. J. Surface Patterning with Fluorescent Molecules Using Click Chemistry Directed by Scanning Electrochemical Microscopy. *J. Am. Chem. Soc.*, **2008**, *130*, 2392-2393. DOI: 10.1021/ja078183d.
- (21) Lummerstorfer, T.; Hoffmann, H. Click Chemistry on Surfaces: 1,3-Dipolar Cycloaddition Reactions of Azide-Terminated Monolayers on Silica. *J. Phys. Chem. B*, **2004**, *108*, 3963-3966. DOI: 10.1021/jp049601t.
- (22) Rohde, R. D.; Agnew, H. D.; Yeo, W.-S.; Bailey, R. C.; Heath, J. R. A Non-Oxidative Approach toward Chemically and Electrochemically Functionalizing Si(111). *J. Am. Chem. Soc.*, **2006**, *128*, 9518-9525. DOI: 10.1021/ja062012b.
- (23) Cao, X. L.; Zhang, T.; Deng, J. Y.; Jiang, L.; Yang, W. T. An Extremely Simple and Effective Strategy to Tailor the Surface Performance of Inorganic Substrates by Two New Photochemical Reactions. *ACS Appl. Mater. Interfaces*, **2013**, *5*, 494—499. DOI: 10.1021/am302582x.
- (24) Chen, C. Z.; Xu, P. C.; Li, X. X. Regioselective Patterning of Multiple SAMs and Applications in Surface-Guided Smart Microfluidics. *ACS Appl. Mater. Interfaces*, **2014**, *6*, 21961—21969. DOI: 10.1021/am508120s.
- (25) Carvalho, R. R.; Pujari, S. P.; Lange, S. C.; Sen, R.; Vrouwe, E. X.; Zuilhof, H. Local Light-Induced Modification of the Inside of Microfluidic Glass Chips. *Langmuir*, **2016**, *32*, 2389—2398. DOI: 10.1021/acs.langmuir.5b04621.
- (26) Carroll, G. T.; Rengifo, H. R.; Grigoras, C.; Mammana, A.; Turro, N. J.; Koberstein, J. T. Photogeneration of “Clickable” Surface-Bound Polymer

- Scaffolds. *J. Polym. Sci. A*, **2017**, *55*, 1151 —1155. DOI: 10.1002/pola.28485.
- (27) Mostegel, F. H.; Ducker, R. E.; Rieger, P. H.; El Zubir, O.; Xia, S. J.; Radl, S. V.; Edler, M.; Cartron, M. L.; Hunter, C. N.; Leggett, G. J.; Griesser, T. Versatile Thiol-based Reactions for Micrometer- and Nanometer-scale Photopatterning of Polymers and Biomolecules *J. Mater. Chem. B*, **2015**, *3*, 4431 —4438. DOI: doi.org/10.1039/C5TB00345H.
- (28) Carvalho, R. R.; Pujari, S. P.; Gahtory, D.; Vrouwe, E. X.; Albada, B.; Zuilhof, H. Mild Photochemical Biofunctionalization of Glass Microchannels. *Langmuir*, **2017**, *33*, 8624 —8631. DOI: 10.1021/acs.langmuir.6b03931.
- (29) Qin, G. T.; Yam, C. M.; Kumar, A.; Lopez-Romero, J. M.; Li, S.; Huynh, T.; Li, Y.; Yang, B.; Contreras-Caceres, R.; Cai, C. Z. Preparation, characterization, and protein-resistance of films derived from a series of  $\alpha$ -oligo(ethylene glycol)- $\omega$ -alkenes on H-Si(111) surfaces. *RSC Adv.*, **2017**, *7*, 14466 —1447. DOI: 10.1039/C6RA28497C.
- (30) Intemann, J. J.; Yao, K.; Li, Y. X.; Yip, H. L.; Xu, Y. X.; Liang, P. W.; Chueh, C. C.; Ding, F. Z.; Yang, X.; Li, X.; Chen, Y.; Jen, A. K. Y. Highly Efficient Inverted Organic Solar Cells through Material and Interfacial Engineering of Indacenodithieno[3,2-b]Thiophene-Based Polymers and Devices. *Adv. Funct. Mater.* **2014**, *24* (10), 1465–1473. DOI: 10.1002/adfm.201302426.
- (31) Yang, J.; Oshima, T.; Yindeesuk, W.; Pan, Z.; Zhong, X.; Shen, Q. Influence of Linker Molecules on Interfacial Electron Transfer and Photovoltaic Performance of Quantum Dot Sensitized Solar Cells. *J. Mater. Chem. A*, **2014**,

- 2 (48), 20882–20888. DOI: 10.1039/C4TA04353G.
- (32) Leo, N.; Liu, J.; Archbold, I.; Tang, Y.; Zeng, X. Ionic Strength, Surface Charge, and Packing Density Effects on the Properties of Peptide Self-Assembled Monolayers. *Langmuir*, **2017**, *33* (8), 2050–2058. DOI: 10.1021/acs.langmuir.6b04038.
- (33) Stettner, J.; Winkler, A. Characterization of Alkanethiol Self-Assembled Monolayers on Gold by Thermal Desorption Spectroscopy. *Langmuir*, **2010**, *26* (12), 9659–9665. DOI: 10.1021/la100245a.
- (34) Gotesman, G.; Naaman, R. Selective Surface Patterning for the Coadsorption of Self-Assembled Gold and Semiconductor Nanoparticles. *Langmuir*, **2008**, *24* (12), 5981–5983. DOI: 10.1021/la800184z.
- (35) Herzer, N.; Hoepfner, S.; Schubert, U.S. Fabrication of patterned silane based self-assembled monolayers by photolithography and surface reactions on silicon-oxide substrates. *Chem. Commun.*, **2010**, *46*, 5634–5652. DOI: 10.1039/C0CC00674B.
- (36) Wang, L.; Schubert, U. S.; Hoepfner, S. Surface Chemical Reactions on Self-Assembled Silane Based Monolayers. *Chem. Soc. Rev.* **2021**, *50* (11), 6507–6540. DOI: 10.1039/D0CS01220C.
- (37) Wasserman, S. R.; Tao, Y.T.; Whitesides, G.M. Structure and Reactivity of Alkylsiloxane Monolayers formed by Reaction of Alkyltrichlorosilanes on Silicon Substrate. *Langmuir*, **1989**, *5*, 4, 1074–1087. DOI: 10.1021/la00088a035.

- (38) Ishani, M., Dekamin, M. G.; Alirezvani, Z. Superparamagnetic silica core-shell hybrid attached to graphene oxide as a promising recoverable catalyst for expeditious synthesis of TMS-protected cyanohydrins. *J. Colloid Interface Sci.* **2018**, *521*, 232–24. DOI: 10.1016/j.jcis.2018.02.060.
- (39) Ulman, A. Formation and Structure of Self-Assembled Monolayers. *Chem. Rev.* **1996**, *96* (4), 1533–1554. DOI: 10.1021/cr9502357.
- (40) Ni, Y.; Zheng, S. Supramolecular Inclusion Complexation of Polyhedral Oligomeric Silsesquioxane Capped Poly( $\epsilon$ -Caprolactone) with  $\alpha$ -Cyclodextrin. *J. Polym. Sci. A Polym. Chem.* **2007**, *45* (7), 1247–1259. DOI: 10.1002/pola.20999.
- (41) Chougala, B. M.; Samundeeswari, S.; Holiyachi, M.; Shastri, L. A. Mild, Efficient and Catalyst-Free Hydroxylation of Alkyl Halides in Water: Significant Enhancement of Water Nucleophilicity in Dipolar Solvents. *ChemistrySelect* **2017**, *2* (3), 1290–1296. DOI: 10.1002/slct.201601444.
- (42) Hutchins, R.O.; Taffer, I. M. Aqueous Polar Aprotic Solvents. Efficient Sources of Nucleophilic Oxygen. *J. Org. Chem.* **1983**, *48* (8), 1360–1362. DOI: 10.1021/jo00156a045.
- (43) Menchikov, L. G.; Vorogushin, A. V.; Korneva, O. S.; Nefedov, O. M. An Effective Method for Alcohol Preparation by Hydrolysis of Organohalides in the Presence of Copper and Its Salts in Aqueous DMSO. *Mendeleev Commun.* **1995**, *5* (6), 223–224. DOI: 10.1070/MC1995v005n06ABEH000536.
- (44) Krishnamurty, K.V.; Harris, G. M. The Chemistry of the Metal Oxalato

- Complexes. *Chem. Rev.* **1961**, *61* (3), 213–246. DOI: 10.1021/cr60211a001.
- (45) Delle Chiaie, K. R.; Biernesser, A. B.; Ortuño, M. A.; Dereli, B.; Iovan, D. A.; Wilding, M. J. T.; Li, B.; Cramer, C. J.; Byers, J. A. The Role of Ligand Redox Non-Innocence in Ring-Opening Polymerization Reactions Catalysed by Bis(Imino)Pyridine Iron Alkoxide Complexes. *Dalton Trans.*, **2017**, *46* (38), 12971–12980. DOI: 10.1039/C7DT03067C.
- (46) Fetsch, C.; Gaitzsch, J.; Messenger, L.; Battaglia, G.; Luxenhofer, R. Self-Assembly of Amphiphilic Block Copolypeptoids – Micelles, Worms and Polymersomes. *Sci Rep*, **2016**, *6* (1), 1–13. DOI: 10.1038/srep33491.
- (47) Thunig, D.; Semen, J.; Elias, H.-G. Carbon Dioxide Influence on NCA Polymerizations. *Die Makromol. Chem.* **1977**, *178* (2), 603–607. DOI: 10.1002/macp.1977.021780229.
- (48) Aliferis, T.; Iatrou, H.; Hadjichristidis, N. Living Polypeptides. *Biomacromolecules* **2004**, *5* (5), 1653–1656. DOI: 10.1021/bm0497217.
- (49) Zou, J.; Fan, J.; He, X.; Zhang, S.; Wang, H.; Wooley, K. L. A Facile Glovebox-Free Strategy to Significantly Accelerate the Syntheses of Well-Defined Polypeptides by N -Carboxyanhydride (NCA) Ring-Opening Polymerizations. *Macromolecules* **2013**, *46* (10), 4223–4226. DOI: 10.1021/ma4007939.
- (50) Pangborn, A. B.; Giardello, M. A.; Grubbs, R. H.; Rosen, R. K.; Timmers, F. J. Safe and Convenient Procedure for Solvent Purification. *Organometallics* **1996**, *15* (5), 1518–1520. DOI: 10.1021/om9503712.

- (51) Biernesser, A. B.; Li, B.; Byers, J. A. Redox-Controlled Polymerization of Lactide Catalyzed by Bis(Imino)Pyridine Iron Bis(Alkoxide) Complexes. *J. Am. Chem. Soc.* **2013**, *135* (44), 16553–16560. DOI: 10.1021/ja407920d.
- (52) Biernesser, A. B.; Chiaie, K. R. D.; Curley, J. B.; Byers, J. A. Block Copolymerization of Lactide and an Epoxide Facilitated by a Redox Switchable Iron-Based Catalyst. *Angew. Chem. Int. Ed.* **2016**, *55* (17), 5251–5254. DOI: 10.1002/anie.201511793.
- (53) Hoertz, P. G.; Chen, Z.; Kent, C. A.; Meyer, T. J. Application of High Surface Area Tin-Doped Indium Oxide Nanoparticle Films as Transparent Conducting Electrodes. *Inorg. Chem.* **2010**, *49* (18), 8179–8181. DOI: 10.1021/ic100719r.